



**Hurricane Weather Research and Forecasting
(HWRF) Model:
2014 Scientific Documentation**

September 2014 – HWRF v3.6a

Vijay Tallapragada

NOAA/NWS/NCEP Environmental Modeling Center, College Park, MD

Ligia Bernardet

NOAA Earth System Research Laboratory, CIRES / University of Colorado, and Developmental Testbed Center, Boulder, CO

Mrinal K Biswas

National Center for Atmospheric Research and Developmental Testbed Center, Boulder, CO

Sundararaman Gopalakrishnan

NOAA/AOML, Hurricane Research Division, Miami, FL

Young Kwon

NOAA/NWS/NCEP Environmental Modeling Center and IMSG Inc., College Park, MD

Qingfu Liu

NOAA/NWS/NCEP Environmental Modeling Center, College Park, MD

Timothy Marchok

NOAA/OAR/Geophysical Fluid Dynamics Laboratory, Princeton, NJ

Dmitry Sheinin

NOAA/NWS/NCEP Environmental Modeling Center and IMSG Inc., College Park, MD

Mingjing Tong

NOAA/NWS/NCEP Environmental Modeling Center and UCAR, College Park, MD

Samuel Trahan

NOAA/NWS/NCEP Environmental Modeling Center and IMSG Inc., College Park, MD

Robert Tuleya

Center for Coastal Physical Oceanography, Old Dominion University, Norfolk, VA

Richard Yablonsky

Graduate School of Oceanography, University of Rhode Island, Narragansett, RI

Xuejin Zhang

NOAA/AOML Hurricane Research Division and RSMAS/CIMAS, University of Miami, Miami, FL

Acknowledgments

The authors wish to acknowledge the Development Testbed Center (DTC) for facilitating the coordination of writing this document amongst the following institutions: NOAA/NWS/NCEP Environmental Modeling Center; NOAA/ESRL Global Systems Division; NOAA/AOML Hurricane Research Division; NOAA/OAR Geophysical Fluid Dynamics Laboratory; IM Systems Group Inc.; Graduate School of Oceanography, University of Rhode Island; RSMAS/CIMAS, University of Miami; and CIRES University of Colorado, Boulder, CO. Thanks to Karen Griggs of NCAR for offering her desktop publishing expertise in the preparation of this document.

Table of Contents

Acknowledgments	2
An Introduction to the Hurricane Weather Research and Forecast (HWRP) System	5
1.0 HWRP Initialization	18
1.1 Introduction	18
1.2 HWRP cycling system.....	18
1.3 Bogus vortex used to correct weak storms.....	22
1.4 Correction of vortex in previous 6-h HWRP or GDAS forecast	23
1.5 Data assimilation through GSI in HWRP	35
2.0 MPI Princeton Ocean Model for Tropical Cyclones (MPIPOM-TC)	44
2.1 Introduction.....	44
2.2 Purpose.....	45
2.3 Grid size, spacing, configuration, arrangement, coordinate system, and numerical scheme.....	45
2.4 Initialization.....	47
2.5 Physics and dynamics	48
2.6 Coupling.....	49
2.7 Output fields for diagnostics	50
3.0 Physics Packages in HWRP	51
3.1 HWRP physics	51
3.2 Microphysics parameterization.....	52
3.3 Cumulus parameterization	54
3.4 Surface-layer parameterization.....	56
3.5 Land-surface model.....	61
3.6 Planetary boundary-layer parameterization	63
3.7 Atmospheric radiation parameterization.....	66
3.8 Physics interactions.....	68
4.0 Design of Moving Nest	69
4.1 Grid Structure.....	69
4.2 Terrain Treatment.....	70
4.3 Moving Nest Algorithm	72
4.4 Fine Grid Initialization.....	72
4.5 Lateral Boundary Conditions.....	74
4.6 Feedback	75

5.0 Use of the GFDL Vortex Tracker	76
5.1 Introduction	76
5.2 Design of the tracking system.....	78
5.3 Parameters used for tracking	83
5.4 Intensity and wind radii parameters.....	85
5.5 Thermodynamic phase parameters.....	85
5.6 Detecting genesis and tracking new storms.....	86
5.7 Tracker output.....	88
6.0 The idealized HWRF framework	95
7.0 References	98

An Introduction to the Hurricane Weather Research and Forecast (HWRF) System

The Environmental Modeling Center (EMC) at the National Centers for Environmental Prediction (NCEP) provides high-resolution deterministic tropical cyclone forecast guidance in real time to the National Hurricane Center (NHC) for the North Atlantic and Eastern North Pacific basins; to the Central Pacific Hurricane Center (CPHC) for the Central North Pacific basin; and to the United States (US) Navy's Joint Typhoon Warning Center (JTWC) for all other tropical ocean basins including Western North Pacific, North Indian, South Indian and South Pacific. Figure I.1 shows the regions where HWRF model is currently operated in real time.

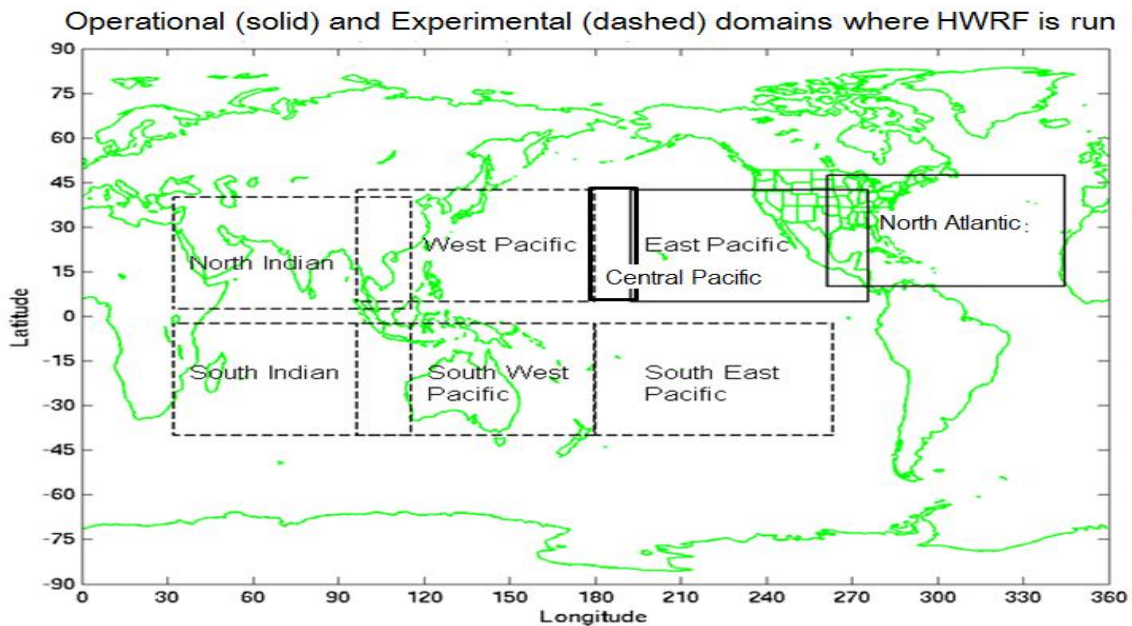


Figure I.1: Tropical oceanic basins covered by the HWRF model for providing real-time TC forecasts. Solid lines represent operational HWRF domains at NCEP. Dashed lines show the areas where experimental forecasts are provided by HWRF in real time.

The Hurricane Weather Research and Forecast (HWRF) system became operational at NCEP starting with the 2007 hurricane season. Development of the HWRF began in 2002 at EMC in collaboration with the Geophysical Fluid Dynamics Laboratory (GFDL) of the National Oceanic and Atmospheric Administration (NOAA) and the University of Rhode Island (URI). To meet operational implementation requirements, skill of the track forecasts from the HWRF and GFDL hurricane models needed to be comparable. Because the GFDL model evolved as primary guidance for track prediction used by NHC, CPHC, and JTWC after becoming operational in 1994, the strategy for HWRF development was to take advantage of the advancements made to improve tropical cyclone track, intensity, structure and rainfall predictions through a focused collaboration between EMC, GFDL, and URI, and then transition those modeling advancements to the HWRF. This strategy ensured comparable track and intensity forecast skill to the GFDL

for initial implementation in 2007. Additionally, features of the GFDL hurricane model that led to demonstrated skill for intensity forecasts, such as ocean coupling, upgraded air-sea physics, and improvements to microphysics, were also incorporated into the newly developed HWRF system.

Upgrades to the HWRF system are performed on an annual cycle that is dependent on the hurricane season and on upgrades to the Global Data Assimilation System (GDAS) and the Global Forecast System (GFS) that both provide initial and boundary conditions for HWRF. Every year, prior to the start of the Eastern North Pacific and Atlantic hurricane seasons (15 May and 1 June, respectively), HWRF upgrades are provided to NHC by EMC so that NHC forecasters have improved hurricane guidance at the start of each new hurricane season. These upgrades are chosen based on extensive testing and evaluation (T&E) of model forecasts for at least two recent past hurricane seasons. There are basically two phases of development. The first is developmental testing that occurs prior to and during the hurricane season (roughly 1 April to 30 October) where potential upgrades to the system are tested individually in a systematic and coordinated manner. The pre-implementation testing starts in November and is designed to test the most promising developments assessed in the development phase to define the HWRF configuration for the upcoming hurricane season. The results of the pre-implementation testing must be completed and the final HWRF configuration locked down by 15 March for each annual upgrade. Once frozen, the system is handed off to NCEP Central Operations (NCO) for implementation by about 1 June. The cycle is then repeated for the next set of proposed upgrades to the HWRF system. During the hurricane season (1 June to 30 November) changes are not made to the operational HWRF so that forecasters are provided with consistent and documented numerical guidance performance characteristics.

Since its initial implementation in 2007, HWRF has been upgraded every year to meet specific scientific goals addressed through the aforementioned pre-implementation T&E. Changes to the vortex initialization and convective parameterization were the focal areas for the 2008 HWRF implementation. Infrastructure upgrades and transitioning to the new IBM machine were dominant for the 2009 HWRF implementation. For 2010 upgrades, the HWRF team at EMC worked on further improving the vortex initialization, including gravity wave drag parameterization and modifying the surface physics based on observations. Limiting rapid growth of initial intensity errors was one of the focal areas for the 2011 HWRF implementation, along with major upgrades to model dynamical core from WRF v2.0 to community-based WRF v3.2, bridging the gap between the operational and community versions of the WRF model. Other significant developments in year 2011 were to make the operational HWRF model available to the research community through the Developmental Testbed Center (DTC), and to draw the codes from the community repository maintained and supported by DTC, ensuring that the operational and research HWRF codes remain synchronized (Bernardet et al. 2014).

To significantly improve hurricane forecast skill, the hurricane modeling team at NCEP/EMC, with support from NOAA's Hurricane Forecast Improvement Project (HFIP) and in collaboration with the Hurricane Research Division (HRD) of the NOAA Atlantic Oceanographic and Meteorological Laboratory (AOML) and several partners

within NOAA as well as academia, implemented major changes to the 2012 version of operational HWRf. The biggest improvement was the triple-nest capability that included a cloud-resolving innermost grid operating at 3-km horizontal resolution. Other major HWRf upgrades implemented for the 2012 hurricane season include a centroid-based nest-movement algorithm; explicit representation of moist processes in the innermost grid; inclusion of shallow convection in the Simplified Arakawa Schubert (SAS) convective parameterization; observation-based modifications to the convective, microphysics, Planetary Boundary Layer (PBL) and surface parameterizations, making them suitable for higher resolution; re-design of the vortex initialization for 3-km resolution with improved interpolation algorithms and better representation of the composite storm; improved Princeton Ocean Model for TCs (POM-TC) initialization in the Atlantic domain and new 1-D ocean coupling for the Eastern North Pacific basin; upgrade of the Gridpoint Statistical Interpolator (GSI) data assimilation system; improved HWRf Unified Post Processor (UPP) to generate simulated microwave satellite imagery products; and very high-resolution (every 5 s) storm tracker output to support NHC operations. The HWRf codes were optimized to ensure that the 2012 model ran in the time slot allotted for operational products at NCEP and with few additional computer resources.

Apart from obtaining significant improvements in the track forecast skill compared to previous versions, 2012 version of the operational HWRf has conclusively demonstrated the positive impact of resolution on storm size and structure forecasts (Tallapragada et al. 2014). Figure I.2 shows the verification of the mean 34-kt (R34), 50-kt (R50) and 65-kt (R65) radii for the NATL and EPAC basins for the 2010-2011 hurricane seasons. Here, the R34 at each quadrant is defined as the radius at which the mean tangential wind is equal to 34-kt (and similarly for R50 and R65), and the mean radii are obtained by taking an average of the radii in four different quadrants. It is apparent in Fig. I.2 that improvements of the various storm radii are radical for both basins. Except for the R34 in the NATL basin, the overall reduction of the errors is nearly 80% at all forecast lead times, particularly for R50 and R65. Such large reduction of the strong wind radii indicates that the high-resolution HWRf model forecasts were able to capture the inner-core region of the storms more realistically. This is expected as storm structure and fine-scale processes are believed to be better resolved with higher resolution.

The 2013 version of the operational HWRf made significant gains in improving track, intensity and structural prediction of TCs by taking further advantage of the high-resolution capability built in the 2012 HWRf. Major upgrades for the 2013 HWRf include changes in model configuration, such as use of a larger innermost 3-km domain and higher frequency of physics calls; an advanced parent-nest interpolation method; a more sophisticated vortex-following algorithm based on nine different parameters as in GFDL vortex tracker; upgrades to the PBL parameterization to fit observed structures of both the hurricane area and the outer environmental region; modifications of the vortex initialization method with adjusted filter size, storm-size correction, and weak-storm treatment; and for the first time, implementation of the Hurricane Data Assimilation System (HDAS), a GSI-based one-way hybrid ensemble-variational data assimilation scheme to assimilate inner-core observations from the NOAA P3 aircraft Tail Doppler

Radar (TDR) data, when available; improved ocean model; and further improvements to the forecast products.

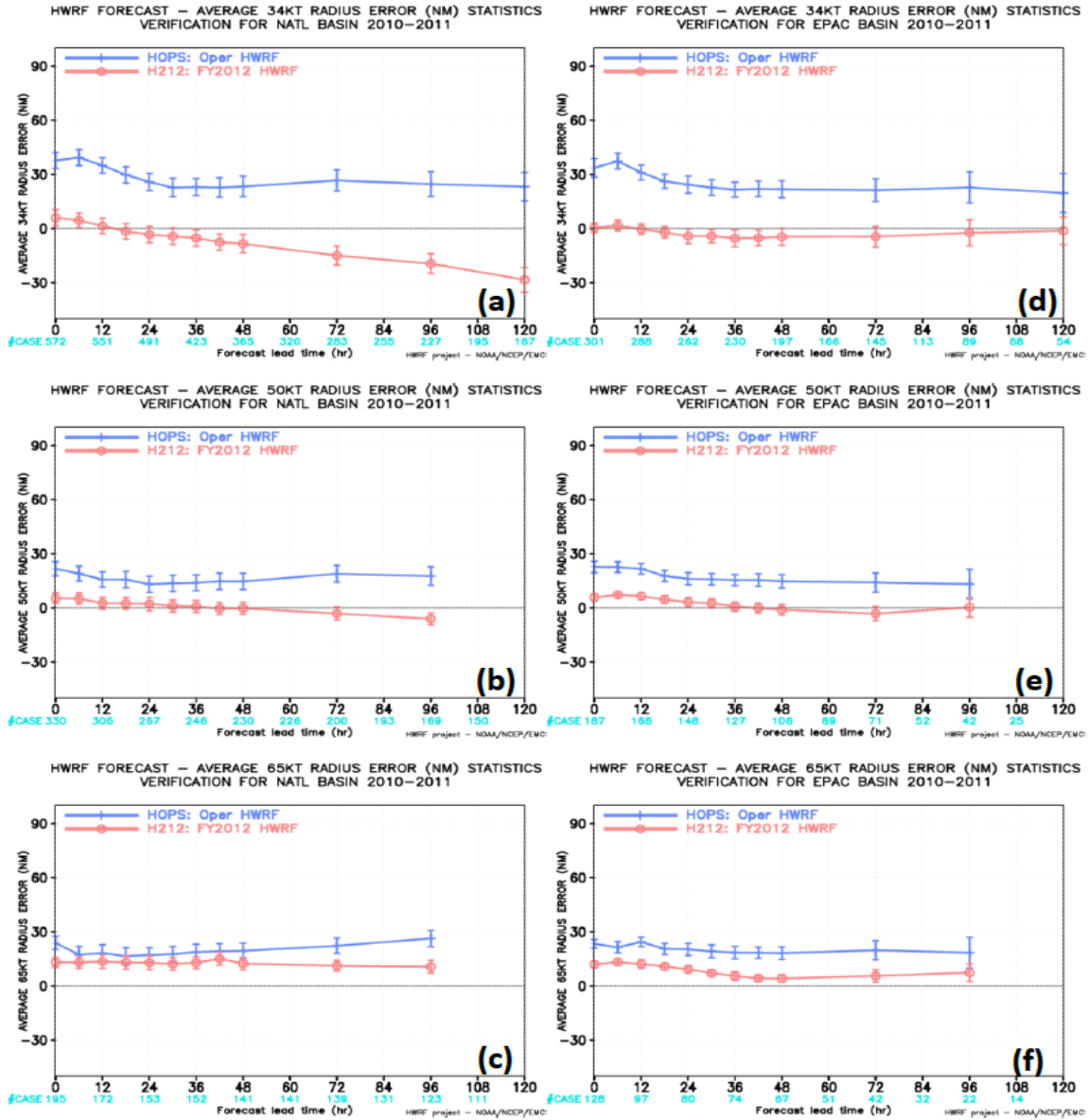


Figure I.2: Comparison of the statistics of the radii verification of the mean 34 kt, 50 kt, and 65kt radius during the 2010-2011 hurricane seasons between the operational HWRf version (blue, HOPS) and the newly implemented HWRf configuration (red, H212) for the Atlantic basin (left panels) and Eastern Pacific basin (right panels). The number below the x-axis denote the number of cases (cycles) during the implementation. Here the mean radii verification is calculated by using the simple arithmetic mean of the radii in the SE, SW, NE, and NW quadrant. (Taken from Tallapragada et al. 2014)

One of the highlights of the 2013 HWRf configuration retrospective T&E, performed on a vast sample of three hurricane seasons (2010-2012), was the remarkable intensity forecast skill. Results shown in Fig. I.3 indicated that the HWRf model outperformed

the statistical models for intensity prediction in the 2 to 3-day forecast period. Historically, statistical models have been more skillful than dynamical models for hurricane intensity prediction. These HWRF results demonstrate, for the first time, the potential of an operational dynamical model as a viable hurricane intensity prediction tool. Track forecast skills from the 2013 HWRF have also been significantly improved compared to the 2012 HWRF, and are now comparable to the best-performing GFS model.

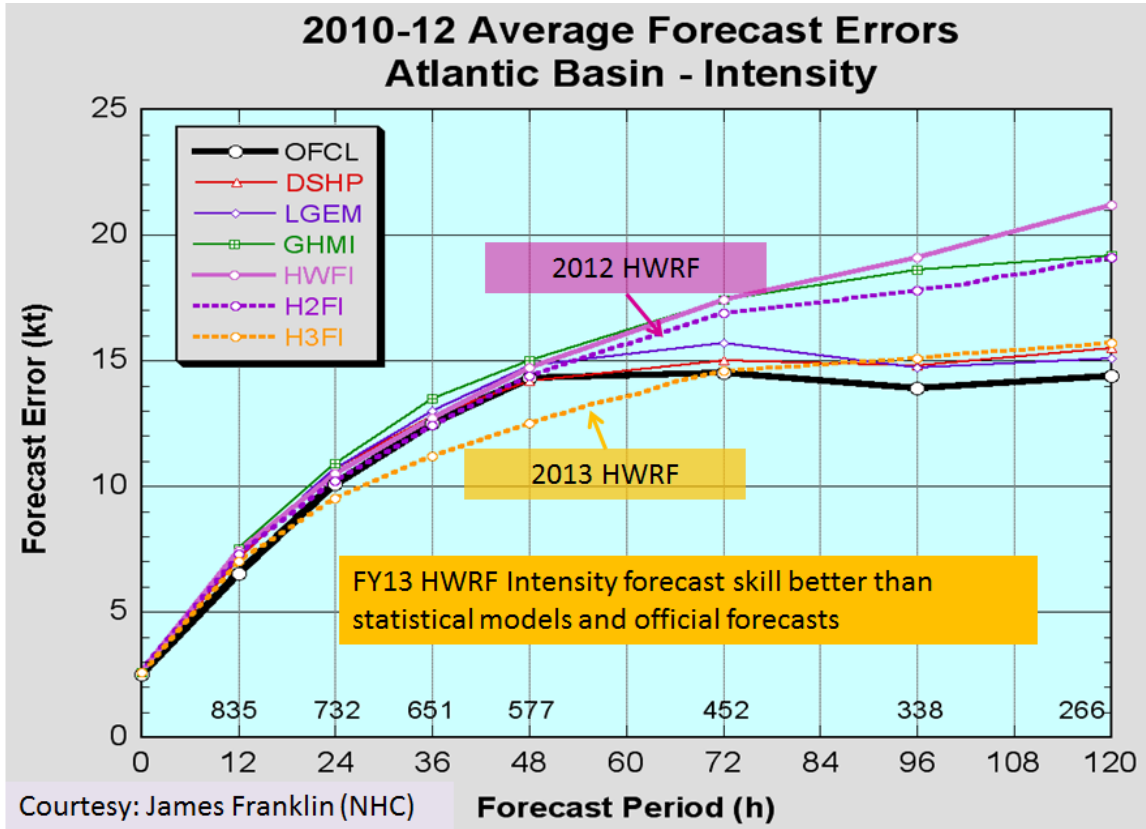


Figure I.3: Average intensity forecast errors for 2010-2012 hurricane seasons from 2013 version of HWRF model (H3FI) compared to 2012 version (H2FI), operational HWRF (HWFI), GFDL model (GHMI), statistical models LGEM (Linear Growth Equation Model) and DSHP (Decay Statistical Hurricane Intensity Prediction System). Dark black line represents NHC Official Forecast errors as a function of time, and the number of cases verified at each forecast period is shown along the x-axis.

Major upgrades for the 2014 version of the operational HWRF include increased vertical resolution (61 levels) and higher model top (2 hPa), inclusion of aircraft reconnaissance dropsonde data in the inner core, implementation of a new, high-resolution version of POM-TC (MPIPOM-TC), with a single, transatlantic ocean domain for NATL and 3-D coupling for the EPAC basins. Evaluation of 2014 HWRF upgrades have shown further improvements in track and intensity forecasts, with the track errors now comparable to the best performing GFS model and intensity errors better than NHC official forecasts at all forecast lead times. Fig. I.4 shows the cumulative improvements obtained from the

operational HWRF during the last four years (2011-2014), highlighting the role of HWRF in providing more accurate track and intensity forecast guidance for NHC. HWRF model's progress towards accomplishing 5-year goals of HFIP is also highlighted in this figure.

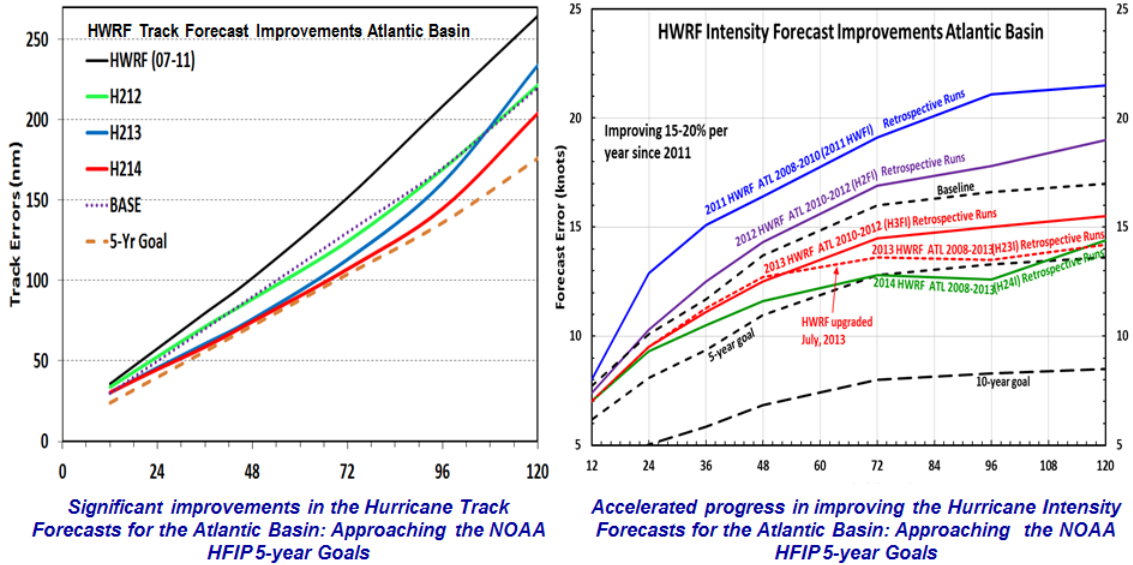


Figure I.4: Cumulative forecast improvements in the NATL basin from operational HWRF over the years since 2011. Each configuration of HWRF was evaluated for multiple hurricane seasons. The dashed lines show HFIP baseline (BASE) and 5-year goal for track and intensity errors.

This documentation provides a description of HWRF v3.6a, which is functionally equivalent to the model implemented for the 2014 hurricane season. The list of upgrades to the HWRF for the hurricane seasons from 2008 through 2014 is available on EMC's HWRF website (<http://www.emc.ncep.noaa.gov/index.php?branch=HWRF>). These details will also be made available on the WRF for Hurricanes website hosted by DTC (<http://www.dtcenter.org/HurrWRF/users>).

The HWRF system is composed of the WRF model software infrastructure, the Non-Hydrostatic Mesoscale Model (NMM) dynamic core, the MPIPOM-TC, and the NCEP coupler. HWRF employs a suite of advanced physics developed for tropical cyclone applications. These include GFDL surface physics to account for air-sea interaction over warm water and under high-wind conditions, GFDL land-surface model and radiation, Ferrier Microphysics, NCEP GFS boundary layer, and GFS SAS deep and shallow convection. Figure I.5 illustrates all components of HWRF supported by the DTC, which also include the WRF Pre-Processor System (WPS), *prep_hybrid* (used to process spectral coefficients of GDAS and GFS in their native vertical coordinates), a sophisticated vortex initialization package designed for HWRF, the regional hybrid Ensemble Kalman Filter (EnKF) - three-dimensional variational data assimilation system (3D-VAR) GSI, UPP, and the GFDL vortex tracker.

It should be noted that, although the HWRF uses the same dynamic core as the NMM in the Arakawa E-staggered grid (NMM-E) developed at NCEP, HWRF was customized for hurricane/tropical forecast applications, and is very different from other operational models that employ NMM-E, such as the High-Resolution Windows (HRW) and the Short-Range Ensemble Forecast (SREF) System. HWRF also differs substantially from the North American Mesoscale (NAM) model, which now employs the NMM dynamic core in the Arakawa-B grid (NMM-B). The HWRF is an atmosphere-ocean model configured with a parent grid and two telescopic, high-resolution, movable 2-way nested grids that follow the storm, using a unique physics suite and diffusion treatment. The HWRF also contains a sophisticated initialization of both the ocean- and the storm-scale circulation. Additionally, unlike other NCEP forecast systems that run continuously throughout the year, the HWRF and GFDL hurricane models are launched for operational use only when NHC or JTWC determines that a disturbed area of weather has the potential to evolve into a depression anywhere over their area of responsibility. After an initial HWRF run is triggered, new runs are launched in cycled mode at 6-h intervals, until either the storm dissipates after making landfall, becomes extra-tropical, or degenerates into a remnant low, typically identified when convection becomes disorganized around the center of circulation. Currently, the HWRF model is run in NCEP Central Operations (NCO) for the NATL, EPAC, and CPAC basins, and experimentally on HFIP computational resources for all other basins, four times daily producing 126-h forecasts of TC track, intensity, structure, and rainfall to meet the operational forecast and warning process objectives.

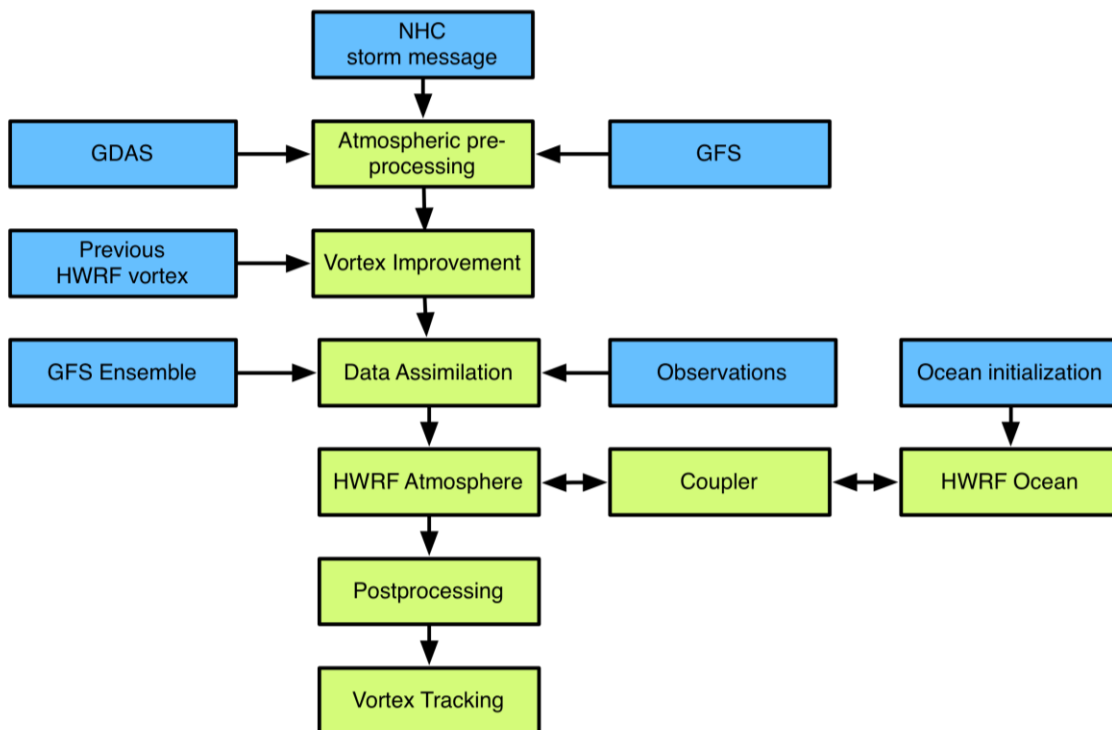


Figure I.5. A simplified overview of the HWRF system for the case in which TDR data are not available. Components include the atmospheric initialization (WPS and prep_hybrid), the vortex improvement, the GSI data assimilation, the HWRF atmospheric model, the atmosphere-ocean coupler, the ocean initialization, the MPIPOM-TC, the post processor, and the vortex tracker. When TDR data are available, the data assimilation in the parent domain is not used as an input to the vortex improvement. Additionally, a second run of GSI is performed on the high-resolution grid after the vortex improvement (more details in Section 1).

The following paragraphs present an overview of the sections contained in this documentation. A concluding paragraph provides proposed future enhancements to the HWRF system for advancing track, intensity, and structure prediction, along with modeling advancements to address issues of storm surge, inland flooding, and coastal inundation for landfalling storms.

HWRF Atmospheric Initialization

The HWRF vortex initialization consists of several major steps: definition of the HWRF domain based on the observed storm center position; interpolation of the HDAS fields onto the HWRF parent domain; removal of the global model vortex and insertion of a modified mesoscale vortex obtained from the previous cycle's HWRF 6-hr forecast (when available), from HDAS, or from a synthetic vortex (cold start). The modification of the mesoscale hurricane vortex in the first-guess field is a critical aspect of the initialization problem. Modifications include corrections to the storm size and to the three-dimensional structure based on observed parameters, including Radius of Maximum Wind (RMW), radius of 34-kt winds (R34) and/or Radius of Outermost Closed Isobar (ROCI), maximum sustained 10-m winds (intensity), and minimum mean sea-level pressure (MSLP). Each of these corrections requires careful rebalancing between the model winds, temperature, pressure, and moisture fields. This procedure is described in Section 1.

An advancement of the HWRF system over the GFDL model bogus vortex initialization is the capability of the HWRF to run in cycles to improve the three-dimensional structure of the hurricane vortex. This capability provides a significant opportunity to add more realistic structure to the forecast storm and is a critical step towards advancing hurricane intensity/structure prediction.

The operational HWRF initialization procedure mentioned above, and described in Section 1, utilizes the community GSI with a regional hybrid EnKF-3DVAR data assimilation procedure that includes assimilation of TDR data from the NOAA P3 aircraft, when available. The NCEP operational GFS 80-member ensemble forecast provides the ensemble background error covariances for HDAS. Apart from the NOAA P3 TDR, dropsonde data from aircraft reconnaissance missions, conventional observations, and clear-sky radiance datasets from several geostationary and polar orbiting satellites are also assimilated in the hurricane environment using GSI. Section 1 provides more details on the application of GSI in the HWRF modeling system. Unlike in past HWRF configuration, in 2014 HWRF, GFS analysis is used for HWRF initial

conditions in the outer domain while GSI data assimilation procedure is applied only for the 9-km intermediate and 3-km inner most nest domains. Hurricane data assimilation is one of the high-priority areas of research that holds promise for improved representation of initial structure of the hurricane vortex and its environment.

Ocean Coupling

In 2001, the GFDL was coupled to POM-TC, a three-dimensional version of the POM modified for hurricane applications over the Atlantic basin. GFDL was the first coupled air-sea hurricane model to be implemented for hurricane prediction into NCEP's operational modeling suite. Prior to implementation, many experiments were conducted over multiple hurricane seasons that clearly demonstrated the positive impact of the ocean coupling on both the GFDL track and intensity forecasts. Given the demonstrated improvements in the Sea Surface Temperature (SST) analyses and forecasts, this capability was also developed for the HWRF 2007 implementation.

Because early experiments had shown the impact on intensity of storms traversing over a cold-water wake, particular attention was given to the generation of the hurricane-induced cold wake in the initialization of the POM-TC. Some of the most recent improvements to the ocean initialization include feature-based modifications of the temperature and salinity to produce more realistic ocean structures than climatology can provide. These feature-based modifications include better initialization of the Gulf Stream, the Loop Current, and both warm and cold-core eddies in the Gulf of Mexico (GOM). The GOM features have shown importance for more accurate predictions in the GFDL model of intensification and weakening in Hurricanes Katrina, Rita, Gustav, and Ike.

To increase the resolution of POM-TC and provide the framework for flexible ocean initialization options, POM-TC has now been replaced in HWRF with a new, Message Passing Interface (MPI) version of POM-TC, called MPIPOM-TC. While the implementation of MPIPOM-TC has so far led to modest improvements in HWRF intensity forecasts, the new MPIPOM-TC system will facilitate more rapid improvements in subsequent years. Section 2 describes the configuration of MPIPOM-TC used in HWRF and its initialization.

From 2007 to 2011, the operational HWRF was coupled only in the North Atlantic basin. In 2012 and 2013, the operational HWRF was coupled to a 1-D version of POM-TC in the Eastern North Pacific basin. Starting with the 2014 hurricane season, the operational HWRF is now coupled to the 3-D MPIPOM-TC in both the North Atlantic and eastern North Pacific basins. HWRF/MPIPOM-TC coupling also exists in other worldwide ocean basins, with a variety of potential ocean initialization options, but these other basins are not being released to the community until the developers have completed sufficient testing and evaluation.

Much research is currently underway in the atmospheric/oceanic hurricane community to prioritize and determine the model complexity necessary to simulate realistic air-sea interactions. This complexity may include coupling to an adaptable multi-grid wave model (WAVEWATCH III – WW3) and simulating wave-current interactions that may

prove important to solve coastal inundation problems for landfalling hurricanes. The NCEP operational hurricane wave model driven by HWRP forcing has shown significant improvements in forecasting the significant wave heights. Starting with 2014 hurricane season, NCEP Hurricane WW3 model will become a downstream model for HWRP, replacing the wind forcing from GFDL model forecasts with high-resolution HWRP hourly wind forecasts.

HWRP Physics

Some of the physics in the HWRP evolved from a significant amount of development work carried out over the past 15 years in advancing model prediction of hurricane track with global models, such as the NCEP GFS, the Navy Operational Global Atmospheric Prediction System (NOGAPS), the United Kingdom Met Office (UKMO) model, and subsequently with the higher-resolution GFDL hurricane model that demonstrated improvement in hurricane intensity forecasts. These physics include representations of the surface layer, planetary boundary layer, microphysics, deep convection, radiative processes, and land surface. Commensurate with increasing interest in the ocean impact on hurricanes in the late 1990s and the operational implementation of the coupled GFDL model in 2001, collaboration increased between the atmospheric/oceanic research and operational communities that culminated in the Navy's field experiment, the Coupled Boundary Layer Air-Sea Transfer (CBLAST), carried out in the Eastern Atlantic in 2004. During CBLAST, important observations were recorded that helped confirm that drag coefficients used in hurricane models were incorrect under high-wind regimes. Since then, surface fluxes of both momentum and enthalpy under hurricanes remain an active area of hurricane scientific/modeling interest and are being examined in simple air-sea coupled systems and three-dimensional air-sea coupled systems with increasing complexity, including coupling of air-sea to wave models. Surface physics parameterization schemes used in the GFDL and HWRP models have continuously been calibrated to match the air-sea exchange coefficients based on findings from various observational campaigns and laboratory experiments. Recent research findings based on extensive dropsonde data collected from NOAA P3 aircraft and analyzed by scientists at NOAA/AOML have led to the improved representation of the vertical mixing in the hurricane planetary boundary layer (PBL) formulation in HWRP (Gopalakrishnan et al. 2012). Further improvements to the PBL scheme include formulation of variable critical Richardson number based on surface-wind speed and calibration of PBL height and inflow angle to match the analysis provided by the observations from various field campaigns. The moist physics (convection and microphysics) used in the HWRP model has also been constantly improved to obtain improved hurricane intensity forecast skill. Dependency of convection scheme on model resolution requires adopting more sophisticated scale-aware physics; however, convection is explicitly resolved in the inner-core region covered by the 3-km nest. While there have been lot of efforts evaluating the impact of advanced microphysics schemes like the double-moment Thompson scheme, the results so far did not yield the desired benefits in improving hurricane intensity forecasts. Therefore, HWRP still employs the most successful Ferrier scheme modified for hurricane applications. Accurate representation of cloud-radiative feedback and land-surface processes, improved interactions between various components

of the physics and dynamics, and testing of next-generation scale-aware and stochastic physics continue to be a high-priority area of research for the HWRP model improvements.

A detailed treatment of the HWRP physics is presented in Section 3. However, it must be re-emphasized that these physics, along with other HWRP upgrades, are subject to modification or change on an annual basis to coincide with continuous advancement to the components of this system.

Grid Configuration, Moving Nest and Vortex Tracker

The current HWRP configuration used in operations (starting with the 2012 hurricane season) contains three domains: a parent domain with 27-km horizontal grid spacing and two two-way interactive telescopic moving nests with 9- and 3-km spacing respectively, to capture multi-scale interactions. The parent domain covers roughly $80^{\circ} \times 80^{\circ}$ on a rotated latitude/longitude E-staggered grid. The large parent domain allows for rapidly accelerating storms moving to the north typically seen over the mid-Atlantic within a given 5-day forecast. The intermediate nest domain at 9-km resolution spans approximately $12^{\circ} \times 12^{\circ}$ and the innermost nest domain at 3-km resolution covers an area of about $7.1^{\circ} \times 7.1^{\circ}$. Both the intermediate and innermost grids are centered over the initial storm location, and are configured to follow the projected path of the storm.

The HWRP movable nested grids and the internal mechanism that ensures the nested grids follow the storm are described in Section 4. A major upgrade for 2013 HWRP is the redesign of the nest movement technique, now based on nine different atmospheric parameters used to accurately determine the storm center at every nest movement time step. Further improvements to the nest movement algorithm and nest-parent interpolations have been introduced in the 2014 HWRP configuration to provide the much desired high resolution atmospheric domains near the storm area and faithfully track the model storms throughout the model integration. The overall development of the movable nested grids required substantial testing to determine optimal grid configurations, lateral boundary conditions, and domain sizes to accommodate the required 5-day operational hurricane forecasts with consideration for multiple storm scenarios occurring in either the Atlantic or Eastern North Pacific basins. When more than one storm becomes active, a separate HWRP run is launched with its unique storm-following nested grids.

After the forecast is run, a post-processing step includes running the GFDL vortex tracker on the model output to extract attributes of the forecast storm. The GFDL vortex tracker is described in Section 5.

Future HWRP Direction

Starting with the 2011 hurricane season, all components of HWRP have been synchronized with their community code repositories to facilitate transition of developments from Research to Operations (R2O). This effort, led by the DTC, has enabled closer collaboration among HWRP developers and allowed accelerated R2O

transfer from government laboratories and academic institutions to the operational HWRF.

The major HWRF upgrades for the 2013 and 2014 hurricane seasons, previously listed, provide a solid foundation for improved tropical cyclone intensity prediction. Future advancements to the HWRF system include implementing advanced physics packages, such as land-surface model (LSM), radiation, PBL, and microphysics.

Future advancements to atmospheric initialization include assimilation of cloudy and all-sky radiances from various satellites, and additional observations from aircraft and/or Unmanned Aerial Vehicles (UAVs). Those include flight-level data, dropsondes, and surface winds obtained with the Stepped-Frequency Microwave Radiometer (SFMR). It should be noted that, to support future data-assimilation efforts for the hurricane core, NOAA acquired the G-IV aircraft in the mid 1990s to supplement the data obtained by NOAA's P-3s. The high altitude of the G-IV allows for observations that help define the three-dimensional core structure from the outflow layer to the near surface. For storms approaching landfall, the coastal 88-D high-resolution radar data is also available.

To make use of these newly expanded observations, several advanced data assimilation techniques are being explored within the operational and research hurricane modeling communities, including EnKF and hybrid EnKF-4D-VAR approaches. The improvement of hurricane initialization has become a top priority in both the research and operational communities.

Enhancements to the HWRF modeling infrastructure include a much larger outer domain with multiple movable grids, and an eventual transition to NOAA's Environmental Modeling System (NEMS), which can provide a global-to-local scale modeling framework.

The initialization of the MPIPOM-TC ocean component (i.e. the feature-based model in the Atlantic and the GDEM climatology in the eastern North Pacific) may be replaced with HYCOM in the near future to be consistent with EMC's general ocean model development plan for all EMC coupled applications. The HYCOM has its own data assimilation system that includes assimilation of altimetry data and data from other remote-based and conventional *in situ* ocean data platforms. This system will also assimilate Airborne eXpendable BathyThermograph (AXBT) data obtained by NOAA's P-3s for selected storm scenarios over the GOM. Also, to include the dynamic feedback of surface waves on air-sea processes and the ocean, HWRF will be coupled to an advanced version of the NCEP wave model, the Wave Watch III (WW3). Further advancement of the WW3 to a multi-grid wave model (MWW3) will incorporate 2-way interactive grids at different resolutions. Eventually, this system will be fully coupled to a dynamic storm-surge model for more accurate prediction of storm surge and forecasts of waves on top of storm surge for advanced prediction of landfalling storms' impacts on coasts. Moreover, to address inland flooding and inundation associated with landfalling storms, HWRF will also be coupled to a comprehensive Land Surface Model (Noah LSM) to provide better precipitation forecasts for landfalling storms and to provide improved input for hydrology and inland inundation models.

Other advancements to the HWRF modeling system include advanced products tailored to serve Weather Forecast Offices (WFOs) along the coastal regions, enhanced model diagnostics capabilities, and high-resolution ensembles. Figure I.6 shows the fully coupled proposed operational hurricane system, with 2-way interaction between the atmosphere-land-ocean-wave models, providing feedback to high-resolution bay and estuary hydrodynamic models that predict storm-surge inundation.

Hurricane-Wave-Ocean-Surge-Inundation Coupled Models

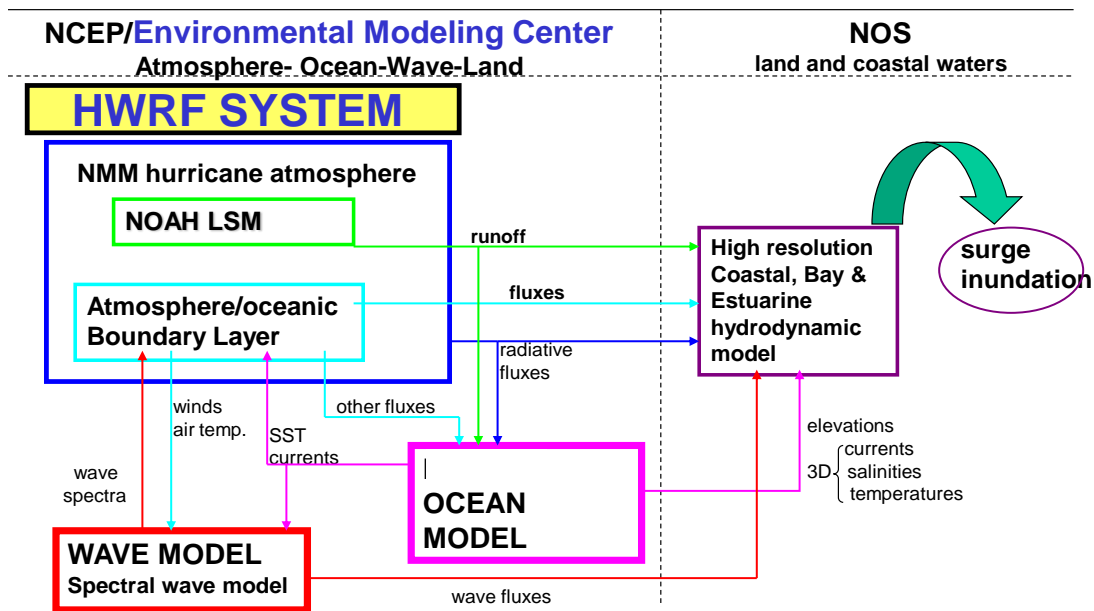


Figure I.6. Proposed future operational coupled hurricane forecast system. The left/right parts of the diagram refer to the responsibilities of the National Weather Service and National Ocean Service (NOS), respectively.

1.0 HWRF Initialization

1.1 Introduction

The 2014 operational initialization of hurricanes in the HWRF model involves several steps to prepare the analysis at various scales. The environmental fields in the parent domain are derived from the GFS analysis, and the fields in the nest domains are derived from 6-h forecast from GDAS, enhanced through the vortex relocation and HDAS. The vortex-scale fields are generated by inserting a vortex corrected using TC Vitals data, onto the large-scale fields. The vortex may originate from GDAS 6-h forecast, from the previous HWRF 6-h forecast, or from a bogus calculation, depending on the storm intensity and on the availability of a previous HWRF forecast. Additionally, vortex scale data assimilation is performed with conventional observations, satellite observations and NOAA P3 Tail Doppler Radar radial velocities (whenever available) assimilated in the TC vortex area and its near environment. Finally, the analyses are interpolated onto the HWRF outer domain and two inner domains to initialize the forecast.

The data assimilation systems for the GFS and for HWRF (GDAS and HDAS, respectively) follow similar procedures, but are run on different grids (global for GDAS and regional for HWRF). Both systems employ the community GSI, which is supported by the DTC.

The original design for the HWRF initialization (Liu et al. 2006a) was to continually cycle the HWRF large-scale fields and apply the vortex relocation technique (Liu et al. 2000, 2006b) at every model initialization time. However, the results were problematic. Large-scale flows can drift and the errors increased as cycles passed. To address this issue, the environmental fields from the GFS analysis are now used at every initialization time.

This section discusses the details of the atmospheric initialization, while the ocean initialization is described in Section 2.

1.2 HWRF cycling system

The location of the HWRF outer and inner domains algorithm is based on the observed hurricane's current and projected center position based on the NHC storm message. Therefore, if a storm is moving, the outer domain will not be in the same location for subsequent cycles.

Once the domains have been defined, the vortex replacement cycle and HDAS analysis are used to create the initial nest fields. If a previous 6-h HWRF forecast is available, and the observed intensity of the storm is greater than or equal to 14 ms^{-1} , the vortex is extracted from that forecast and corrected to be included in the current initialization. If the previous 6-hr HWRF forecast is not available, or the observed storm has a maximum wind speed of less than 14 ms^{-1} , the HDAS vortex is corrected using the vortex correction procedure and added to the current initialization.

The vortex correction process involves the following steps, partially represented in Figure 1.1.

1. Interpolate the GFS analysis fields onto the HWRF model parent grids (these data will be used in the final merge after HDAS analysis).
2. Interpolate the GDAS 6-h forecast onto the HWRF model parent grid, and interpolate this parent data onto nest grids and ghost grids. These ghost domains are created for inner-core data assimilation only, and have the same resolutions as the inner nests (0.06° and 0.02°). The domain size for ghost2 is $20^\circ \times 20^\circ$, and for ghost3 it's $10^\circ \times 10^\circ$.
3. Remove the vortex from the GDAS 6-h forecast. The remaining large-scale flow is termed the “environmental field.”
4. Determine which vortex will be added to the environmental fields (create a new $30^\circ \times 30^\circ$ dataset with 0.02° resolution). Check the availability of the HWRF 6-h forecast from the previous run (initialized 6 h before the current run) and the observed storm intensity.
 - a. If the forecast is not available:
 - i. if the observed storm maximum wind speed is greater than, or equal to, 20 ms^{-1} , use a bogus vortex; or
 - ii. if the observed maximum wind speed is less than 20 ms^{-1} , use a corrected GDAS 6-h forecast vortex.
 - b. If the forecast is available:
 - i. if the observed maximum wind speed is equal to or more than 14 ms^{-1} , extract the vortex from the forecast fields and correct it based on the TCVitals; or
 - ii. if the observed maximum wind speed is less than 14 ms^{-1} , use a corrected GDAS 6-h forecast vortex.
 - c. Interpolate the $30^\circ \times 30^\circ$ new data onto ghost2 and ghost3 domains.

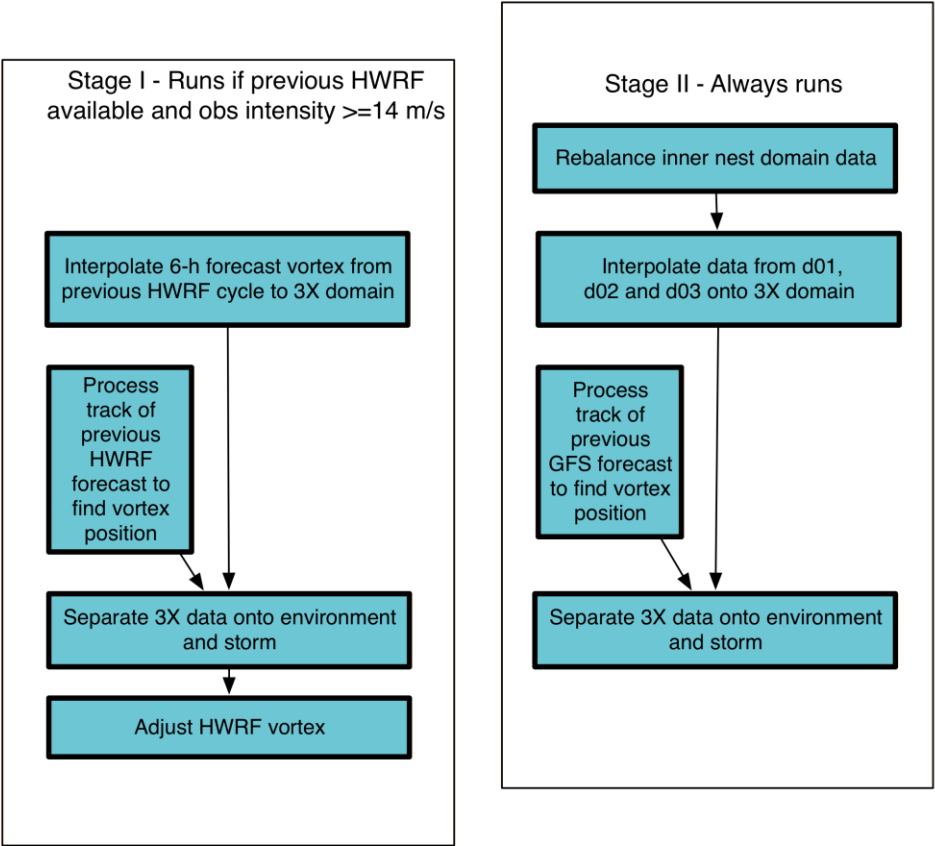
Note that, for each HWRF forecast, steps 2 and 3 are performed three times: 3 h before, 3 h after, and at the HWRF initialization time. These three time levels are necessary to support the GSI *define* (FGAT), as described later in this chapter.

5. Perform two one-way hybrid ensemble-3DVAR GSI analyses, using all observation data and the GFS 80-member ensemble background error

correlation, to create HDAS analysis fields for the HWRf ghost2 and ghost3 domains (see section 1.5).

- 6. Merge the data obtained from Step 5 onto the parent and nest domains.
- 7. Run the HWRf forecast model.

a) HWRf Vortex Initialization - Stages I and II



Stage I is used to split the previous HWRf forecast onto storm and environment so that the vortex can be adjusted and relocated. This is not done when the storm is very weak as it is best to use the GFS vortex in that case.

Stage II is used to split the global forecast to get the environment.

b) HWRF Vortex Initialization - Stage III - Always runs

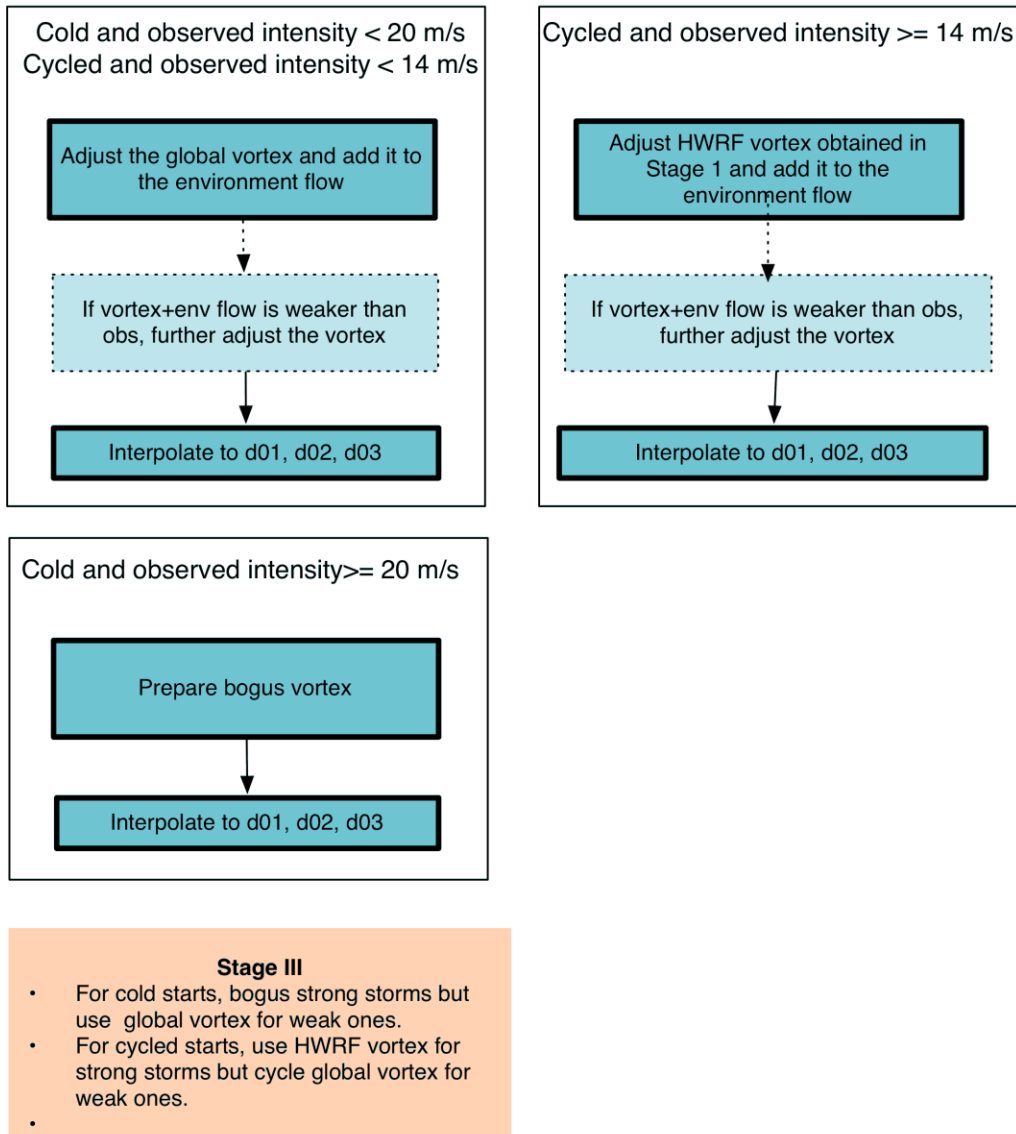


Figure 1.1. Simplified flow diagram for HWRF vortex initialization describing a) the split of the HWRF forecast between vortex and environment, b) the split of the background fields between vortex and analysis, and c) the insertion of the corrected vortex in the environmental field.

The vortex correction, as described in Section 1.4, adjusts its location, size, and structure based on the TCVitals:

- storm location (data used: storm center position);
- storm size (data used: radius of maximum surface wind speed, 34-kt wind radii, and radius of the outmost closed isobar); and
- storm intensity (data used: maximum surface wind speed and, secondarily, the minimum sea level pressure).

As noted above, a bogus vortex (described in Section 1.3) is only used in the initialization of strong storms (intensity greater than 20 ms^{-1}) when HWRF 6-h forecast is not available. Generally speaking, a bogus vortex does not produce the best intensity forecast. Also, cycling very weak storms (less than 14 ms^{-1}) without inner-core data assimilation often leads to large errors in intensity forecasts. To reduce the intensity forecast errors for cold starts and weak storms, the corrected GDAS 6-h forecast vortex is used in the 2014 operational HWRF. These changes improve the intensity forecast for the first several cycles, as well as for weak storms (less than 14 ms^{-1}).

1.3 Bogus vortex used to correct weak storms

The bogus vortex discussed here is primarily used to cold-start strong storms (observed intensity greater than or equal to 20 ms^{-1}) and to increase the storm intensity when the storm in the HWRF 6-h forecast is weaker than that of the observation (see Section 1.4.2). This is in contrast with previous HWRF implementations, in which a bogus vortex was used in all cold starts. This change significantly improves the intensity forecasts in the first 1-3 cycles of a storm.

The bogus vortex is created from a 2D axi-symmetric synthetic vortex generated from a past model forecast. The 2D vortex only needs to be recreated when the model physics has undergone changes that strongly affect the storm structure. We currently have two composite storms, one created in 2007 for strong deep storms, another one created in 2012 for shallow and medium depth storms.

For the creation of the 2D vortex, a forecast storm (over the ocean) with small size and near axi-symmetric structure is selected. The 3D storm is separated from its environment fields, and the 2D axi-symmetric part of the storm is calculated. The 2D vortex includes the hurricane perturbations of horizontal wind component, temperature, specific humidity, and sea-level pressure. This 2D axi-symmetric storm is used to create the bogus storm.

To create the bogus storm, the wind profile of the 2D vortex is smoothed until its RMW or maximum wind speed matches the observed values. Next, the storm size and intensity are corrected following a procedure similar to the cycled system.

The vortex in medium-depth and deep storms, receives identical treatment, while the vortex in shallow storms undergoes two final corrections: the vortex top is set to 400 hPa and the warm core structures are removed (this shallow storm correction is only for bogus storm, not for the cycled vortex).

1.4 Correction of vortex in previous 6-h HWRf or GDAS forecast

1.4.1 Storm size correction

Before starting to describe the storm size correction, some frequently used terms will be defined. Composite vortex refers to the 2D axi-symmetric storm, which is created once and used for all forecasts. The bogus vortex is created from the composite vortex by smoothing and performing size (and/or intensity) corrections. The background field, or guess field, is the output of the vortex initialization procedure, to which inner-core observations can be added through data assimilation. The environment field is defined as the HDAS analysis field after removing the vortex component.

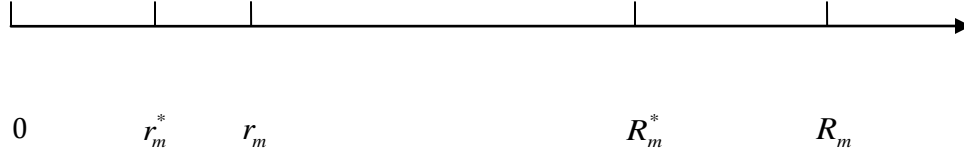
For hurricane data assimilation, we need a good background field. Storms in the background field (this background field can be the GFS analysis or, as in the operational HWRf, the previous 6-h forecast of GDAS) may be too large or too small, so the storm size needs to be corrected based on observations. We use two parameters, namely the radius of maximum winds and the radius of the outermost closed isobar to correct the storm size.

The storm size correction can be achieved by stretching/compressing the model grid. Let's consider a storm of the wrong size in cylindrical coordinates. Assume the grid size is linearly stretched along the radial direction

$$\alpha_i = \frac{\Delta r_i^*}{\Delta r_i} = a + b r_i, \quad (1.4.1.1)$$

where a and b are constants. r and r^* are the distances from the storm center before and after the model grid is stretched. Index i represents the i^{th} grid point.

Let r_m and R_m denote the radius of the maximum wind and radius of the outermost closed isobar (the minimum sea-level pressure is always scaled to the observed value before calculating this radius) for the storm in the background field, respectively. Let r_m^* and R_m^* be the observed radius of maximum wind and radius of the outermost closed isobar (which can be redefined if \square in Equation [1.4.1.1] is set to be a constant). If the high-resolution model is able to resolve the hurricane eyewall structure, r_m^*/r_m will be close to 1; therefore, we can set $b = 0$ in Equation (1.4.1.1) and $\alpha = r_m^*/r_m$ is a constant. However, if the model doesn't handle the eyewall structure well (r_m^*/r_m will be smaller than R_m^*/R_m) within the background fields, we need to use Equation (1.4.1.1) to stretch/compress the model grid.



Integrating Equation (1.4.1.1), we have

$$r^* = f(r) = \int_0^r \alpha(r) dr = \int_0^r (a + br) dr = ar + \frac{1}{2} br^2. \quad (1.4.1.2)$$

We compress/stretch the model grids such that

$$\text{At } r = r_m, \quad r^* = f(r_m) = r_m^* \quad (1.4.1.3)$$

$$\text{At } r = R_m, \quad r^* = f(R_m) = R_m^*. \quad (1.4.1.4)$$

Substituting (1.4.1.3) and (1.4.1.4) into (1.4.1.2), we have

$$ar_m + \frac{1}{2} br_m^2 = r_m^* \quad (1.4.1.5)$$

$$aR_m + \frac{1}{2} bR_m^2 = R_m^*. \quad (1.4.1.6)$$

Solving for a and b, we have

$$a = \frac{r_m^* R_m^2 - r_m^2 R_m^*}{R_m r_m (R_m - r_m)}, \quad b = 2 \frac{R_m^* r_m - R_m r_m^*}{R_m r_m (R_m - r_m)}. \quad (1.4.1.7)$$

Therefore,

$$r^* = f(r) = \frac{r_m^* R_m^2 - r_m^2 R_m^*}{R_m r_m (R_m - r_m)} r + \frac{R_m^* r_m - R_m r_m^*}{R_m r_m (R_m - r_m)} r^2 \quad (1.4.1.8)$$

One special case is α being constant, so that

$$\alpha = \alpha_m = \frac{r_m^*}{r_m} = \frac{R_m^*}{R_m} \quad (1.4.1.9)$$

where $b = 0$ in equation (1.4.1.1), and the storm size correction is based on one parameter only (this procedure was used in the initial implementation of the operational HWRF model in 2007).

To calculate the radius of the outmost closed isobar, it is necessary to scale the minimum surface pressure to the observed value as discussed below. A detailed discussion is given in the following. We define two functions, f_1 and f_2 , such that

for the 6-h HWRF or HDAS vortex (vortex #1),

$$f_1 = \frac{\Delta p_1}{\Delta p_{1c}} \Delta p_{obs} \quad (1.4.1.10)$$

and for composite storm (vortex #2),

$$f_2 = \frac{\Delta p_2}{\Delta p_{2c}} \Delta p_{obs} \quad (1.4.1.11)$$

where Δp_1 and Δp_2 are the 2D surface perturbation pressures for vortices #1 and #2, respectively. Δp_{1c} and Δp_{2c} are the minimum values of Δp_1 and Δp_2 , while Δp_{obs} is the observed minimum perturbation pressure.

The radius of the outmost closed isobar for vortices #1 and #2 can be defined as the radius of the 1 hPa contour from f_1 and f_2 , respectively.

We can show that after the storm size correction for vortices #1 and #2, the radius of the outmost closed isobar is unchanged for any combination of the vortices #1 and #2. For example (c is a constant),

$$\Delta p_1 + c\Delta p_2 = \frac{\Delta p_1}{\Delta p_{1c}} \Delta p_{1c} + c \frac{\Delta p_2}{\Delta p_{2c}} \Delta p_{2c}$$

At the radius of the 1-hPa contour, we have $f_1=1$ and $f_2=1$, or

$$\frac{\Delta p_1}{\Delta p_{1c}} = \frac{\Delta p_2}{\Delta p_{2c}} = \frac{1}{\Delta p_{obs}}$$

so,

$$\Delta p_1 + c\Delta p_2 = \frac{\Delta p_1}{\Delta p_{1c}} \Delta p_{1c} + c \frac{\Delta p_2}{\Delta p_{2c}} \Delta p_{2c} = \frac{1}{\Delta p_{obs}} (\Delta p_{1c} + c\Delta p_{2c}) = 1$$

where we have used

$$(\Delta p_{1c} + c\Delta p_{2c}) = \Delta p_{obs}. \quad (1.4.1.12)$$

Similarly, to calculate the radius of 34-kt winds, we need to scale the maximum wind speed for vortices #1 and #2. We define two functions, g_1 and g_2 , such that for the 6-h HWRf or GDAS vortex (vortex #1),

$$g_1 = \frac{v_1}{v_{1m}}(v_{obs} - \bar{v}_m) ; \quad (1.4.1.13)$$

for the composite storm (vortex #2),

$$g_2 = \frac{v_2}{v_{2m}}(v_{obs} - \bar{v}_m) ; \quad (1.4.1.14)$$

where v_{1m} and v_{2m} are the maximum wind speed for vortices #1 and #2, respectively, and $(v_{obs} - \bar{v}_m)$ is the observed maximum wind speed minus the environment wind. The environment wind is defined as

$$\bar{v}_m = \max(0, U_{1m} - v_{1m}), \quad (1.4.1.15)$$

where U_{1m} is the maximum wind speed at the 6-h forecast.

The radius of 34-kt wind for vortices #1 and #2 are calculated by setting both g_1 and g_2 to be 34 kt.

After the storm size correction, the combination of vortices #1 and #2 can be written as

$$v_1 + \beta v_2 = \frac{v_1}{v_{1m}} v_{1m} + \beta \frac{v_2}{v_{2m}} v_{2m} .$$

At the 34-kt radius, we have ($g_1=34, g_2=34$)

$$v_1 + \beta v_2 = \frac{v_1}{v_{1m}} v_{1m} + \beta \frac{v_2}{v_{2m}} v_{2m} = \frac{34}{v_{obs} - \bar{v}_m} (v_{1m} + \beta v_{2m}) = 34 .$$

Note we have used,

$$(v_{1m} + \beta v_{2m}) + \bar{v}_m = v_{obs} . \quad (1.4.1.16)$$

In the 2010 operational HWRf initialization, only one parameter (radius of the maximum wind) was used in the storm size correction. The radius of the outermost closed isobar was calculated, but never used. Since the 2011 upgrade, a second parameter (radius of the

outermost closed isobar or radius of the average 34-kt wind for hurricanes) was added by Kevin Yeh (HRD). Specifically, in the 2010 HWRF initialization, Equation (1.4.1.12) was used for storm size correction, and b was set to zero in Equation (1.4.1.1). In the new operational models, a and b are calculated using Equation (1.4.1.7).

Storm size correction can be problematic. The reason is that the eyewall size produced in the model can be larger than the observed one, and the model does not support observed small-size eyewalls. For example, the radius of maximum winds for 2005's Hurricane Wilma was 9 km at 140 kt for several cycles. The model-produced radius of maximum wind was larger than 20 km. If we compress the radius of maximum winds to 9 km, the eyewall will collapse and significant spin-down will occur. So the minimum value for storm eyewall is currently set to 19 km. The eyewall size in the model is related to model resolution, model dynamics, and model physics.

In the storm size correction procedure, we do not match the observed radius of maximum winds. Instead, we replace r_m^* as the average between the model value and the observation. We also limit the correction to be 15% of the model value. In the 2013 version, the limit is set as follows (the settings are the same as those in the 2012 version): 10% if r_m^* is smaller than 20 km; 10-15% if r_m^* is between 20 and 40km; and 15% if r_m^* is larger than 40 km. For the radius of the outermost closed isobar (or average 34-kt wind if storm intensity is larger than 64 kt), the correction limit is set to 15% of the model value.

Even with the current settings, major spin-down may occur if the eyewall size is small and lasts for many cycles (due to the consecutive reduction of the storm eyewall size in the initialization). To fix this problem, size reduction is stopped if the model storm size (measured by the average radius of the filter domain) is smaller than the radius of the outermost closed isobar.

1.4.1.1 Surface pressure adjustment after the storm size correction

In our approximation, we only correct the surface pressure of the axi-symmetric part of the storm. The governing equation for the axi-symmetric components along the radial direction is

$$\frac{\partial u}{\partial t} + u \frac{\partial u}{\partial r} + w \frac{\partial u}{\partial z} - v \left(\frac{v}{r} + f_0 \right) + \frac{1}{\rho} \frac{\partial p}{\partial r} = F_r \quad (1.4.1.1.1)$$

where u , v and w are the radial, tangential, and vertical velocity components, respectively.

F_r is friction and $F_r \approx -C_d \frac{u}{H_B} v$ where H_B is the top of the boundary layer. F_r can be

estimated as $F_r \approx -10^{-6} v$ away from the storm center, and $F_r \approx -10^{-5} v$ near the storm center. Dropping the small terms, Equation (1.4.1.1.1) is close to the gradient wind balance.

Because we separate the hurricane component from its environment, the contribution from the environment flow to the average tangential wind speed can be neglected. From now on, the tangential velocity we discussed refers to the vortex component.

We define the gradient wind stream function ψ as

$$\frac{\partial \psi}{\partial r} = \frac{v^2}{rf_0} + v \quad (1.4.1.1.2)$$

and

$$\psi = \int_{\infty}^r \left(\frac{v^2}{rf_0} + v \right) dr. \quad (1.4.1.1.3)$$

Due to the coordinate change, Equation (1.4.1.1.2) can be rewritten as the following,

$$\frac{\partial \psi}{\partial r} = \frac{\partial \psi}{\partial r^*} \frac{\partial r^*}{\partial r} = \alpha \frac{\partial \psi}{\partial r^*}$$

$$\frac{v^2}{rf_0} + v = \frac{v^2}{r^*} \frac{r^*}{rf_0} + v = \frac{v^2}{r^*} \frac{f(r)}{rf_0} + v \quad (r = r(r^*)).$$

Therefore, the gradient wind stream function becomes (due to the coordinate transformation)

$$\psi = \int_{\infty}^{r^*} \frac{1}{\alpha(r^*)} \left[\frac{v^2}{r^*} \frac{f(r^*)}{r(r^*)f_0} + v(r^*) \right] dr^*. \quad (1.4.1.1.4)$$

We can also define a new gradient wind stream function for the new vortex as

$$\frac{\partial \psi^*}{\partial r^*} = \frac{v^2}{r^* f_0} + v, \quad (1.4.1.1.5)$$

where v is a function of r^* . Therefore,

$$\psi^* = \int_{\infty}^{r^*} \left(\frac{v^2}{r^* f_0} + v \right) dr^*. \quad (1.4.1.1.6)$$

Assuming the hurricane sea-level pressure component is proportional to the gradient wind stream function at the top of the boundary layer (roughly 850mb level), i.e.,

$$\Delta p(r^*) = c(r^*) \psi(r^*) \quad (1.4.1.1.7)$$

and

$$\Delta p^*(r^*) = c(r^*)\psi^*(r^*), \quad (1.4.1.1.8)$$

where $c(r^*)$ is a function of r^* and represents the impact of friction on the gradient wind balance. If friction is neglected, $c(r^*) = 1.0$, we have gradient wind balance.

From equations (1.4.1.1.7) and (1.4.1.1.8), we have

$$\Delta p^* = \Delta p \frac{\psi^*}{\psi}, \quad (1.4.1.1.9)$$

where $\Delta p = p_s - p_e$ and $\Delta p^* = p_s^* - p_e$ are the hurricane sea-level pressure perturbations before and after the adjustment, and p_e is the environment sea-level pressure.

Note that the pressure adjustment is minor due to the grid stretching. For example, if in Equation (1.4.1.1) α is a constant, we can show that Equation (1.4.1.1.4) becomes

$$\psi = \int_{\infty}^{r^*} \left(\frac{v^2}{r^* f_0} + \frac{1}{\alpha} v \right) dr^*. \quad (1.4.1.1.10)$$

This value is very close to that of Equation (1.4.1.1.6) since the first term dominates.

1.4.1.2 Temperature adjustment

Once the surface pressure is corrected, we need to correct the temperature field.

Let's consider the vertical equation of motion. Neglecting the Coriolis, water load, and viscous terms, we have,

$$\frac{dw}{dt} = -\frac{1}{\rho} \frac{\partial p}{\partial z} - g. \quad (1.4.1.2.1)$$

The first term on the right-hand side is the pressure gradient force, and g is gravity. dw/dt is the total derivative (or Lagrangian air-parcel acceleration) which, in the large-scale environment, is small when compared to either of the last two terms. Therefore, we have,

$$-\frac{1}{\rho} \frac{\partial p}{\partial z} - g = 0$$

or

$$\frac{\partial p}{\partial z} = -\frac{p}{RT_v} g \quad (1.4.1.2.2)$$

Applying equation (1.4.1.2.2) to the environmental field and integrating from surface to model top, we get:

$$\ln \frac{p_s}{p_T} = \frac{g}{R} \int_0^H \frac{dz}{\bar{T}_v} \quad (1.4.1.2.3)$$

where H and p_T are the height and pressure at the model top, respectively. \bar{T}_v is the virtual temperature of the environment.

The hydrostatic equation for the total field (environment field + vortex) is

$$\ln \frac{p_s + \Delta p}{p_T} = \frac{g}{R} \int_0^H \frac{dz}{(\bar{T}_v + \Delta T_v)}, \quad (1.4.1.2.4)$$

where Δp and ΔT_v are the sea-level pressure and virtual temperature perturbations for the hurricane vortex. Since $\Delta p \ll p_s$ and $\Delta T_v \ll \bar{T}_v$, we can linearize Equation (1.4.1.2.4)

$$\ln \frac{p_s}{p_T} \left(1 + \frac{\Delta p}{p_s}\right) = \frac{g}{R} \int_0^H \frac{dz}{(\bar{T}_v + \Delta T_v)} \approx \frac{g}{R} \int_0^H \frac{dz}{\bar{T}_v} \left(1 - \frac{\Delta T_v}{\bar{T}_v}\right). \quad (1.4.1.2.5)$$

Subtract Equation (1.4.1.2.3) from Equation (1.4.1.2.5) and we have

$$\ln \left(1 + \frac{\Delta p}{p_s}\right) \approx -\frac{g}{R} \int_0^H \frac{\Delta T_v}{\bar{T}_v^2} dz,$$

or

$$\frac{\Delta p}{p_s} \approx -\frac{g}{R} \int_0^H \frac{\Delta T_v}{\bar{T}_v^2} dz. \quad (1.4.1.2.6)$$

Multiplying Equation (1.4.1.2.6) by $\Gamma(r^*) = \psi^* / \psi$ (Γ is a function of x and y only), we have

$$\frac{\Gamma \Delta p}{p_s} \approx -\frac{g}{R} \int_0^H \frac{\Gamma \Delta T_v}{\bar{T}_v^2} dz. \quad (1.4.1.2.7)$$

We choose a simple solution to equation (1.4.1.2.7), i.e., the virtual temperature correction is proportional to the magnitude of the virtual temperature perturbation. So the new virtual temperature is

$$T_v^* = \bar{T}_v + \Gamma \Delta T_v = T_v + (\Gamma - 1) \Delta T_v \quad (1.4.1.2.8)$$

In terms of the temperature field, we have

$$T^* = \bar{T} + \Gamma \Delta T = T + (\Gamma - 1) \Delta T \quad (1.4.1.2.9)$$

where T is the 3D temperature before the surface-pressure correction, and ΔT is perturbation temperature for vortex #1.

1.4.1.3 Water vapor adjustment

Assume the relative humidity is unchanged before and after the temperature correction, i.e.,

$$RH = \frac{e}{e_s(T)} \approx \frac{e^*}{e_s(T^*)} \quad (1.4.1.3.1)$$

where e and $e_s(T)$ are the vapor pressure and the saturation vapor pressure in the model guess fields, respectively. e^* and $e_s(T^*)$ are the vapor pressure and the saturation vapor pressure respectively, after the temperature adjustment.

Using the definition of the mixing ratio,

$$q = 0.622 \frac{e}{p - e} \quad (1.4.1.3.2)$$

at the same pressure level and from Equation (1.4.1.3.1)

$$\frac{q^*}{q} \gg \frac{e^*}{e} \gg \frac{e_s(T^*)}{e_s(T)}. \quad (1.4.1.3.3)$$

Therefore, the new mixing ratio becomes

$$q^* \approx \frac{e^*}{e} q \approx \frac{e_s^*}{e_s} q \approx q + \left(\frac{e_s^*}{e_s} - 1 \right) q. \quad (1.4.1.3.4)$$

From the saturation water pressure

$$e_s(T) = 6.112 \exp \left[7.67 \frac{(T - 273.16)}{(T - 29.66)} \right] \quad (1.4.1.3.5)$$

we can write

$$\frac{e_s^*}{e_s} = \exp \left[\frac{17.67 * 2435 (T^* - T)}{(T^* - 29.66)(T - 29.66)} \right]. \quad (1.4.1.3.6)$$

Substituting Equation (1.4.1.3.6) into (1.4.1.3.4), we have the new mixing ratio after the temperature field is adjusted.

1.4.2 Storm intensity correction

Generally speaking, the storm in the background field has a different maximum wind speed compared to the observations. We need to correct the storm intensity based on the observations, which is discussed in detail in the following sections.

1.4.2.1 Computation of intensity correction factor β

Let's consider the general formulation in the traditional x, y, and z coordinates; where u_1^* and v_1^* are the background horizontal velocity, and u_2 and v_2 are the vortex horizontal velocity to be added to the background fields. We define

$$F_1 = \sqrt{(u_1^* + u_2)^2 + (v_1^* + v_2)^2} \quad (1.4.2.1.1)$$

and

$$F_2 = \sqrt{(u_1^* + \beta u_2)^2 + (v_1^* + \beta v_2)^2} . \quad (1.4.2.1.2)$$

Function F_1 is the wind speed if we simply add a vortex to the environment (or background fields). Function F_2 is the new wind speed after the intensity correction.

We consider two cases here.

Case I: F_1 is larger than the observational maximum wind speed. We set u_1^* and v_1^* to be the environment wind component; i.e., $u_1^* = U$ and $v_1^* = V$ (the vortex is removed and the field is relatively smooth); and $u_2 = u_1$ and $v_2 = v_1$ are the vortex horizontal wind components from the previous cycle's 6-h forecast (we call it vortex #1, which contains both the axi-symmetric and asymmetric parts of the vortex).

Case II: F_1 is smaller than the observational maximum wind speed. We add the vortex back into the environment fields after the grid stretching, i.e., $u_1^* = U + u_1$ and $v_1^* = V + v_1$. We choose u_2 and v_2 to be an axi-symmetric composite vortex (vortex #2) which has the same radius of maximum wind as that of the first vortex.

In both cases, we can assume that the maximum wind speed for F_1 and F_2 are at the same model grid point. To find β , we first locate the model grid point where F_1 is at its maximum. Let's denote the wind components at this model grid point as u_1^m , v_1^m , u_2^m , and v_2^m (for convenience, we drop the superscript m), so that

$$(u_1^* + \beta u_2)^2 + (v_1^* + \beta v_2)^2 = v_{obs}^2 \quad (1.4.2.1.3)$$

where v_{obs} is the 10-m observed wind converted to the first model level.

Solving for β , we have

$$\beta = \frac{-u_1^* u_2 - v_1^* v_2 + \sqrt{v_{obs}^2 (u_2^2 + v_2^2) - (u_1^* v_2 - v_1^* u_2)^2}}{(u_2^2 + v_2^2)}. \quad (1.4.2.1.4)$$

The procedure to correct wind speed is as follows.

First, we calculate the maximum wind speed from Equation (1.4.2.1.1) by adding the vortex into the environment fields. If the maximum of F_1 is larger than the observed wind speed, we classify it as Case I and calculate the value of β . If the maximum of F_1 is smaller than the observed wind speed, we classify it as Case II. The reason we classify it as Case II is that we don't want to amplify the asymmetric part of the storm. Amplifying it may negatively affect the track forecasts. In Case II, we first add the original vortex to the environment fields after the storm size correction, then add a small portion of an axisymmetric composite storm. The composite storm portion is calculated from Equation (1.4.2.1.4). Finally, the new vortex 3D wind field becomes

$$u(x, y, z) = u_1^*(x, y, z) + \beta u_2(x, y, z)$$

$$v(x, y, z) = v_1^*(x, y, z) + \beta v_2(x, y, z).$$

1.4.2.2 Surface pressure, temperature, and moisture adjustments after the intensity correction

If the background fields are produced by high-resolution models (such as in HWRF), the intensity corrections are minor and the correction of the storm structure is not necessary. The guess fields should be close to the observations; therefore, we have

In Case I β is close to 1;

In Case II β is close to 0.

After the wind-speed correction, we need to adjust the sea-level pressure, 3D temperature, and the water vapor fields. These adjustments are described below.

In Case I, β is close to 1. Following the discussion in Section.1.4.1.1, we define the gradient wind stream function ψ as

$$\frac{\partial \psi}{\partial r} = \frac{v_2}{rf_0} + v_2 \quad (1.4.2.2.1)$$

and

$$\psi_2 = \int_{\infty}^r \left(\frac{v_2^2}{rf_0} + v_2 \right) dr. \quad (1.4.2.2.2)$$

The new gradient wind stream function is

$$\psi^{new} = \int_{\infty}^r \left[\frac{(\beta v_2)^2}{rf_0} + \beta v_2 \right] dr. \quad (1.4.2.2.3)$$

The new sea-level pressure perturbation is

$$\Delta p^{new} = \Delta p \frac{\psi^{new}}{\psi_2} \quad (1.4.2.2.4)$$

where $\Delta p = p_s - p_e$ and $\Delta p^{new} = p_s^{new} - p_e$ are the hurricane sea-level pressure perturbations before and after the adjustment and p_e is the environment sea-level pressure.

In Case II, β is close to 0. Let's define

$$\psi_1 = \int_{\infty}^r \left(\frac{v_1^2}{rf_0} + v_1 \right) dr, \quad (1.4.2.2.5)$$

and the new gradient wind stream function is

$$\psi^{new} = \int_{\infty}^r \left[\frac{(v_1 + \beta v_2)^2}{rf_0} + (v_1 + \beta v_2) \right] dr. \quad (1.4.2.2.6)$$

And the new sea-level pressure perturbation is calculated as,

$$\Delta p^{new} = \Delta p \frac{\psi^{new}}{\psi_1}. \quad (1.4.2.2.7)$$

Equations (1.4.2.2.4) and (1.4.2.2.7) are supposed to be close to the observed surface pressure. However, if the model has an incorrect surface pressure-wind relationship, Equations (1.4.2.2.4) and (1.4.2.2.7) may have a large surface pressure difference from the observation. In 2013 HWRF, the pressure-wind relationship is further improved, and we can set the limit to be 10% off the observation Δp_{obs} without producing large spin up/spin down problems.

The correction of the temperature field is as follows,

In Case I, we define

$$\Gamma = \frac{\psi^{new}}{\psi_2}. \quad (1.4.2.2.8)$$

Then we use the following equation to correct the temperature fields.

$$T^* = T_e + \Gamma \Delta T_1 = T + (\Gamma - 1) \Delta T_1 \quad (1.4.2.2.9)$$

In Case II, we define

$$\Gamma = \frac{\psi^{new}}{\psi_1} \quad (1.4.2.2.10)$$

and

$$T^* = T_e + \Delta T_1 + (\Gamma - 1) \Delta T_2 = T + (\Gamma - 1) \Delta T_2, \quad (1.4.2.2.11)$$

where T is the 3D background temperature field (environment+vortex1), and ΔT_2 is the temperature perturbation of the axi-symmetric composite vortex.

The corrections of water vapor in both cases are the same as those discussed in Section 1.4.1.3.

We would like to mention that the storm intensity correction is, in fact, a data analysis. The observation data used here is the surface maximum wind speed (single point data), and the background error correlations are flow dependent and based on the storm structure. The storm structure used for the background error correlation is vortex #1 in Case I, and vortex #2 in Case II (except for water vapor which still uses the vortex #1 structure). Vortex #2 is an axi-symmetric vortex. If the storm structure in vortex #1 could be trusted, one could choose vortex #2 as the axi-symmetric part of vortex #1. In HWRF, the structure of vortex #1 is not completely trusted when the background storm is weak, and therefore an axi-symmetric composite vortex from old model forecasts is employed as vortex #2.

1.5 Data assimilation through GSI in HWRF

The major upgrade of data assimilation for 2014 operational HWRF is the assimilation of satellite observations into HWRF. The model and data assimilation configurations have been changed to facilitate the assimilation of satellite radiance observations. The capability of using global-regional blended coordinates in GSI analysis has been developed to address issues associated with satellite radiance data assimilation for regional models such as HWRF.

Before 2014 upgrade, the model top of HWRF was set to be 50 hPa, which is too low to allow upper-level microwave and infrared channels to be assimilated into HWRF. The model top has been raised to 2 hPa with the vertical levels increasing from 43 to 61 levels

for 2014 implementation. However, 2 hPa is still not sufficient for some high peaking channels.

In order to properly assimilate satellite radiance observations, biases between the observed radiances and those simulated from the model first guess must be corrected. The biases could be from systematic errors in the data (e.g. due to pool calibration), inadequacies in the observation operator (e.g. interpolation or radiative transfer errors), or biases in the forecast model (Derber and Wu 1998; McNally et al. 2000; Harris and Kelly 2001). In GSI, the coefficients of the chosen bias predictors are treated as additional control variables estimated simultaneously with the rest of the analysis variables (Derber and Wu 1998, McNally et al. 2000). However, HWRF is only run for tropical cyclones. The short cycling period and variable sample size due to movable forecast domains make the spin up of bias correction problematic. An alternative is to use bias correction coefficients estimated from the GDAS. However, direct utilization of global bias correction coefficients in regional analysis may not be appropriate, because the vertical coordinates and the radiance data assimilated, which directly affect the result of bias correction, are different.

A solution is to use a global-regional blended vertical coordinate in GSI analysis. The GFS and HWRF model levels are blended together in the stratosphere, changing smoothly from HWRF coordinate to GFS coordinate. With the blended coordinate, the vertical resolution in the stratosphere is increased and the model top is further extended to 0.26 hPa with vertical levels increased to 76 levels. The GDAS forecast valid at the same time is added in the additional levels as the first guess. Using the blended vertical coordinate significantly improved the data usage and model fit to observation for both microwave (MW) and infrared (IR) instruments.

HWRF does not provide ozone profiles, which are used in the radiative transfer calculation, to obtain simulated brightness temperature. The lack of ozone profiles can lead to biased analyses, especially for IR instruments. To mitigate this deficiency, the ozone profiles from the GDAS forecast are used in HWRF analysis. Using global ozone profiles greatly improved the data coverage and model fit to observation across the entire IR spectrum.

Using the global and regional (HWRF) blended coordinate in analysis along with the use of the global ozone profile improved the assimilation of satellite radiance data into HWRF. On the other hand, this significantly increased the computational resource requirement because not only are the vertical levels of the analysis grid increased by 15 levels, the 80-member ensemble has to be interpolated to the new analysis grid for hybrid analysis, which requires high memory usage. This makes the analysis of the original ghost domain ($20^{\circ} \times 20^{\circ}$, 0.02° horizontal resolution) especially hard to fit into the computational resource and running-time limit of the operational HWRF. Therefore, the data assimilation domains have to be reconfigured. It has been found through repeated experiments that regional analysis at the same resolution barely shows any benefit over

global analysis for large-scale TC environment. Therefore, we chose not to perform data assimilation on HWRF outer domain ($75^{\circ} \times 75^{\circ}$, 0.18° horizontal resolution). Instead, the GFS analysis is directly interpolated to the outer domain. This helps us focus on vortex scale analysis. Data assimilation is now performed on two new ghost domains – ghost d02 ($20^{\circ} \times 20^{\circ}$, 0.06° horizontal resolution) and ghost d03 ($10^{\circ} \times 10^{\circ}$, 0.02° horizontal resolution). Ghost d02 can cover the entire storm and its near environment. Ghost d03 is specifically used to assimilate high-resolution aircraft reconnaissance observations. The new data assimilation domains as well as the model forecast domains are shown in Fig. 1.2.

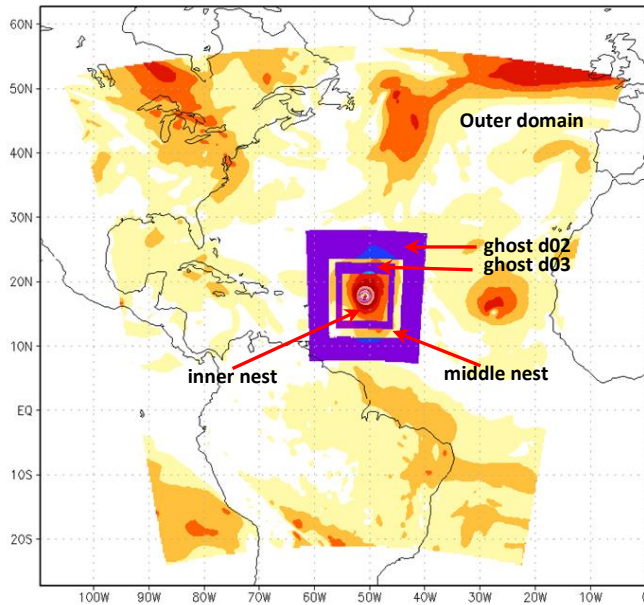


Figure 1.2. HWRF data assimilation and model forecast domains.

The hybrid ensemble-variational data assimilation scheme continues to be used in 2014 HWRF. The background error covariance of the hybrid scheme is a combination of the static background error covariance obtained through the National Meteorological Center (now NCEP) method and the flow-dependent background error covariance estimated from the short term ensemble forecast. The hybrid method provides better analysis compared to stand-alone ensemble-based method (e.g. Ensemble Kalman filter, EnKF), especially when the ensemble size is small or large model error is present (Wang et al. 2007b).

In GSI, the ensemble covariance is incorporated into the variational scheme through the extended control variable method (Lorenz 2003; Buehner 2005). The following description of the algorithm follows Wang (2010).

The analysis increment, denoted as \mathbf{x}' , is a sum of two terms:

$$\mathbf{x}' = \mathbf{x}'_1 + \sum_{k=1}^K (\boldsymbol{\alpha}_k \cdot \mathbf{x}_k^e), \quad (1.5.1)$$

where \mathbf{x}'_1 is the increment associated with the GSI static background covariance and the second term is the increment associated with the flow-dependent ensemble covariance. In the second term \mathbf{x}_k^e is the k^{th} ensemble perturbation normalized by $(K - 1)^{1/2}$, where K is the ensemble size. The vector $\boldsymbol{\alpha}_k, k = 1, \dots, K$, contains the extended control variables for each ensemble member. The second term represents a local linear combination of ensemble perturbations, and $\boldsymbol{\alpha}_k$ is the weight applied to the k^{th} ensemble perturbation.

The cost function minimized to obtain \mathbf{x}' is

$$J(\mathbf{x}'_1, \boldsymbol{\alpha}) = \beta_1 (\mathbf{x}'_1)^T \mathbf{B}_1^{-1} (\mathbf{x}'_1) + \beta_2 (\boldsymbol{\alpha})^T \mathbf{A}^{-1} (\boldsymbol{\alpha}) + (\mathbf{y}^{o'} - \mathbf{H}\mathbf{x}')^T \mathbf{R}^{-1} (\mathbf{y}^{o'} - \mathbf{H}\mathbf{x}') + J_c, \quad (1.5.2)$$

where

\mathbf{B}_1 is the static background error covariance matrix;

β_1 is the weight applied to the static background error covariance;

\mathbf{A} defines the spatial correlation of $\boldsymbol{\alpha}$;

β_2 is the weight applied to the ensemble covariance;

\mathbf{y} is the innovation vector;

\mathbf{R} is the observational and representativeness error covariance matrix;

\mathbf{H} is the observation operator; and

J_c is the constraint term.

Wang (2007a) proved the equivalence of using (1.5.1) and (1.5.2) to find the solution to that, with the ensemble covariance explicitly included as part of the background covariance. It is also shown in this paper that matrix \mathbf{A} determines the covariance localization on the ensemble covariance.

The same conjugate gradient minimization algorithm used for the 3DVAR scheme is used to find the optimal solution for the analysis problem (1.5.1.) and (1.5.2), except the control variable and the background covariance are extended as

$$\mathbf{x} = \begin{pmatrix} \mathbf{x}'_1 \\ \boldsymbol{\alpha} \end{pmatrix}, \quad (1.5.3)$$

and

$$\mathbf{B} = \begin{pmatrix} \frac{1}{\beta_1} \mathbf{B}_1 & \mathbf{0} \\ \mathbf{0} & \frac{1}{\beta_2} \mathbf{A} \end{pmatrix}. \quad (1.5.4)$$

More information about the hybrid algorithm can be found in Wang (2010). The iteration algorithm can be found in the [GSI User's Guide](#) Chapter 6, Section 6.1. Two outer loops with 50 iterations each are used for HWRF (miter=2, niter[1]=50, niter[2]=50). The outer loop consists of more complete (nonlinear) observation operators and quality control. Usually, simpler observation operators are used in the inner loop. The nonlinear variational quality control, which is part of the inner loop, is turned on for HWRF (niter_no_qc[1]=20).

The analysis variables are: streamfunction, unbalanced part of velocity potential, unbalanced part of temperature, unbalanced part of surface pressure, pseudo-relative humidity (qoption = 1) or normalized relative humidity (qoption = 2), surface skin temperature (sea-surface temperature, skin temperature over land, skin temperature over ice), and the extended control variable α . The definition of the normalized relative humidity allows for a multivariate coupling of the moisture, temperature, and pressure increments, as well as flow dependence (Kleist et al. 2009). Therefore this option is used for HWRF. The accurate specification of the surface-skin temperature can be extremely important in the estimation of the simulated brightness temperature (Derber and Wu 1998). Therefore, it is included as an analysis variable, but is not introduced into the forecast model (Derber and Wu 1998). Ozone and cloud variables are not analyzed. Since global bias correction coefficients are directly used in HWRF analysis, the bias correction coefficients are not updated through analysis (upd_pred=0).

The 2014 HWRF data assimilation system is still a one-way hybrid system, because it does not include a HWRF ensemble forecast and the associated EnKF analysis components.. It uses the global hybrid EnKF/Var system run at T254L64 to provide ensemble perturbations (Fig. 1.3). The HWRF hybrid analysis does not feed back to the updated ensemble perturbations through EnKF, as is the case with the global hybrid system. The first guesses of the HWRF hybrid analysis at each analysis time are the global GDAS 3, 6 and 9-hr forecasts at T574L64 plus the relocated, size and, intensity corrected vortexes from HWRF or GDAS (see section 1.4) 3, 6 and 9-hr forecasts. First Guess at Appropriate Time (FGAT) is used to allow data within 6 hours (minus 3 hours to plus 3 hours) time window be better assimilated. In traditional 3DVAR data assimilation schemes, observations are assumed to be valid at the analysis time. With FGAT, observations are compared with the first guess at the observation time to obtain the innovation. The first guess at observation time is obtained by interpolating the two closest time levels of background fields within GSI. Therefore multiple time levels of first guesses, here 3, 6 and 9-hour forecasts, are required.

For the HWRF hybrid analysis, 6-hour forecasts of the GFS 80-member ensemble are used to provide ensemble covariance. For both ghost d02 and ghost d03 domains, β_1^{-1} (beta1_inv in GSI namelist) is set to 0.2, which means 80% of the weight is placed on the ensemble covariance.

As mentioned earlier, matrix \mathbf{A} in (1.5.2) effectively conducts the covariance localization on the ensemble covariance. In GSI, a recursive filter is used to approximate the static background error covariance \mathbf{B}_1 , as well as \mathbf{A} . The correlation length scale of the recursive filter used to approximate \mathbf{A} , prescribes the covariance localization length scale for ensemble covariance. The parameters in the GSI namelist that define the horizontal and vertical localization length scales refer to the recursive filter e-folding length scale. In most EnKF applications, the correlation function given by Eq. (4.10) of Gaspari and Cohn (1999) is used for covariance localization. The Gaspari-Cohn type of localization length scale refers to the distance at which the covariance is forced to be zero, which is roughly equivalent to the e-folding length scale divided by 0.388. For the ghost d02/d03 domain analysis, the horizontal localization length scale is set to 300/150 km ($s_{ens_h}=300/150$). The vertical localization length scales for both analysis domains are set to be 0.5 in units of $\ln p$ ($s_{ens_v}=-0.5$), where p is the pressure in units of cb. Note that if the vertical localization length scale is measured in units of $\ln p$, s_{ens_v} is expressed as a negative value and the length scale is the absolute value of s_{ens_v} .

When using GSI with HWRF, 'wrf_nmm_regional' and 'uv_hyb_ens' in the GSI namelist should be set to "true." The use of "uv_hyb_ens=.true." means that ensemble perturbations contain the zonal and meridional components of the wind instead of stream function and velocity potential.

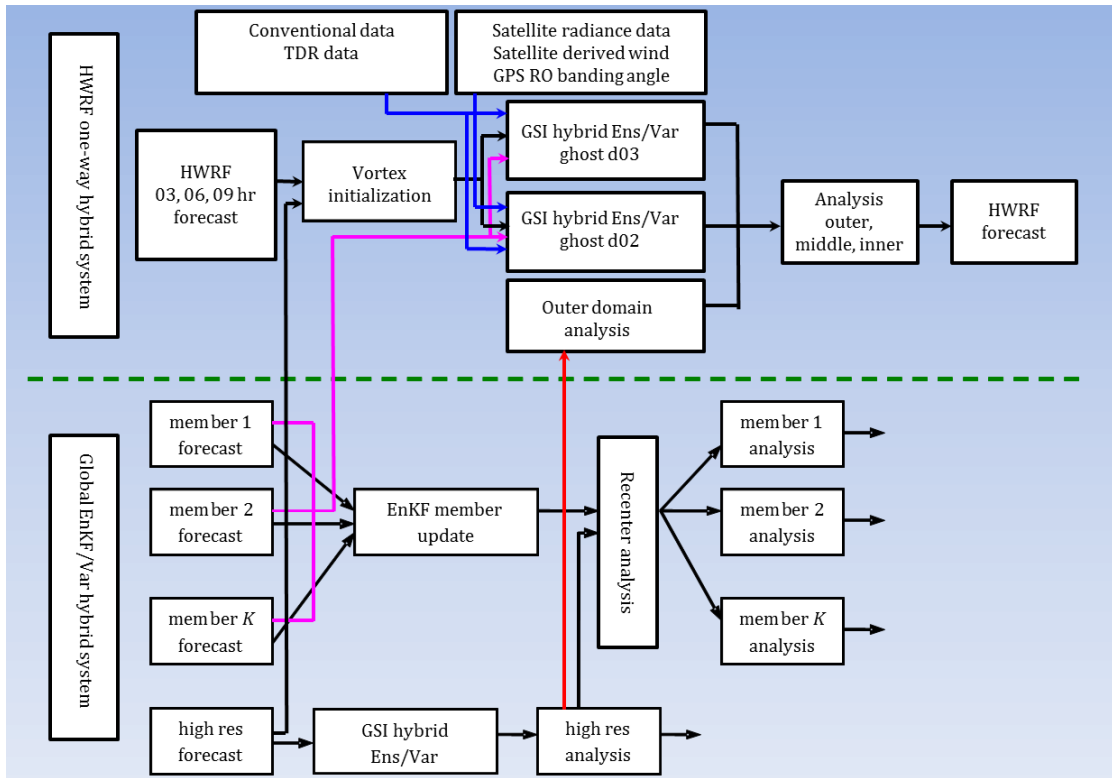


Figure 1.3. Flow diagram of HWRf and GFS hybrid data assimilation systems. Processes described by the black and magenta lines always run, while those described by the red and blue lines run when inner-core data assimilation is performed or is not performed, respectively.

Because data assimilation is no longer performed on HWRf outer domain and satellite data are regularly available (unlike aircraft reconnaissance data), the combination of vortex initialization and data assimilation is not as complex as that in 2013 HWRf. Vortex initialization is performed before data assimilation as shown in Fig. 1.3. The observations assimilated into ghost d02 include all conventional data, satellite radiance data, satellite derived wind data, blending angle from GPS Radio Occultation and NOAA P3 tail Doppler radar (TDR) radial winds. Our initial intention was to assimilate satellite data on both ghost domains. However, it was noted that the assimilation of satellite data in the inner core, no matter radiance or satellite wind, can degrade the intensity forecast. Therefore, only conventional data and P3 TDR radial winds are assimilated in ghost d03 domain.

Conventional observations (contained in prepbufr file) assimilated in ghost d02 and ghost d03 domains include:

- radiosondes;
- dropwindsondes;

- aircraft reports (AIREP/PIREP, RECCO , MDCRS-ACARS, TAMDAR , AMDAR);
- surface ship and buoy observations;
- surface observations over land;
- pibal winds;
- wind profilers;
- radar-derived Velocity Azimuth Display (VAD) wind;
- WindSat scatterometer winds; and
- integrated precipitable water derived from the Global Positioning System.

Satellite observations assimilated in ghost d02 domain include:

- Radiances from IR instruments: HIRS, AIRS, IASI, GOES Sounders
- Radiances from MW instruments: AMSU-A, MHS, ATMS
- Satellite derived wind: IR/VIS cloud drift winds, water vapor winds

The dropwindsonde observations could be obtained from US Air Force WC-13J, NOAA P3, and G-IV aircrafts. Dropwindsonde wind reports within a radius of 111 km or three times the RMW, whichever is larger, and surface-pressure reports near the storm center are flagged (a large quality control [QC] mark is assigned) in the prepbuf file. Those data will be rejected in GSI analysis according to their QC mark. We performed experiments to investigate the impact of those data and discovered that they do negatively impact the forecast. Therefore, those dropwindsonde reports are not assimilated. All other dropwindsonde reports, including temperature and moisture profiles, are assimilated.

The NOAA P3 TDR, using the Fore-Aft Scanning Technique (FAST) probes the three-dimensional wind field in the inner cores of the hurricanes (Gamache et al. 1995). The antenna is programmed to scan as much as 25° fore or aft of the plane perpendicular to the fuselage. Major quality control of the radial velocity data, including: (1) removing the projection of the aircraft motion on the observed Doppler velocity; (2) removing the reflection of the main lobe and side lobes off the sea surface; (3) removing noise; and (4) unfolding, are conducted aboard the P3 aircraft before the data are sent to the ground. The TDR data in Binary Universal Form for the Representation of meteorological data (BUFR) format contain quality-controlled radial velocities averaged over 8 gates along the radial direction. Further data thinning to the model resolution and quality control of the TDR radial velocities are performed before the data are assimilated. Figure 1.4 is an example of the TDR radial velocity data assimilated for Hurricane Earl at 12 Z on August 29, 2010. The observation error, including the representative error, of the radial velocity data is set to be 5 ms⁻¹. When the difference between the observation and the background field is more than 10 ms⁻¹, the observation error gradually increases to 10 ms⁻¹.

Observations differing from the background more than 20 ms^{-1} are rejected. Positive impact of assimilating TDR data into HWRF was found in a real time demo experiment performed during the 2012 hurricane season. The data have been assimilated into the operational HWRF since 2013 hurricane season.

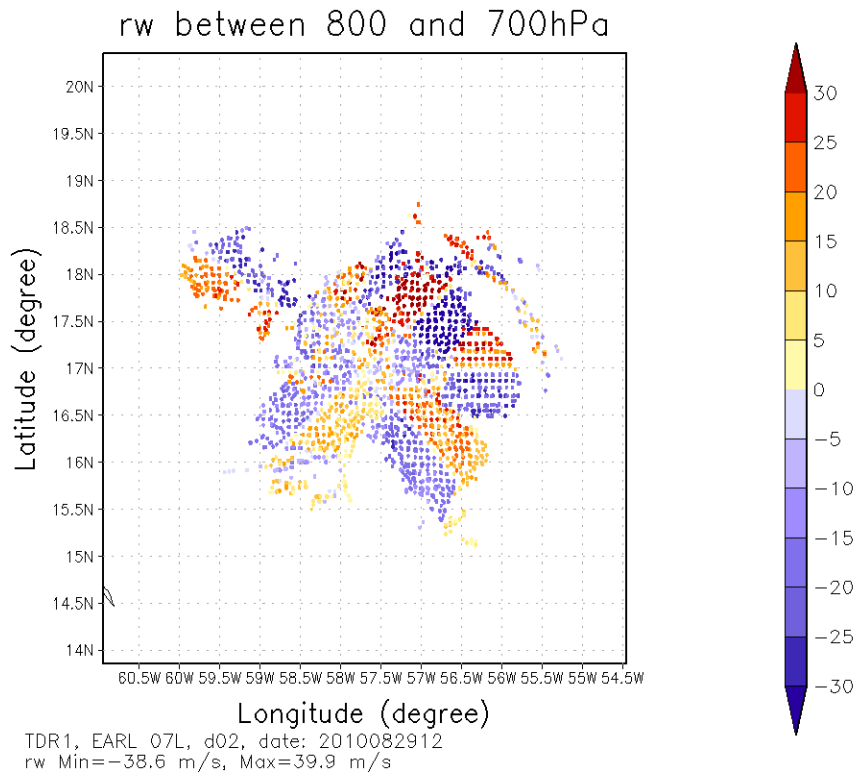


Figure 1.4. NOAA TDR radial velocities between 800 hPa and 700 hPa assimilated at 12 Z on August 29, 2010.

2.0 MPI Princeton Ocean Model for Tropical Cyclones (MPIPOM-TC)

2.1 Introduction

The three-dimensional, primitive equation, numerical ocean model that has become widely known as the POM was originally developed by Alan F. Blumberg and George L. Mellor in the late 1970s. One of the more popularly cited references for the early version of POM is Blumberg and Mellor (1987), in which the model was principally used for a variety of coastal ocean circulation applications. Through the 1990s and 2000s, the number of POM users increased enormously, reaching over 3,500 registered users as of October 2009. During this time, many changes were made to the POM code by a variety of users, and some of these changes were included in the “official” versions of the code housed at Princeton University, which has since been moved to Old Dominion University (ODU, <http://www.ccpo.odu.edu/POMWEB/>). Mellor (2004), currently available on the aforementioned website, is the latest version of the POM User’s Guide and is an excellent reference for understanding the details of the more recent versions of the official POM code.

In 1994, a version of POM available at the time was transferred to URI for the purpose of coupling to the GFDL hurricane model. At this point, POM code changes were made specifically to address the problem of the ocean’s response to hurricane wind forcing in order to create a more realistic Sea Surface Temperature (SST) field for input to the hurricane model, and ultimately to improve 3-5 day hurricane intensity forecasts in the model. Initial testing showed hurricane intensity forecast improvements when ocean coupling was included (Bender and Ginis 2000). Since operational implementation of the coupled GFDL/POM model at NCEP in 2001, additional changes to POM were made at URI and subsequently implemented in the operational GFDL model, including improved ocean initialization (Falkovich et al. 2005, Bender et al. 2007, Yablonsky and Ginis 2008). This POM version was then coupled to the atmospheric component of the HWRF model in the North Atlantic Ocean (but not in the eastern North Pacific Ocean) before operational implementation of HWRF at NCEP/EMC in 2007. Then for the 2012 operational implementation of HWRF, a simplified one-dimensional (vertical columnar) version of POM was coupled to the atmospheric component of HWRF in the eastern North Pacific Ocean, as in the 2012 (and earlier) operational GFDL model. This version of POM, used as the ocean component of the operational HWRF model through 2013 to forecast tropical cyclones in the North Atlantic and North Pacific Oceans, is known as POM-TC (Yablonsky et al. 2014a).

The remainder of this chapter primarily describes URI’s new version of POM-TC with Message Passing Interface (MPI) capabilities, adopted from sbPOM (Jordi and Wang 2012); this new ocean model version will henceforth be called MPIPOM-TC (Yablonsky et al. 2014b; Figure 2.1). Important features of MPIPOM-TC include: 1) MPI (to run on multiple processors); 2) higher resolution; 3) larger, relocatable ocean domain; 4)

improved physics; 5) 18 years of community-based improvements and bug fixes; and 6) flexible initialization options.

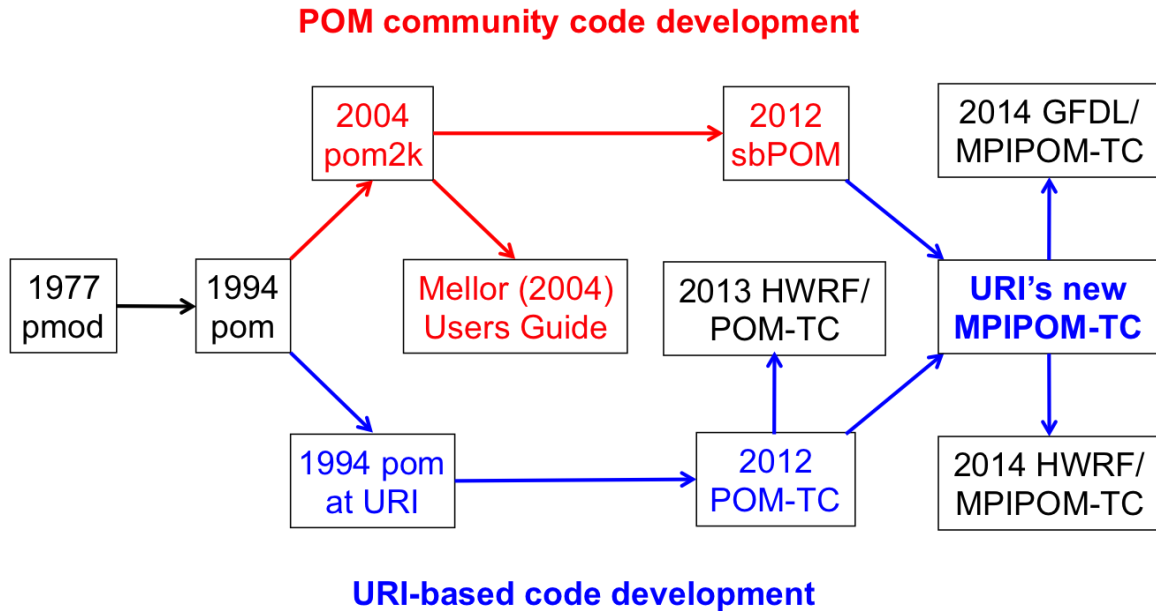


Figure 2.1. History of MIPOM-TC development (adapted from Yablonsky et al. 2014b).

2.2 Purpose

The primary purpose of coupling MIPOM-TC (or any fully three-dimensional ocean model) to the HWRF (or to any hurricane model) is to create an accurate SST field for input into the hurricane model. The SST field is subsequently used by the HWRF to calculate the surface heat and moisture fluxes from the ocean to the atmosphere. An uncoupled hurricane model with a static SST field is restricted by its inability to account for SST changes during model integration, which can contribute to high intensity bias (e.g. Bender and Ginis 2000). Similarly, a hurricane model coupled to an ocean model that does not account for fully three-dimensional ocean dynamics may only account for some of the hurricane-induced SST changes during model integration (e.g. Yablonsky and Ginis 2009, 2013).

2.3 Grid size, spacing, configuration, arrangement, coordinate system, and numerical scheme

The horizontal MIPOM-TC grid uses curvilinear orthogonal coordinates. There is one MIPOM-TC grid in the North Atlantic Ocean and one MIPOM-TC grid in the eastern North Pacific Ocean (unlike POM-TC, which had two, smaller North Atlantic POM-TC grids called “United” and “East Atlantic” (Figure 2.2). The North Atlantic grid covers the transatlantic region, which is bounded by 10°N to 47.5°N, and 98.5°W longitude to the

west, and 15.3°W longitude to the east. The North Pacific grid covers the East Pacific region, which is bounded by 5°N to 42.5°N, 167.5°W longitude to the west, and 84.3°W longitude to the east. In both ocean regions, there are 449 latitudinal grid points and 869 longitudinal grid points, yielding ~9-km grid spacing in both the latitudinal and longitudinal directions. Additional grids have been developed for other worldwide ocean regions and for an idealized ocean region, but these grids are not yet supported to the community as part of the HWRF system.

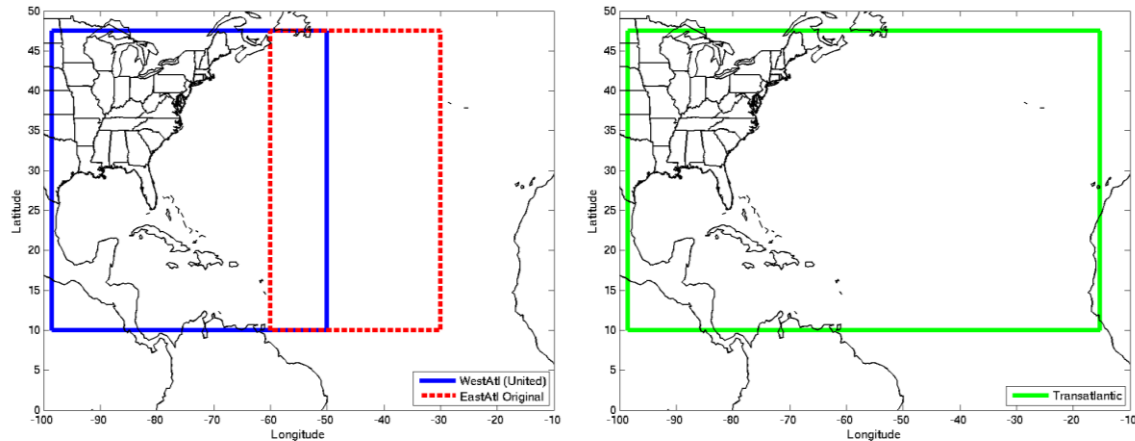


Figure 2.2. Overlapping United (blue) and East Atlantic (red) POM-TC ocean domains (in the 2013 operational HWRF), each of which had ~18-km horizontal grid spacing (left panel), and the new, transatlantic (green) MPIPOM-TC ocean domain (in the 2014 operational HWRF), which has ~9-km horizontal grid spacing (right panel).

The vertical coordinate is the terrain-following sigma coordinate system (Phillips 1957; Mellor 2004; Figure 1 and Appendix D). There are 23 vertical levels, where the level placement is scaled based on the bathymetry of the ocean at a given location. The largest vertical spacing occurs where the ocean depth is 5500 m; here, the 23 full-sigma vertical levels (“Z” in Mellor 2004) are located at 0, 10, 20, 30, 40, 50, 60, 70, 85, 100, 120, 150, 200, 300, 450, 650, 900, 1300, 1800, 2400, 3200, 4200, and 5500 m depth, and the 23 half-sigma vertical levels (“ZZ” in Mellor 2004) are located at 5, 15, 25, 35, 45, 55, 65, 77.5, 92.5, 110, 135, 175, 250, 375, 550, 775, 1100, 1550, 2100, 2800, 3700, 4850, and 5500 m depth.

During model integration, horizontal spatial differencing of the MPIPOM-TC variables occurs on the so-called staggered Arakawa-C grid. With this grid arrangement, some model variables are calculated at a horizontally shifted location from other model variables. See Mellor (2004, Section 4) for a detailed description and pictorial representations of MPIPOM-TC’s Arakawa-C grid.

MPIPOM-TC has a free surface and a split timestep. The external mode is two-dimensional and uses a short timestep (6 s) based on the well-known Courant-Friedrichs-Lewy (CFL) condition and the external wave speed. The internal mode is three-dimensional and uses a longer timestep (4.5 min) based on the CFL condition and the

internal wave speed. Horizontal time differencing is explicit, whereas the vertical time differencing is implicit. The latter eliminates time constraints for the vertical coordinate and permits the use of fine vertical resolution in the surface and bottom boundary layers. See Mellor (2004, Section 4) for a detailed description and pictorial representations of MPIPOM-TC's numerical scheme.

2.4 Initialization

Prior to coupled model integration of the HWRF/MPIPOM-TC, MPIPOM-TC is initialized with a realistic, three-dimensional temperature (T) and salinity (S) field and subsequently integrated to generate realistic ocean currents and incorporate the pre-existing hurricane-generated cold wake. The starting point for the ocean initialization in the North Atlantic Ocean is the Generalized Digital Environmental Model (GDEM) monthly ocean T and S climatology (Teague et al. 1990), which has $1/2^\circ$ horizontal grid spacing and 33 vertical z-levels located at 0, 10, 20, 30, 50, 75, 100, 125, 150, 200, 250, 300, 400, 500, 600, 700, 800, 900, 1000, 1100, 1200, 1300, 1400, 1500, 1750, 2000, 2500, 3000, 3500, 4000, 4500, 5000, and 5500 m depth. This GDEM climatology is then modified diagnostically by interpolating it in time to the MPIPOM-TC initialization date (using two months of GDEM data), horizontally interpolating it onto the MPIPOM-TC transatlantic grid, assimilating a land/sea mask and bathymetry data, and employing a feature-based modeling procedure that incorporates historical and near-real time observations of the ocean in the western portion of the grid to 50°W longitude (i.e. the old POM-TC United grid; Falkovich et al. 2005; Yablonsky and Ginis 2008). This feature-based modeling procedure has also been configured to utilize alternative T and S climatologies with $1/4^\circ$ grid spacing, including a newer GDEM climatology and a Levitus climatology (Boyer and Levitus 1997), but tests with these climatologies in the North Atlantic Ocean in the GFDL model do not show increased skill over the original GDEM climatology used operationally (Yablonsky et al. 2006). To prevent T and S discontinuities across 50°W longitude, the GDEM T and S values that have been modified by the feature-based modeling procedure west of this longitude are blended with the raw GDEM T and S values that have not been modified by the feature-based modeling procedure east 50°W longitude. In the eastern North Pacific region, a more recent version of the GDEM monthly ocean T and S climatology (GDEMv3; Carnes 2009), which has $1/4^\circ$ horizontal grid spacing and 78 vertical z-levels, is used to initialize the ocean. Only the first 73 GDEMv3 levels are utilized, however, because the MPIPOM-TC depth is not permitted to exceed 5500 m. These 73 vertical z-levels are located at: 0, 2, 4, 6, 8, 10, 15, 20, 25, 30, 35, 40, 45, 50, 55, 60, 65, 70, 75, 80, 85, 90, 95, 100, 110, 120, 130, 140, 150, 160, 170, 180, 190, 200, 220, 240, 260, 280, 300, 350, 400, 500, 600, 700, 800, 900, 1000, 1100, 1200, 1300, 1400, 1500, 1600, 1800, 2000, 2200, 2400, 2600, 2800, 3000, 3200, 3400, 3600, 3800, 4000, 4200, 4400, 4600, 4800, 5000, 5200, 5400, and 5600 m depth.

The basic premise of the feature-based modeling procedure is that major oceanic fronts and eddies in the western North Atlantic Ocean, namely the Gulf Stream (GS), the Loop Current (LC), and Loop Current warm and cold core rings (WCRs and CCRs), are poorly represented by the GDEM climatology's T and S fields. By defining the spatial structure

of these fronts and eddies using historical observations gathered from various field experiments (Falkovich et al. 2005, Section 3), cross-frontal “sharpening” of the GDEM T and S fields can be performed to obtain more realistic fields. These sharpened fields yield stronger geostrophically adjusted ocean currents along the front than would be obtained directly from GDEM, causing the former to be more consistent with observations than the latter. In addition, algorithms were incorporated into the feature-based modeling procedure to initialize the GS and LC with prescribed paths, and to insert WCRs and CCRs in the Gulf of Mexico based on guidance from near real-time observations, such as satellite altimetry (Yablonsky and Ginis 2008, Section 2).

After the aforementioned diagnostic modifications to the GDEM climatology (including the feature-based modifications in the transatlantic region), at the beginning of what is referred to as ocean spinup “phase 1” (also commonly known as “phase 3” for historical reasons), the upper ocean temperature field is modified by assimilating the real-time daily SST data (with 1° grid spacing) that is used in the operational NCEP GFS global analysis (hereafter NCEP SST; Reynolds and Smith 1994). Further details of the SST assimilation procedure can be found in Yablonsky and Ginis (2008, Section 2). Finally, the three-dimensional T and S fields are interpolated from the GDEM z-levels onto the MPIPOM-TC vertical sigma levels, and the density (RHO) is calculated using the modified United Nations Educational, Scientific, and Cultural Organization (UNESCO) equation of state (Mellor 1991), ending the diagnostic portion of the ocean initialization.

Ocean spinup phase 1 involves 48 h of MPIPOM-TC integration, primarily for dynamic adjustment of the T and S (and ultimately, RHO) fields and generation of geostrophically adjusted currents. During phase 1, SST is held constant. Once phase 1 is complete, the phase 1 output is used to initialize ocean spinup “phase 2” (also commonly known as “phase 4” for historical reasons). During phase 2, the cold wake at the ocean surface and the currents produced by the hurricane prior to the beginning of the coupled model forecast are generated by a 72-h integration of MPIPOM-TC with the observed hurricane surface wind distribution provided by NOAA’s NHC along the storm track. Or, if the observed wind field is very weak, phase 2 is skipped. Once phase 2 is complete (or skipped), the phase 2 output (or phase 1 output) is used to initialize the MPIPOM-TC component of the coupled HWRF.

2.5 Physics and dynamics

As previously stated, the primary purpose of coupling the MPIPOM-TC to the HWRF is to create an accurate SST field for input into the HWRF. An accurate SST field requires ocean physics that can generate accurate SST change in response to wind (and to a lesser extent, thermal) forcing at the air-sea interface. The leading order mechanism driving SST change induced by wind forcing is vertical mixing and entrainment in the upper ocean. Vertical mixing occurs because wind stress generates ocean surface-layer currents, and the resulting vertical current shear leads to turbulence, which then mixes the upper ocean and entrains colder water from the thermocline up into the well-mixed ocean surface layer, ultimately cooling the SST. In MPIPOM-TC, turbulence is parameterized using a second moment turbulence closure submodel, which provides the vertical mixing

coefficients. This submodel is widely known as the Mellor-Yamada Level 2.5 turbulence closure model (Mellor and Yamada 1982; Mellor 2004, Sections 1 and 14).

If vertical mixing (and the resulting entrainment) was the only ocean response to hurricane wind forcing that impacted SST, then a one-dimensional (vertical columnar) ocean model would be sufficient. However, idealized experiments comparing three-dimensional and one-dimensional versions of POM-TC (or equivalently, MPIPOM-TC), show that the one-dimensional (MPI)POM-TC underestimates SST cooling for slow-moving hurricanes (Yablonsky and Ginis 2009). This finding is consistent with previous studies (e.g. Price 1981). The primary reason a one-dimensional ocean model fails to capture the magnitude of SST cooling for slow-moving storms is the neglect of upwelling, which is a fully three-dimensional process. The cyclonic wind stress induced by a hurricane creates divergent surface currents in the upper ocean, causing upwelling of cooler water from the thermocline towards the sea surface. For slow-moving storms, this upwelling increases the efficiency with which vertical mixing can entrain cooler water from the thermocline into the well-mixed ocean surface layer, ultimately cooling the SST. Finally, horizontal advection, which is also neglected by one-dimensional ocean models, may impact the SST distribution, especially in oceanic fronts and eddies where strong background currents exist (Yablonsky and Ginis 2013). Horizontal diffusion in MPIPOM-TC, which generally has relatively little impact on the SST over the time scale of the hurricane, uses Smagorinsky diffusivity (Smagorinsky 1963).

2.6 Coupling

At NCEP, a coupler was developed to act as an independent interface between the HWRF atmospheric component and the MPIPOM-TC. While the technology of the atmosphere-ocean coupling in HWRF differs from the GFDL model, the purpose is the same. During forecast integration of HWRF, the east-west and north-south momentum fluxes at the air-sea interface (“wusurf” and “wvsurf” in Mellor 2004) are passed from the atmosphere to the ocean, along with temperature flux (“wtsurf”) and the shortwave radiation incident on the ocean surface (“swrad”). Prior to a change made in the operational HWRF in between the 2012 and 2013 Atlantic hurricane seasons, all four of these fluxes (wusurf, wvsurf, wtsurf, and swrad) were first reduced by 25% before being passed from the atmosphere to the ocean to mitigate excessive SST cooling. This 25% flux reduction has since been eliminated, based on testing that showed improved SST cooling prediction and improved HWRF intensity prediction in the absence of the 25% flux reduction. During forecast integration of MPIPOM-TC, the SST is passed from the ocean to the atmosphere.

The time integration of the coupled system is carried out with three executables working in Multiple Program Multiple Data (MPMD) mode for the HWRF atmospheric component, MPIPOM-TC, and the coupler. The coupler serves as a hub for MPI communications between HWRF atmosphere and MPIPOM-TC and performs the interpolation of the surface fluxes from the fixed and moving HWRF atmospheric grids to the MPIPOM-TC grid and of the SST from the MPIPOM-TC grid to the two outermost HWRF atmospheric grids. A generalized bilinear interpolation for non-rectangular quadrilateral grid cells is used. Only sea-point values of the surface fields are employed for the interpolation. For missing values due to model domain inconsistencies, a limited

extrapolation within the relevant connected component of the model sea surface is used. The computations that establish the mutual configuration of the grids (interpolation initialization) are performed prior to the forecast, using an algorithm with the number of operations reduced to the order of N^3 , where N is the number of points in a grid row. The coupler also provides run-time analysis and diagnostics of the surface data.

Finally, the coupler includes the non-operational capability for three-way coupling, where the third model component is the WAVEWATCH III wave model. With the three-way option activated, HWRF atmosphere supplies WAVEWATCH III with surface wind data and the hurricane's current geographical position, which is taken to be a circle circumscribed around HWRF's moving domain. WAVEWATCH III is not currently supported by the DTC.

2.7 Output fields for diagnostics

Some of the two-dimensional and three-dimensional MPIPOM-TC variables are saved in netCDF output files for diagnostic purposes every 24 hours (by default). The format of the names of these netCDF output files is "name.NNNN.nc" where "name" is the storm name and "NNNN" is the four-digit file number. The first output time is always the model initialization time (for the particular model phase being simulated), and can therefore be used to diagnose the current model phase's initial condition. The netCDF utility "ncdump" can be used to see a listing of the variables and their sizes and units in the netCDF output files. Note that variables in these netCDF output files retain their native MPIPOM-TC C-grid and sigma level navigation information, so "u," "v," "wusurf," and "wvsurf," for example, are defined at a horizontally-shifted locations from "t" and "s," and "q2" and "w" are defined at vertically-shifted locations from "t" and "s." Therefore, it may be necessary to post process the variables in these netCDF output files in order to make meaningful spatial plots and/or vertical cross sections. Efforts are currently underway to create more comprehensive diagnostic packages for MPIPOM-TC visualization within the HWRF system.

3.0 Physics Packages in HWRF

The HWRF system was designed to utilize the strengths of the WRF software system, the well tested NMM dynamic core, and the physics packages of the GFDL and GFS forecast systems. Since the HWRF system became operational in 2007, the physics packages of the HWRF model have been upgraded on a yearly basis, and this document describes the HWRF physics suites implemented for the 2014 hurricane season.

Examples of recent improvements include surface layer and PBL parameterization changes designed to bring the HWRF physics packages more in line with observations of surface roughness, enthalpy and momentum surface fluxes, and PBL height. The physics packages of HWRF will be briefly described and contrasted with other NOAA models such as GFS, GFDL and NAM. A GFS model and physics descriptions can be found at <http://www.emc.ncep.noaa.gov/GFS/doc.php>, while more information on additional physics available in the WRF model are available in Skamarock et al. (2008) and at http://www.mmm.ucar.edu/wrf/users/tutorial/201207/Basic/WRF_Physics_Dudhia.pdf. See Bender et al. (2007) for more information on the GFDL hurricane model. Note that the POM coupling component of HWRF is described in Section 2.

3.1 HWRF physics

This section outlines the physical parameterizations used in the operational HWRF model, which fall into the following categories: (1) microphysics, (2) cumulus parameterization, (3) surface layer, (4) PBL (5) LSM, and (6) radiation. It closely follows the basic WRF physics tutorial of Jimmy Dudhia mentioned above. Horizontal diffusion, which may also be considered part of the physics, is not described in this section. The WRF system has been expanded to include all HWRF physics and, for each category, the operational HWRF employs a specific choice within the WRF spectrum of physics options. As mentioned above, the HWRF physics initially followed the physics suite used by the benchmark operational GFDL hurricane model, but in the last few years several modifications have been introduced.

In the WRF framework, the physics section is insulated from the rest of the dynamics solver by the use of physics drivers. These drivers are located between the following solver-dependent steps: pre-physics preparations and post-physics modifications of the tendencies. The physics preparation involves filling arrays with physics-required variables, such as temperature, pressure, heights, layer thicknesses, and other state variables in MKS units at half-level and full levels. The velocities are de-staggered so that the physics code is independent of the dynamical solver's velocity staggering. Since HWRF uses the E-grid on the rotated lat-long projection of the WRF-NMM dynamic core, this velocity de-staggering involves interpolating the momentum variables from the velocity to the mass grid points. Physics packages compute tendencies for the un-staggered velocity components, potential temperature, and moisture fields. The solver-dependent post-physics step re-staggeres the tendencies as necessary, couples tendencies with coordinate metrics, and converts to variables or units appropriate to the dynamics

solver. As in other regional models, the physics tendencies are generally calculated less frequently than dynamic tendencies for computational expediency. The interval of physics calls is controlled by namelist parameters.

3.2 Microphysics parameterization

Microphysics parameterizations explicitly handle the behaviors of hydrometeor species by solving prognostic equations for their mixing ratio and/or number concentration, so they are sometimes called explicit cloud schemes (or gridscale cloud schemes) in contrast to cumulus schemes, which parameterize sub-grid scale convection. The adjustment of water vapor exceeding saturation values is also included inside the microphysics. The treatment of water species such as rain, cloud, ice, and graupel was first utilized in the development of cloud models, which simulated individual clouds and their interactions. Gradually, as it became more computationally feasible to run at high-grid resolutions, microphysics schemes were incorporated into regional atmospheric models. At high enough resolution (~1 km or less), convective parameterization of cloud processes may not be needed because convection can be resolved explicitly by a microphysics scheme. In the simpler microphysics schemes (single-moment schemes), such as the one used in HWRF, only the mixing ratios of the water species are carried as predicted variables, while the number concentration of the variables is assumed to follow standard distributions. If number concentrations are also predicted, the schemes are coined “double moment.” A further sophistication in microphysics schemes is introduced if the water species are predicted as a function of size. This added level of complexity is coined a “bin” scheme. The present HWRF model, like the NAM and GFDL models, uses the Ferrier scheme, which is simplified so that the cloud microphysical variables are considered in the physical column, but only the combined sum of the microphysical variables, the total cloud condensate, is advected horizontally and vertically. A possible upgrade of HWRF microphysics would be to extend the Ferrier scheme to handle advection of cloud species. Note that the 2012 modifications were made to the HWRF model such that it can now be run in research mode with a variety of microphysics packages, including the Thompson and WRF single-moment 6-class (WSM6) parameterizations.

The Ferrier scheme

The present HWRF Ferrier microphysics scheme is based on the Eta Grid-scale Cloud and Precipitation scheme developed in 2001 and known as the EGCP01 scheme (Ferrier 2005). The WRF model has three versions of the Ferrier microphysics; one for general applications (used in the old WRF-based NAM model), one for higher resolution (used operationally in the 4-km grid spacing High-Resolution Windows application), and one tailored for the tropics (used in HWRF). The latter duplicates some features used in the GFDL model implementation. For example, the number concentration of droplets is set to 60 cm^{-3} and 100 cm^{-3} in the HWRF and old WRF-based NAM versions, respectively. In addition, the onset of condensation above the planetary boundary layer in the parent grid of the tropical Ferrier is set to 97.5%, while the standard value of 100 % relative humidity is used throughout the domain in the old WRF-based NAM version. These changes for

the tropics were implemented primarily to obtain a more realistic intensity distribution in HWRF and GFDL forecasts. The scheme predicts changes in water vapor and condensate in the forms of cloud water, rain, cloud ice, and precipitation ice (snow/graupel/sleet). The individual hydrometeor fields are combined into total condensate, and it is the water vapor and total condensate that are advected in the model. This is done for computational expediency. Local storage arrays retain first-guess information of the contributions of cloud water, rain, cloud ice, and precipitation ice of variable density in the form of snow, graupel, or sleet (Figure 3.1).

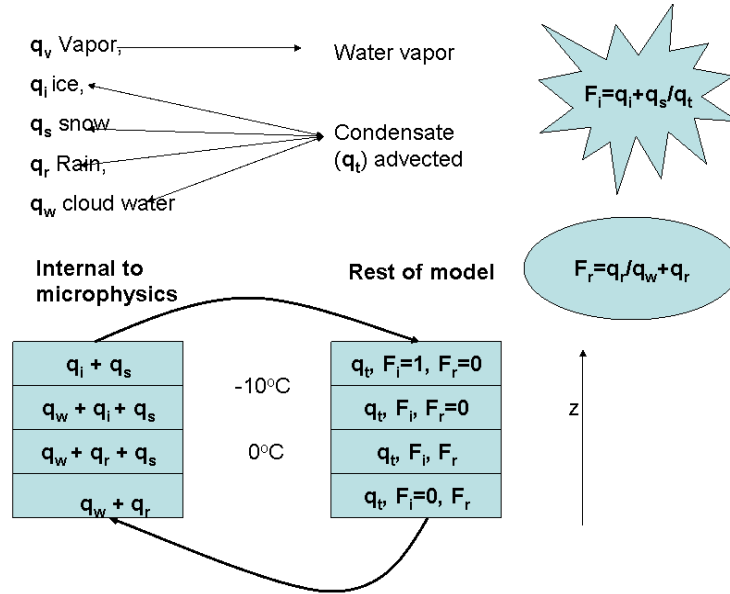


Figure 3.1. Water species used internally in the Ferrier microphysics and their relationship to the total condensate. The left column represents the quantities available inside the microphysics scheme (mixing ratios of vapor, ice, snow, rain, and cloud water). The right column represents the quantities available in the rest of the model: only the water vapor and the total condensate get advected. After advection is carried out, the total condensate is redistributed among the species based on fractions of ice and rain water.

The density of precipitation ice is estimated from a local array that stores information on the total growth of ice by vapor deposition and accretion of liquid water. Sedimentation is treated by partitioning the time-averaged flux of precipitation into a grid box between local storage in the box and fall out through the bottom of the box. This approach, together with modifications in the treatment of rapid microphysical processes, permits large timesteps to be used with stable results. The mean size of precipitation ice is assumed to be a function of temperature following the observational results of Ryan et al. (1996). Mixed-phase processes are now considered at temperatures warmer than -40°C

(previously -10°C), whereas ice saturation is assumed for cloudy conditions at colder temperatures.

Changes were made in three parameters of the Ferrier microphysics scheme for the 2012 HWRF upgrades. Although these changes did not significantly alter the HWRF forecasted track and intensity of a storm, they contributed to produce better mixing ratio forecasts, allowing the creation of more realistic large-scale forecast products, in particular simulated infra-red and water vapor satellite images. The three parameters changed were the maximum allowable ice concentration (NLI_{max}), the number concentration of cloud droplet (NCW) and snow fall speed. NLI_{max} was increased from 2 to 20 L^{-1} and NCW was increased from 60 to 250 cm^{-3} . The reason for the NCW increase was the reduction of the unrealistic widespread spotty drizzle/light rain in the open ocean of the parent domain. Finally, the fall speed of snow particles in the regions of warmer-than-freezing temperature (0°C) was also increased to mimic higher order moment schemes.

Further description of the scheme can be found in Sec. 3.1 of the November 2001 NCEP Technical Procedures Bulletin (TPB) at <http://www.emc.ncep.noaa.gov/mmb/mmbp11/eta12tpbh> and on the COMET page at <http://meted.ucar.edu/nwp/pcu2/etapcp1.htm>.

3.3 Cumulus parameterization

Cumulus parameterization schemes, or convective parameterization schemes, are responsible for the sub-gridscale effects of deep and/or shallow convective clouds. These schemes are intended to represent vertical fluxes unresolved by gridscale microphysics schemes such as updrafts, downdrafts and compensating motion outside the clouds. In its early development, convective parameterization was believed to be necessary to avoid possible numerical instability due to of simulating convection at coarse resolutions. The schemes operate only on individual vertical columns where the scheme is triggered and provide vertical heating and moistening profiles. Some schemes also provide cloud and precipitation field tendencies in the column, and some schemes, such as the one used in HWRF, provide momentum tendencies due to convective transport of momentum. The schemes all provide the convective component of surface rainfall.

Cumulus parameterizations are theoretically only valid for coarser grid sizes, (e.g., greater than 10 km), where they are necessary to properly release latent heat on a realistic time scale in the convective columns. While the assumptions about the convective eddies being entirely sub-grid-scale break down for finer grid sizes, sometimes these schemes have been helpful in triggering convection in 5-10-km grid applications and accurately predicting rainfall patterns. Normally, they should not be used when the model itself can resolve the convective eddies (grid spacing less than approximately 5 km). In the 2013 operational implementation of HWRF, the cumulus parameterization is activated only in the parent domain and in the coarser nest (27- and 9-km horizontal grid spacing, respectively). No convective parameterization is used in the 3-km horizontal grid spacing inner nest.

The Simplified Arakawa-Schubert (SAS) scheme

HWRf uses the SAS cumulus parameterization also employed, with some modifications, in the GFS (Pan and Wu 1995; Hong and Pan 1998; Pan 2003; Han and Pan 2011) and GFDL models. It was made operational in NCEP's global model in 1995 and in the GFDL hurricane model in 2003. This scheme, which is based on Arakawa and Schubert (1974), was simplified by Grell (1993) to consider only one cloud top at a specified time and location and not the spectrum of cloud sizes, as in the computationally expensive original scheme. Since 2011, the GFS and HWRf models use the newly upgraded SAS scheme, which no longer considers a random distribution of cloud tops but one cloud top value in a grid box from various entrainment ensemble averaged parameters. The scheme was revised to make cumulus convection stronger and deeper by increasing the maximum allowable cloud base mass flux and having convective overshooting from a single cloud top.

In addition to the deep convection scheme, the shallow convection parameterization was incorporated in the operational GFS and HWRf models in 2011 and 2012, respectively. The parameter used to differentiate shallow from deep convection is the depth of the convective cloud. When the convective thickness is greater than 150 hPa, convection is defined as deep; otherwise it is treated as shallow. In the HWRf model, precipitation from shallow convection is prohibited when the convection top is located below the PBL top and the thickness of the shallow convection cloud is less than 50 hPa. These customizations were made to remove widespread light precipitation in the model domain over the open ocean areas. Note that because the shallow convection scheme requires knowledge of the PBL height, it needs to be run in conjunction with a PBL parameterization that provides that information. In the current code, only the GFS PBL scheme has been tested to properly communicate the PBL height to the HWRf SAS parameterization.

In SAS, convection depends on the cloud-work function, a quantity derived from the temperature and moisture in each air column of the model, which is similar to the Convective Available Potential Energy (CAPE). When the cloud-work function exceeds a certain critical threshold, which takes into account the cloud-base vertical motion, the parameterizations are triggered and the mass flux of the cloud, M_c , is determined using a quasi-equilibrium assumption. As the large-scale rising motion becomes strong, the cloud-work function is allowed to approach zero (therefore approaching neutral stability).

The temperature and moisture profiles are adjusted towards the equilibrium cloud-work function within a specified time scale using the deduced mass flux, and can be determined on the resolvable scale by:

$$\partial h / \partial t = E(h - \tilde{h}) + D(\tilde{h} - h) + M_c \partial h / \partial z$$

$$\partial q / \partial t = E(q - \tilde{q}) + D(\tilde{q} - q) + M_c \partial q / \partial z$$

where h , l and q are the moist static energy, liquid water, and specific humidity on the resolvable scale and the tilde refers to the environmental values in the entraining (E) and detraining (D) cloud regions.

The cloud model incorporates a downdraft mechanism as well as evaporation of precipitation. Entrainment of the updraft and detrainment of the downdraft in the sub-cloud layers is included. Downdraft strength is based on vertical wind shear through the cloud.

In the revised SAS scheme in HWRF, the cloud-top level is determined by the parcel method to be the level where the parcel becomes stable with respect to the environment. Detrained water is separated into condensate and vapor, with the condensate used as a source of prognostic cloud condensate above the level of the minimum moist static energy. In contrast to HWRF, the GFDL hurricane model version of SAS does not export condensate to the rest of the model.

In the current implementation of SAS, the mass fluxes induced in the updrafts and the downdrafts are allowed to transport momentum (Pan 2003). The momentum exchange is calculated through the mass flux formulation in a manner similar to that of heat and moisture. The introduction of the effect of momentum mixing was made operational in NCEP's GFS model in May 2001 and greatly reduced the generation of spurious vortices (Figure 3.2) in the global model (see Han and Pan 2006). It has also been shown to have a significant positive impact on hurricane tracks in the GFDL model. The effect of the convection-induced pressure gradient force on cumulus momentum transport is parameterized in terms of mass flux and vertical wind shear (Han and Pan 2006). As a result, the cumulus momentum exchange is reduced by about 55 % compared to the full exchange in previous versions. To improve intensity forecasts, the momentum mixing coefficient (*pgcon* in the WRF namelist) has been tuned in the 2013 operational HWRF model to 0.55 and 0.20 in the 27- and 9-km grid spacing domains, respectively. In previous implementations, the same value of *pgcon* was used in both domains (0.20 in 2012 and 0.55 in 2011).

Han and Pan (2011) found that the revised SAS contributed to reductions in the root-mean-squared errors of tropical winds and yielded improved hurricane tracks (Figure 3.3). For more detailed information see: <http://www.emc.ncep.noaa.gov/GFS/doc.php#conv>. For some tests at NCEP and DTC, the HWRF has been configured to use alternate convective schemes: Betts-Miller-Janjic (BMJ - Janjic 1994, 2000 - used in the operational NCEP NAM model), Tiedtke (Tiedtke 1989; Zhang et al. 2011), Kain-Fritsch (modified from Kain and Fritsch 1993), and the New Simplified Arakawa Schubert (NSAS) scheme coded by the Yonsei University (YSU), also based on Han and Pan 2011. Generally speaking, these schemes have not demonstrated superior skill to the operational HWRF SAS scheme, but may serve as a way to create a physics diversity ensemble using WRF.

3.4 Surface-layer parameterization

The surface-layer schemes calculate friction velocities and exchange coefficients that enable the calculation of surface heat, moisture, and momentum fluxes by the LSM. Over water, the surface fluxes and surface diagnostic fields are computed by the surface-layer scheme itself. These fluxes, together with radiative surface fluxes and rainfall, are used as input to the ocean model. Over land, the surface-layer schemes are capable of computing

both momentum and enthalpy fluxes as well. However, if a land model is invoked, only the momentum fluxes are retained and used from the surface-layer scheme. The schemes provide no tendencies, only the stability-dependent information about the surface layer for the land-surface and PBL schemes.

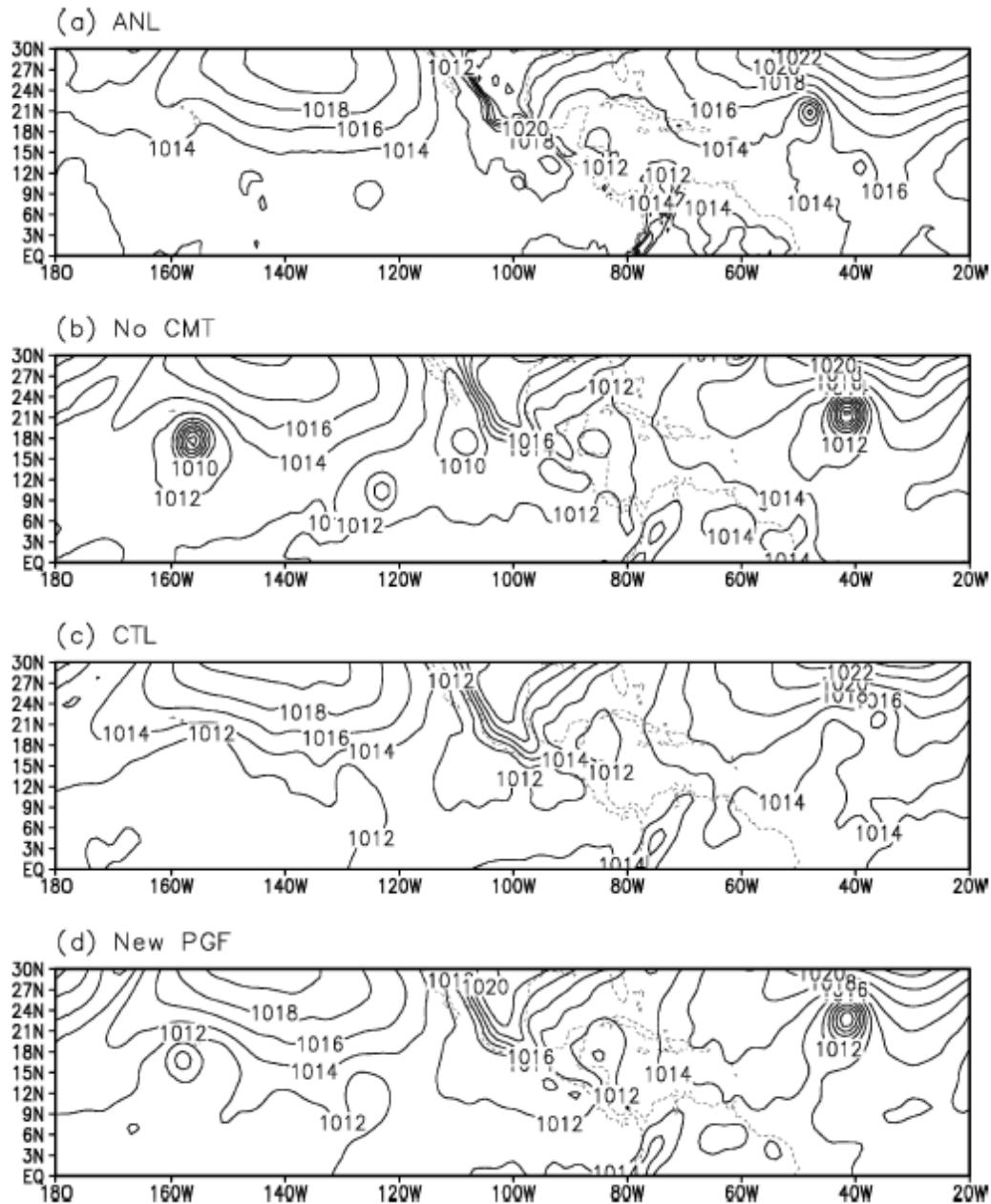


Figure 3.2. Comparison among a) verifying GFS mean sea-level pressure (hPa) analysis and 132-h GFS model forecasts with b) no cumulus momentum mixing and c) and d) with some amount of cumulus momentum mixing. The GFS forecasts were initialized at 0000 UTC 22 Sep 2000. Note several spurious vortices west of 100 W in (b) and (d) (from Han and Pan 2006).

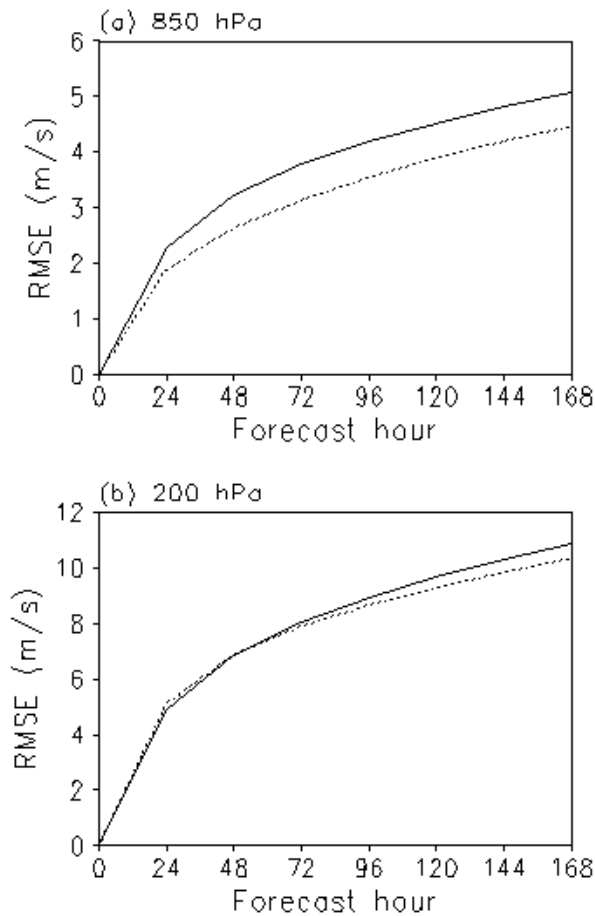


Figure 3.3 Root-mean-square vector wind errors ($m s^{-1}$) at (a) 850 hPa and (b) 200 hPa over the Tropics (20S-20N) from the control (solid line) and revised SAS (dashed line) GFS model forecasts during 20 June–10 November, 2008 (from Han and Pan 2011).

Each surface-layer option is normally tied to a particular boundary-layer option but, in the future, more interchangeability may become available. The HWRF operational model uses a modified GFDL surface layer and the GFS PBL scheme. The GFS surface layer has been used as an alternate configuration of HWRF in some tests at NCEP.

The HWRF surface layer scheme

While the 2009 versions of the HWRF and GFDL surface parameterizations were nearly identical, they have since diverged. Since 2012, HWRF uses a modified surface layer parameterization over water based on Kwon et al. (2010), Powell et al. (2003) and Black et al. (2007). The air-sea flux calculations use a bulk parameterization based on the Monin-Obukhov similarity theory (Sirutis and Miyakoda 1990; Kurihara and Tuleya 1974). The HWRF scheme retained the stability-dependent formulation of the GFDL surface parameterization, with the exchange coefficients now recast to use momentum and enthalpy roughness lengths that conform to observations. In this formulation, the neutral drag coefficient C_d is defined as:

$$C_d = \kappa^2 \left(\ln \frac{z_m}{z_0} \right)^{-2}, \quad (3.4.1)$$

where κ is the von Karman constant ($= 0.4$), z_0 is the roughness length for momentum, and z_m is the lowest model-level height. The neutral heat and humidity coefficients (assumed equal, C_k) are expressed as

$$C_k = \kappa^2 \left(1 + \frac{z_m}{z_0} \right)^{-1} \left(1 + \frac{z_T}{z_0} \right)^{-1} \quad (3.4.2)$$

where z_T is the roughness length for heat and humidity.

In the HWRP implementation of the Monin-Obukov formulations, the C_d and C_k for neutral conditions are prescribed at the lowest model level (~ 35 m). C_k has a constant value of 1.1×10^{-3} based on observations from the Coupled Boundary Layers Air-Sea Transfer (CBLAST) experiment. C_d increases with wind speed until 30 m s^{-1} , when it levels off consistently with field measurements (Powell et al. 2003; Donelan et al. 2004; Emanuel 2003; Moon et al. 2004a,b; Makin 2005; and Black et al. 2007). These prescribed values of C_d and C_k are valid only in neutral conditions. In HWRP, C_d and C_k also depend on atmospheric stability, and are larger in unstable conditions when vertical mixing is more vigorous.

Over land, the roughness in HWRP is specified (as in the NAM model) with $z_0 = z_T$. Over water, the HWRP momentum roughness, z_0 , is obtained by inverting Equation 2.1. The enthalpy roughness, z_T , is obtained by inverting Equation 2.2 above. The resulting formulations for z_0 , as in Moon et al. (2007) and Powell et al. (2003), and z_T , modified from Kwon et al. (2010) and Black et al. (2007), are

$$z_0 = (0.0185/g) \times (7.59 \times 10^{-8} W^2 + 2.46 \times 10^{-4} W)^2, \quad W \leq 12.5 \text{ ms}^{-1}$$

$$z_0 = (7.40 \times 10^{-4} W - 0.58) \times 10^{-3}, \quad 12.5 \text{ ms}^{-1} < W \leq 30 \text{ ms}^{-1}$$

$$z_0 = -1.34 \times 10^{-4} + 3.02 \times 10^{-5} W + 1.52 \times 10^{-6} W^2 - 3.57 \times 10^{-8} W^3 + 2.05 \times 10^{-10} W^4, \quad W > 30 \text{ ms}^{-1}$$

$$z_T = (0.0185/g) \times (7.59 \times 10^{-8} W^2 + 2.46 \times 10^{-4} W)^2, \quad W \leq 7 \text{ ms}^{-1}$$

$$z_T = 2.38 \times 10^{-3} \exp(-0.53 W) + 2.5 \times 10^{-5} \exp(-0.021 W), \quad W > 7 \text{ ms}^{-1}$$

where W (ms^{-1}) is the wind speed at z_m and g is the gravitational acceleration.

In older versions of the GFDL hurricane model, z_0 and z_T were both calculated by the Charnock's relation as $0.0185 u_*^2/g$, where u_* is the friction velocity. C_d kept increasing with wind speed in the original GFDL model, which overestimated the surface drag at

high wind speeds, leading to underestimation of the surface wind speed for a given central pressure in strong hurricanes (Ginis et al. 2004). The surface parameterization scheme used in GFS is also based on Sirutis and Miyakoda (1990) but modified by P. Long in very stable and very unstable situations. The roughness length over ocean is updated with a Charnock formula after the surface stress has been obtained. The GFS thermal roughness over the ocean is based on a formulation derived from the Tropical Ocean Global Atmosphere Coupled Ocean Atmosphere Response Experiment (TOGA COARE, Zeng et al. 1998). Interestingly, the GFS scheme retains the Charnock formulation of roughness for momentum while the GFDL hurricane model retains the Charnock formulation for enthalpy. Therefore there is a distinction between momentum and enthalpy roughness among the HWRF, GFDL, and GFS surface-flux schemes, with correspondingly different momentum and enthalpy coefficients at high wind speed.

Another surface-flux parameterization scheme used experimentally in HWRF is the Mellor-Yamada-Janjic (MYJ) scheme, formerly referred to as the Eta surface layer scheme (Janjic 1996b, 2002) which is based on the similarity theory (Kurihara and Tuleya 1974). The scheme includes parameterizations of a viscous sub-layer. The surface fluxes are computed by an iterative method. This surface-layer scheme is generally run in conjunction with the Eta MYJ PBL scheme, and therefore is referred to as the MYJ surface scheme. As mentioned previously, when the HWRF model is run with the NAM options, including the MYJ scheme, hurricane intensity tends to be reduced. Note that the use of the MYJ PBL and surface-layer parameterizations in HWRF is not supported in the current HWRF code.

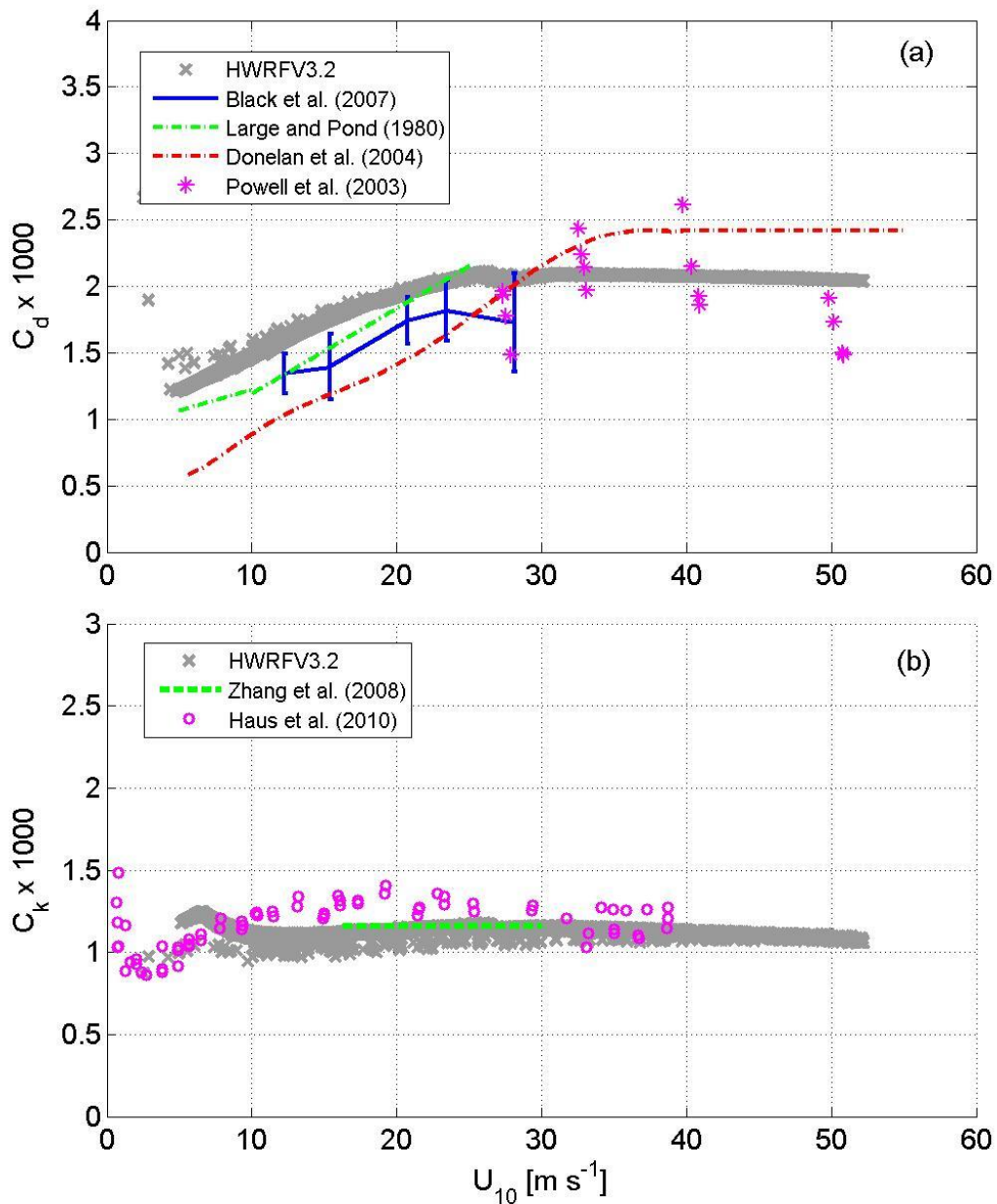


Figure 3.4. Over-water drag coefficients for a) momentum (C_d) and b) enthalpy (C_k) coefficients at a height of 10 m above ground level (Gopalakrishnan et al. 2013). Values for HWRF (grey crosses) are compared against observational estimates by Zhang et al. 2008 (green dashes) and Haus et al. 2010 (pink circles).

3.5 Land-surface model

LSMs use atmospheric information from the surface-layer scheme, radiative forcing from the radiation scheme, and precipitation forcing from the microphysics and convective

schemes, together with internal information on the land's state variables and land-surface properties, to provide heat and moisture fluxes over land points and sea-ice points. These fluxes provide a lower boundary condition for the vertical transport done in the PBL schemes (or the vertical diffusion scheme in the case where a PBL scheme is not run, such as in large-eddy mode). Land-surface models have various degrees of sophistication in dealing with thermal and moisture fluxes in multiple layers of the soil and also may handle vegetation, root, and canopy effects and surface snow-cover prediction. In WRF, the LSM provides no tendencies, but updates the land's state variables which include the ground (skin) temperature, soil temperature profile, soil moisture profile, snow cover, and possibly canopy properties. There is no horizontal interaction between neighboring points in the LSM, so it can be regarded as a one-dimensional column model for each WRF land grid-point, and many LSMs can be run in a stand-alone mode when forced by observations or atmospheric model input. One of the simplest land models involve only one soil layer (slab) and predict surface temperature only. In this formulation, all surface fluxes (both enthalpy and momentum) are predicted by the surface-layer routines. HWRF uses such a simple land model: the GFDL slab option.

The GFDL slab scheme

The GFDL slab model was developed by Tuleya (1994) based on Deardorff (1978). This simple one-level slab model, together with the GFDL radiation package, completed the requirement for realistic tropical cyclone behavior over land during the development of the GFDL hurricane model (see Figure 3.5). The surface temperature, T_* , is the only predicted parameter in this system.

$$\partial T_*/\partial t = (-\sigma T_*^4 - \text{Shfx} - \text{Levp} + (\text{S}+\text{F})) / (\rho_s c_s d), \text{ where}$$

Shfx is the sensible heat flux, Levp is the evaporative flux, $(\text{S}+\text{F})$ is the net downward radiative flux, ρ_s , c_s , and d are the density, specific heat and damping depth of the soil, respectively.

The surface wetness is assumed to be constant during the model forecast, with initial values based on the host model GFS analysis. Note that this simple model is able to realistically simulate the development of the "cool pool" land temperature under landfalling tropical storms, thereby drastically reducing the surface evaporation over land leading to rapid decay over land.

This simple slab model can be contrasted with the Noah LSM developed jointly by NCAR and NCEP, which is a unified code for research and operational purposes, being almost identical to the code used in the NAM Model. This is a 4-layer soil temperature and moisture model with canopy moisture and snow cover prediction. The layer thicknesses are 10, 30, 60 and 100 cm (adding to 2 meters) from the top down. It includes root zone, evapotranspiration, soil drainage, and runoff, taking into account vegetation categories, monthly vegetation fraction, and soil texture. The scheme provides sensible and latent heat fluxes to the boundary-layer scheme. The Noah LSM additionally predicts soil ice, and fractional snow cover effects, has an improved urban treatment, and

considers surface emissivity properties. The Noah LSM is presently being run in test mode in HWRF.

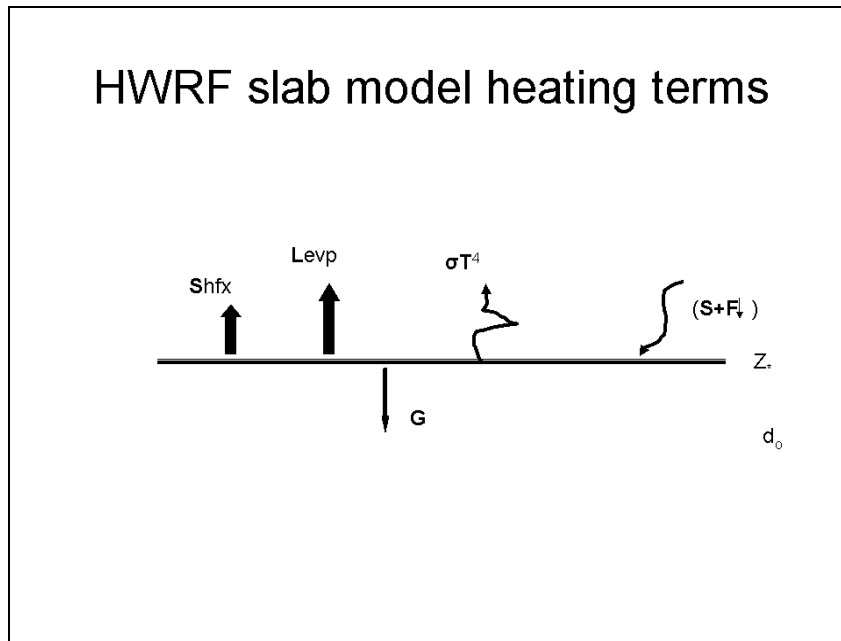


Figure 3.5. Fluxes employed in the LSM used in the GFDL and HWRF hurricane models. The surface land temperature is the only state variable predicted in this scheme. G represents the flux of heat into the ground and all other terms are defined in the text.

3.6 Planetary boundary-layer parameterization

The PBL parameterization is responsible for vertical sub-grid-scale fluxes due to eddy transports in the whole atmospheric column, not just the boundary layer. Thus, when a PBL scheme is activated, no explicit vertical diffusion is activated with the assumption that the PBL scheme will handle this process. Horizontal and vertical mixing are therefore treated independently. The surface fluxes are provided by the surface layer and land-surface schemes. The PBL schemes determine the flux profiles within the well-mixed boundary layer and the stable layer, and thus provide atmospheric tendencies of temperature, moisture (including clouds), and horizontal momentum in the entire atmospheric column. Most PBL schemes consider dry mixing, but can also include saturation effects in the vertical stability that determines the mixing. Conceptually, it is important to keep in mind that PBL parameterization may both complement and conflict with cumulus parameterization. PBL schemes are one-dimensional, and assume that there is a clear scale separation between sub-grid eddies and resolved eddies. This assumption will become less clear at grid sizes below a few hundred meters, where boundary-layer eddies may begin resolving, and in these situations the scheme should be replaced by a fully three-dimensional local sub-grid turbulence scheme, such as the Turbulent Kinetic Energy (TKE) diffusion scheme. HWRF uses a non-local vertical mixing scheme based

on the GFS PBL option with several modifications to fit hurricane and environmental conditions

The HWRF PBL scheme

The HWRF code uses the non-local scheme as the GFDL operational hurricane model (Hong and Pan 1996) which is based on Troen and Mahrt (1986), and was implemented in the GFS in 1995. Note that this scheme is similar, but not quite the same, as the Yonsei University (YSU) scheme and the Medium-Range Forecast (MRF) boundary-layer scheme.

Historically the GFS PBL scheme has given reasonable tropical cyclone tracks for the global GFS and GFDL hurricane models when packaged with the SAS cumulus scheme. The scheme is a first-order vertical diffusion parameterization that uses the surface bulk-Richardson approach to iteratively estimate the PBL height starting from the ground upward. The PBL height (h) depends on the virtual temperature profile between the surface and the PBL top, on the wind speed at the PBL top and on the critical Richardson number (Ric), and is given by

$$h = Ric \times \frac{\theta_{vg} U^2(h)}{g (\theta_v(h) - \theta_s)},$$

where, θ_{vg} and $\theta_v(h)$ are the virtual potential temperature at surface and at the PBL top, $U(h)$ is wind speed at PBL top, and θ_s is the surface potential temperature. Once the PBL height is determined, a preliminary profile of the eddy diffusivity is specified as a cubic function of the PBL height. This value is then refined by matching it with the surface-layer fluxes. The process above determines the local component of the eddy diffusivity, which can be expressed as

$$K_c(z) = \kappa \left(\frac{u_*}{\Phi_m} \right) \left[\alpha \left(1 - \frac{z}{h} \right)^2 \right],$$

where z is the height above ground, Φ_m is a wind profile function evaluated at the top of the surface layer, and α is a parameter that controls the eddy diffusivity magnitude (Zhang et al. 2012).

Additionally, a counter-gradient flux parameterization based on the surface fluxes and on the convective velocity scale (Hong and Pan 1996), is also included. This non-local effect incorporates the contribution of large-scale eddies driven by surface-layer conditions (see Figure 3.6). The overall diffusive tendency of a variable C can be expressed as

$$\frac{\partial C}{\partial t} = \frac{\partial}{\partial z} \left[K_c \left(\frac{\partial C}{\partial z} \right) - \gamma_c \right],$$

where $\partial C / \partial z$ and γ_c are the local and non-local parts, respectively.

In addition, the GFS boundary-layer formulation also considers dissipative heating, the heat produced by molecular friction of air at high wind speeds (Bister and Emanuel 1998). This contribution is controlled by namelist parameter *disheat*.

Previous studies have shown that the class of PBL schemes used in HWRf (GFS/MRF/YSU) often produces too deep a PBL when compared to observations in the hurricane environment (Braun and Tao 2000; Zhang et al. 2012). Because the magnitude of the eddy diffusivity coefficient in the HWRf PBL scheme is directly proportional to the PBL height, a deep PBL causes stronger vertical, which in turn leads to a more diffuse and larger storm. To reduce the feedback mechanism of the HWRf PBL, a couple of modifications were made in the 2013 HWRf upgrades. One was the use of a variable Ric instead of the constant value of 0.25 employed in previous implementations.. This modification was based on Vickers and Mahrt (2004), who performed several tests by using different values of Richardson numbers and Ric to investigate the sensitivity of the PBL height. They concluded that a Ric that varies with the surface Rossby number produced the best solution when compared to all methods of modification of the Richardson number. The surface Rossby number (R_o) and the dependent Ric fit to it using observational data are given by

$$R_o = (U_{10}/fz_0), \text{ and}$$

$$\text{Ric} = 0.16 (10^{-7} R_o)^{-0.18}$$

where U_{10} is the wind speed at 10-m above ground level (AGL) and f is the Coriolis parameter introduced for dimensional purposes. Vickers and Mahrt (2004) stated that there is no evidence that R_o depends on f , so the HWRf model uses a typical value of f , 10^{-4} s^{-1} .

Because the Vickers and Mahrt (2004) study did not use observational data for hurricanes, the archived datasets of the Hurricane Research Division of the NOAA Atlantic Oceanographic and Meteorological Laboratory were used to confirm that this Ric definition is applicable to hurricane conditions. By using the variable Ric method, the PBL height was matched seamlessly around the hurricane and its environment.

In the 2013 HWRf implementation, the artificial decrease of momentum diffusivity in the PBL through the use of a non-zero α parameter was maintained, and its value was increased to 0.7 from 0.5 used in the 2012 HWRf. Although the variable Ric method reduced the diffusivity in hurricane regions, analysis showed that further reduction of diffusivity was still needed to match the observational data.

This GFS PBL scheme can be contrasted with local schemes such as the Mellor-Yamada-Janjic (MYJ) PBL used in NAM, which is an option for experimental, non-supported, versions of HWRf. This parameterization of turbulence in the PBL and in the free atmosphere (Janjic 1990a,b, 1996a, 2002) represents a nonsingular implementation of the Mellor-Yamada Level 2.5 turbulence closure model (Mellor and Yamada 1982) through the full range of atmospheric turbulent regimes. In this implementation, an upper limit is imposed on the master length scale. This upper limit depends on the TKE as well as the buoyancy and shear of the driving flow. In the unstable range, the functional form of the

upper limit is derived from the requirement that the TKE production be nonsingular in the case of growing turbulence. In the stable range, the upper limit is derived from the requirement that the ratio of the variance of the vertical velocity deviation and TKE cannot be smaller than that corresponding to the regime of vanishing turbulence. The TKE production/dissipation differential equation is solved iteratively. The empirical constants used in the original Mellor-Yamada scheme have been revised (Janjic 1996a, 2002). Interestingly, the MYJ PBL scheme is quite similar to the Mellor-Yamada Level 2.5 scheme used in the early operational versions of the GFDL hurricane model. Note that the TKE in the MYJ boundary-layer scheme has a direct connection to the horizontal diffusion formulation in the NNM-E grid and NMM-B grid dynamic cores, but this has been turned off in HWRF.

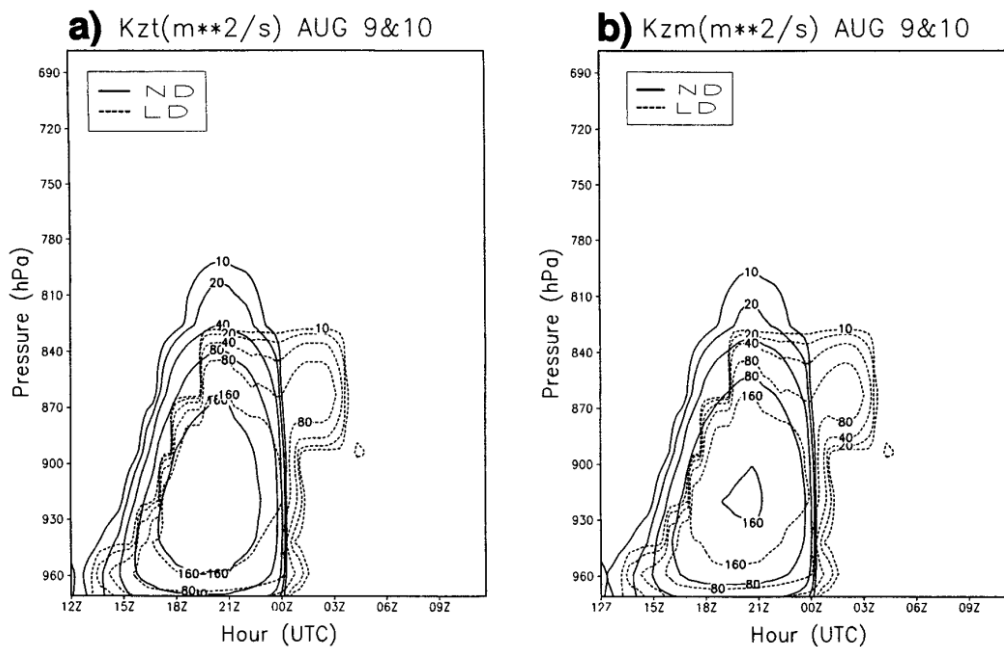


FIG. 2. Time–pressure cross sections of the eddy diffusivity ($\text{m}^2 \text{s}^{-2}$) calculated with the local (dotted) and nonlocal (solid) schemes and for (a) thermal and (b) momentum.

Figure 3.6. Time–pressure cross sections of the eddy diffusivity ($\text{m}^2 \text{s}^{-1}$) calculated with the local (dotted) and nonlocal (solid) schemes and for (a) thermal and (b) momentum. The GFS boundary layer uses the nonlocal formulation in which the eddy mixing is due in part to surface conditions (Hong and Pan 1996).

3.7 Atmospheric radiation parameterization

Radiation schemes provide atmospheric heating due to radiative flux divergence and surface downward longwave and shortwave radiation for the ground heat budget. Longwave radiation includes infrared or thermal radiation absorbed and emitted by gases and surfaces. Upward longwave radiative flux from the ground is determined by the surface emissivity that in turn depends upon land-use type, as well as the ground (skin)

temperature. Shortwave radiation includes visible and surrounding wavelengths that make up the solar spectrum. Hence, the only source is the sun, but processes include absorption, reflection, and scattering in the atmosphere and at surfaces. For shortwave radiation, the upward flux is the reflection due to surface albedo. Within the atmosphere, radiation responds to model-predicted cloud and water vapor distributions, as well as specified carbon dioxide, ozone, and (optionally) trace gas concentrations and particulates. All the radiation schemes in WRF currently are column (one-dimensional) schemes, so each column is treated independently, and the fluxes correspond to those in infinite horizontally uniform planes, which is a good approximation if the vertical thickness of the model layers is much less than the horizontal grid length. This assumption would become less accurate at high horizontal resolution, especially where there is sloping topography. Atmospheric radiation codes are quite complex and computationally intensive and are therefore often invoked at less frequent intervals than the rest of the model physics. The HWRF radiation parameterization used in operations is that from GFDL (see below) and is similar to the one used in the NAM. Compared to extra-tropical phenomena, hurricanes are less dependent on radiative fluxes except when migrating out of the tropics and/or progressing over land. Radiation-cloud interactions may be more important than direct radiative impacts, except during extra-tropical transition.

The Eta GFDL longwave scheme

This longwave radiation scheme follows the simplified exchange method of Fels and Schwarzkopf (1975) and Schwarzkopf and Fels (1991), with calculation over spectral bands associated with carbon dioxide, water vapor, and ozone. Included are Schwarzkopf and Fels (1985) transmission coefficients for carbon dioxide, a Roberts et al. (1976) water-vapor continuum, and the effects of water-vapor carbon dioxide overlap and of a Voigt line-shape correction. The Rodgers (1968) formulation is adopted for ozone absorption. Clouds are randomly overlapped. More recent versions of the GFDL longwave radiation scheme, such as the one used in the NAM model but not adopted in HWRF, contain parameters for urban effects, as well as surface emissivities that can be different than 1.0.

The Eta GFDL shortwave scheme

This shortwave radiation is a GFDL version of the Lacis and Hansen (1974) parameterization. Effects of atmospheric water vapor, ozone (both from Lacis and Hansen 1974), and carbon dioxide (Sasamori et al. 1972) are employed. Clouds are randomly overlapped. Shortwave calculations are made using a daylight-mean cosine solar zenith angle for the specific time and grid location averaged over the time interval (given by the radiation call frequency). The newest version of the GFDL shortwave radiation scheme, used for example in the NAM model but not adopted in HWRF, contains parameters for urban effects.

3.8 Physics interactions

While the model physics parameterizations are categorized in a modular way, it should be noted that there are many interactions between them via the model-state variables (potential temperature, moisture, wind, etc.) and their tendencies, and via the surface fluxes. The surface physics, while not explicitly producing tendencies of atmospheric state variables, is responsible for updating the land-state variables as well as updating fluxes for ocean coupling. Note also that the microphysics does not output tendencies, but updates the atmospheric state at the end of the model time-step. The radiation, cumulus parameterization, and PBL schemes all output tendencies, but the tendencies are not added until later in the solver, so the order of call is not important. Moreover, the physics schemes do not have to be called at the same frequency as each other or at the basic model dynamic time step. When lower frequencies are used, their tendencies are kept constant between calls or time interpolated between the calling intervals. In contrast to HWRF, note that the GFDL hurricane modeling system calls all physics packages once per time step except for radiation. The land-surface and ocean models, excluding simple ones, also require rainfall from the microphysics and cumulus schemes. The boundary-layer scheme is necessarily invoked after the land-surface scheme because it requires the heat and moisture fluxes.

4.0 Design of Moving Nest

HWRF, which uses the NMM dynamic core under the WRF model software framework, supports moving, one- or two-way interactive nests. While WRF-NMM can handle multiple stationary domains at the same nest level, and/or multiple nest levels (telescoping) with two-way interaction, the HWRF configuration employs a single domain per nest level. In HWRF, the 9- and 3-km domains follow the storm, while the 27-km parent domain is stationary. When more than one tropical storm is observed, more than one independent run of HWRF is launched so that every storm has its own high-resolution moving nest.

In the current implementation of the nesting algorithm, only horizontal refinement is available, that is, there is no vertical nesting option. The nested grids adopt ratio 1:3 to refine the resolution of the coarse and fine grids based on Arakawa-E grid staggering structure. Correspondingly, the time-step ratio between the coarse and fine grids is 1:3 as well. The mass points of the nested grids are aligned with those of the coarser grids in which they are nested. The coincidence of grid points between the parent and nested domains simplifies remapping and feedback procedures. The design of constructing nesting grids also conforms to the parallel strategy within the WRF advanced software framework (Michalakes et al. 2004) and enhances code portability of the model for various applications. HWRF inherits time-controlling capabilities of WRF-NMM, which means that HWRF can initialize and terminate the integration of nested grids at any time during the model run. In the operational implementation, nested grids are present throughout the entire forecast.

4.1 Grid Structure

As described in the NMM scientific documentation (Janjic et al. 2010), the WRF-NMM is a non-hydrostatic model formulated on a rotated latitude-longitude, Arakawa E-grid, with a vertical-pressure sigma hybrid vertical coordinate system. The rotated latitude-longitude coordinate is transformed in such a way that the coordinate origin is located in the center of the parent domain, and the x-axis and y-axis are aligned with the new coordinate equator and the prime meridian through the domain center, respectively (Figure 4.1). To address multi-scale forecasting, a horizontal mesh refinement capability was developed for this system. All interpolations from the parent to the nested domain are achieved on a rotated latitude-longitude E-grid. The nested domain can be freely moved anywhere within the grid points of the parent domain, yet the nested domain rotated latitude-longitude lines will always coincide with the rotated latitude-longitude lines on the mass grid of the parent domain at fixed parent-to-nest grid-size ratio 1:3.

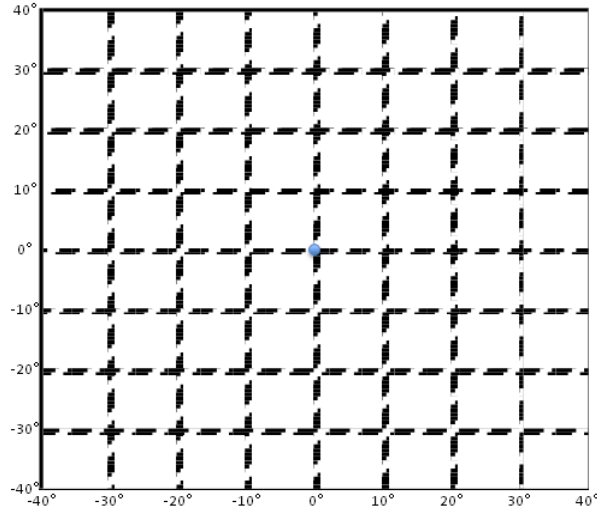


Figure 4.1 Schematic rotated latitude and longitude grid. The blue dot is the rotated latitude-longitude coordinate origin. The origin is the cross point of the new coordinate equator and zero meridian, and can be located anywhere on Earth.

4.2 Terrain Treatment

Terrestrial properties are important external forcing on the dynamics and thermodynamics of any numerical models. The impact of terrain effects on TC track, intensity and structure has been recognized in many previous studies (e.g. Lin 2007). Therefore, careful treatment of static terrestrial conditions such as terrain and land-sea contrast is necessary to contain contamination and possible computational noise in the modeled solution due to improper adjustment from coarse- to fine-resolution terrestrial information.

The terrain treatment in the HWRf system is tailored to the TC problem by using high-resolution topography to account for the detailed topographic effects of the complex islands and landmasses. Before the forecast starts, WPS is used to interpolate topography information from prescribed high-resolution-terrain datasets to the required grid resolution over the entire parent domain to ensure the movable nests always have access to high-resolution topography. For example, in a typical operational forecast at 27 km with two center-aligned movable nests at 9- and 3-km resolutions, terrestrial data are generated at all three resolutions for the entire static parent domain shown in Figure 4.2. This way, it always has access to high-resolution topographic information when the grid moves during the forecast.

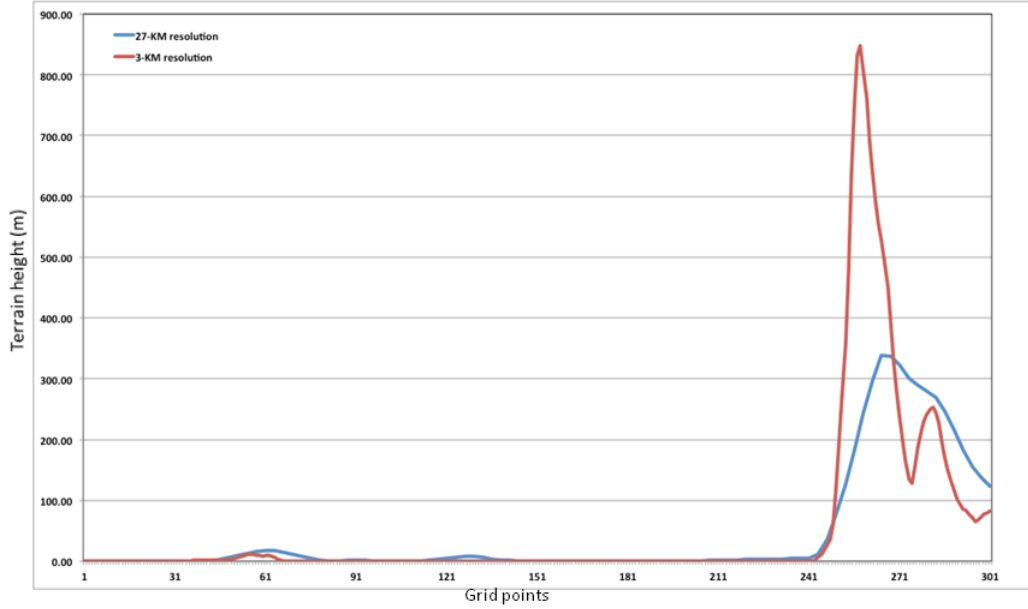


Figure 4.2 An example of topography differences in model for domains at 27- (blue) and 3-km (red) resolutions, respectively. The cross section is along latitude 22°N, between longitudes 85.28°W and 79.32°W. The biggest differences are in the mountainous area of Eastern Cuba.

Topography is the only static dataset generated in high resolution. For pragmatic considerations, all other static terrestrial information for nests is downscaled from the coarser-resolution parent domain.

The terrain within the nest is smoothed before being used. The grids are smoothed through a four-point weighted average with a special treatment at the four corners. Points in the inner part of the domain are smoothed using

$$\bar{t}_{hr}(i, j) = 0.25 * [t_{hr}(i + 1, j) + t_{hr}(i, j + 1) + t_{hr}(i - 1, j) + t_{hr}(i, j - 1)],$$

where t_{hr} is the high-resolution terrain in a nest. Points along the boundary use a modified equation. For example, for the western boundary, the equation is

$$\bar{t}_{hr}(1, j) = 0.125 * [t_{hr}(1, j - 1) + t_{hr}(1, j + 1)] + 0.75 * t_{hr}(1, j).$$

The smoothed topography in the corner points also follows a modified formula. For example, the average terrain at the southwest point is given by

$$\bar{t}_{hr}(1, 1) = 0.75 * t_{hr}(1, 1) + 0.125 * t_{hr}(2, 2) + 0.0625 * [t_{hr}(2, 1) + t_{hr}(1, 2)]$$

Certainly, the high-resolution terrain conforms to land-sea mask binary categories, that is, only land points have terrain assigned.

4.3 Moving Nest Algorithm

The use of enhanced resolution only in the TC region is a pragmatic solution commonly adopted in the tropical cyclone NWP community to reduce computational costs. For the TC to be consistently contained in the highest-resolution domain, that domain has to move to follow the storm.

The nest motion for tropical cyclones and tropical depressions is currently based on the GFDL Vortex Tracker (Section 5). Nine fields are calculated, with pressure-level fields interpolated by $\log(P)$. Vorticity, MSLP and geopotential height fields are smoothed using an iterative smoother. The wind fields are not smoothed – that is a bug fix from last year. Then their extremes, known as *fix locations* are calculated:

1-3. Minimum wind speed at 10 meters, 850 hPa and 700 hPa

4-6. Maximum 10-meter vorticity at 10 meters, 850 hPa and 700 hPa

7. Minimum MSLP

8-9. Minimum geopotential height at 700 and 850 hPa

Once all nine fix locations have been calculated, the standard deviation of the fix locations with respect to the domain center is calculated. Fix locations far from the domain center are discarded. The maximum allowed distance differs by parameter and varies with time, based on prior fix-to-center standard deviations. Once the final set of parameters is chosen, the mean fix location is used as the storm center. The standard deviation of the fix parameters is stored for discarding fix parameters at later time steps. Lastly, the nest is moved if the storm location is more than two parent gridpoints in the Y (rotated north-south) direction or more than one parent gridpoint in the X (rotated east-west) direction. One should note that, while at every time-step numerous fields are passed between domains before and after the grid motion, the interpolation and hydrostatic mass balancing are also applied in the region of the leading edge of the moving nest as described in the next subsection.

4.4 Fine Grid Initialization

The generation of initial conditions for the HWRP parent domain is discussed in Chapter 1. For the nests, all variables, except topography, are initialized using the corresponding variables downscaled from the parent grid during the integration. To alleviate potential problems related to singularities due to high-resolution terrestrial information in the nested domain, the initialization of the land variables, such as land-sea mask, soil temperature, and vegetation type, are exclusively initialized through a nearest-neighbor approach at the initial timestep and the leading edge during the integration.

To obtain the temperature, geopotential, and moisture fields for the nest initialization, hydrostatic mass balance is applied. The first step is to horizontally interpolate coarser-resolution data to the fine-resolution grid. The second step is to apply the high-resolution terrain and the geopotential to determine the surface pressure on the nest. The pressure values in the nest hybrid surfaces are then calculated. The final step is to compute the

geopotential, temperature, and moisture fields on the nest hybrid surfaces using linear interpolation in a logarithm of pressure vertical coordinate. The schematic procedure is illustrated in Figure 4.3. The zonal and meridional components of the wind are obtained by first performing a horizontal interpolation from the parent to the nest grid points using a bi-linear algorithm over the diamond-shaped area indicated in grey in Figure 4.4. The wind components are then linearly interpolated in the vertical from the parent hybrid surfaces onto the nest hybrid surfaces. Note that, while the hybrid levels of the nest and parent in sigma space coincide, the nest and the parent do not have the same levels in pressure or height space. This is due to the differing topography, and consequently different surface pressure between the nest and the parent.

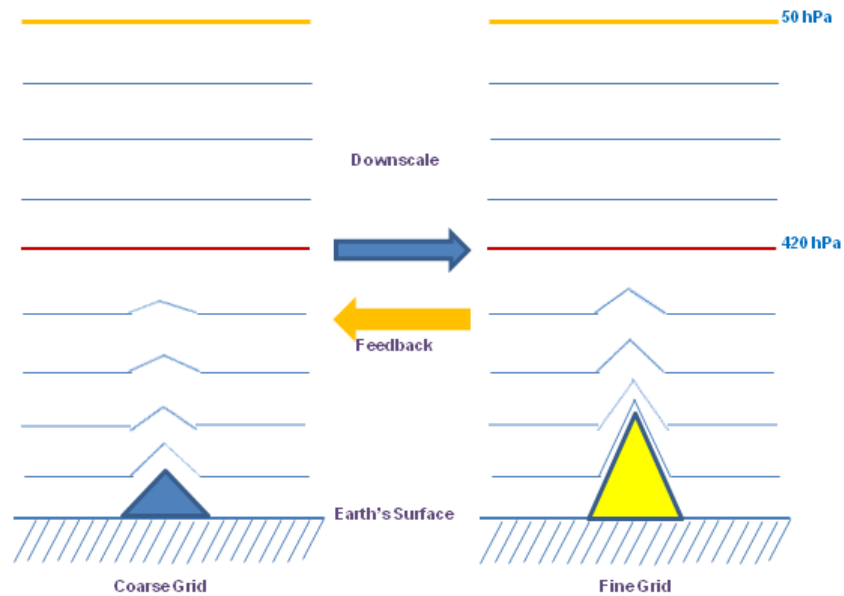


Figure 4.3 An illustration of the vertical interpolation process and mass balance. Hydrostatic balance is assumed during the interpolation process.

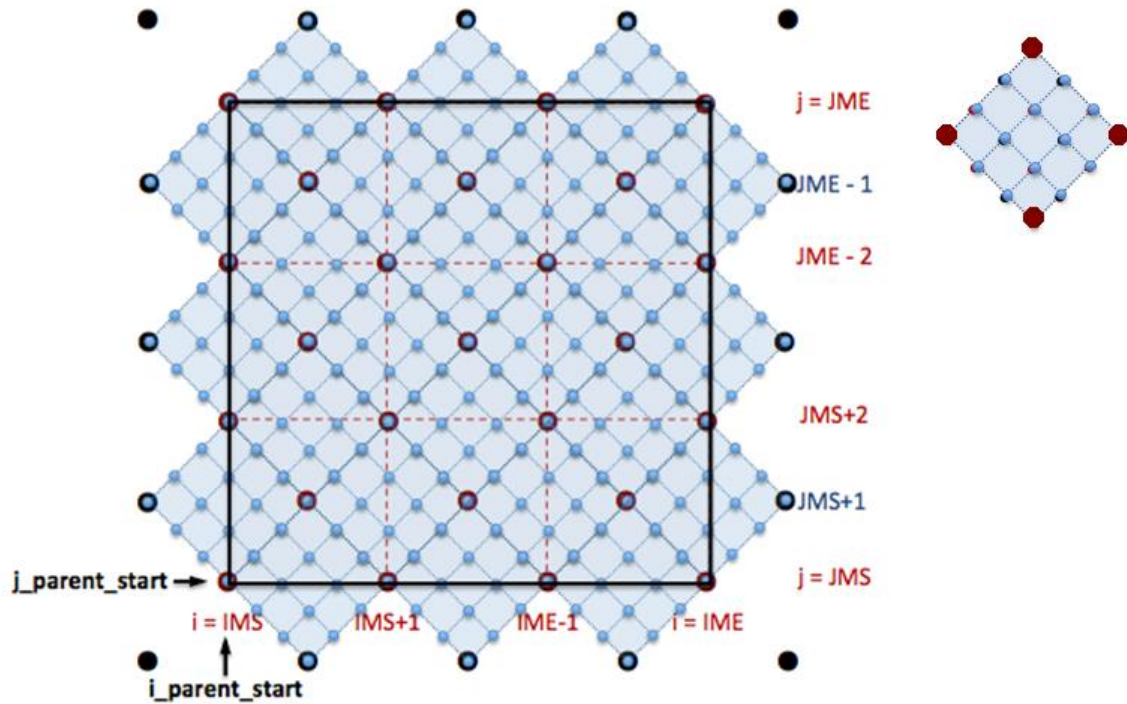


Figure 4.4 The schematic E-grid refinement - dot points represent mass grid. Big and small dots represent coarse- and fine resolution grid points, respectively. The black square represents the nest domain. The diamond square on the right side is composed of four big dot points representing the bilinear interpolation control points.

4.5 Lateral Boundary Conditions

Figure 4.5 illustrates a sample E-grid structure, in which the outermost rows and columns of the nest are termed the prescribed interface, and the third rows and columns are termed the dynamic interface. The prescribed interface is forced to be identical to the parent domain interpolated to the nest grid points. The dynamic interface is obtained from internal computations within the nest. The second rows and columns are a blend of the first and third rows/columns. Because the prescribed interface is well separated from the dynamic interface in the E-grid structure, nested boundaries can be updated at every time step of the parent domain exactly the same way as the parent domain boundary is updated from the external data source. This is done using bi-linear interpolation and extrapolation using the same mass adjustment procedure previously described. This approach is simple, and yet produces an effective way of updating the interface without excessive distortion or noise.

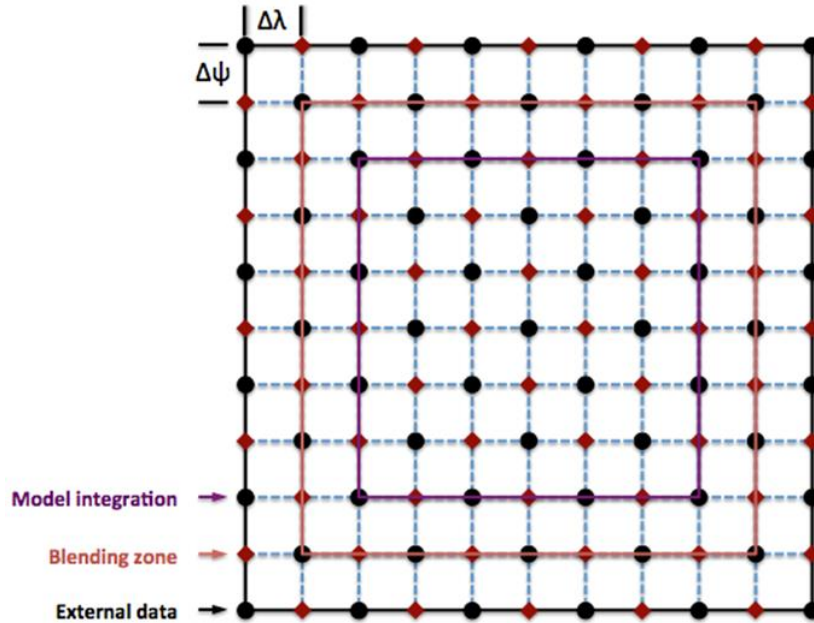


Figure 4.5 Lateral boundary-condition buffer zone - the outmost column and row are prescribed by external data from either a global model or regional model. The blending zone is an average of data prescribed by global or regional models and those predicted in the HWRF domain. Model integration is the solution predicted by HWRF. $\Delta\psi$ and $\Delta\lambda$ are the grid increment in the rotated latitude-longitude coordinate.

4.6 Feedback

The feedback from fine-resolution domain to coarse-resolution domain is an important process for a hurricane forecast model. It reflects the multiple-scale physical interactions in the hurricane environment. This is done using the same mass adjustment procedure previously described, except that the parent pressure is retained. In addition, rather than horizontal interpolation, horizontal averaging is used: the nine fine-grid points surrounding a coarser-resolution grid point are used before the mass adjustment process. Furthermore, feedback is done with a 0.5 weighting factor, replacing the coarse-grid data with the average of the coarse and fine-grid data. In addition, to avoid a nest directly modifying its boundary conditions, a one-parent gridpoint row and column buffer region is maintained in the parent domain, that does not receive data from the nest. In cases with multiple nests at the same level (which does not happen in the operational 2014 HWRF configuration), nests feed back to the parent in numerical order (grid 1, then 2, then 3, etc.) Each has 50% feedback, resulting in a smoothed average in the parent, in regions where nest domains overlap.

5.0 Use of the GFDL Vortex Tracker

5.1 Introduction

Numerical modeling has become an increasingly important component of hurricane research and operational hurricane forecasting. Advances in modeling techniques, as well as in fundamental understanding of the dynamics of tropical cyclones, have enabled numerical simulations of hurricanes to become more realistic and contributed to more skillful hurricane forecasts. One critical element of assessing the performance of a hurricane model is the evaluation of its track and intensity forecasts. These forecasts are typically represented in the form of text data that are output either directly from the forecast model or in a post-processing step of the modeling system using an external vortex tracker. This document provides a description of the GFDL vortex tracker (Marchok 2002), which operates as a standalone tracking system in a post-processing step. The GFDL vortex tracker has been used as an operational tool by NCEP since 1998, and it is flexible enough to operate on a variety of regional and global models of varying resolutions. The tracker was updated in 2012 enabling it to function in a mode in which it will also detect new cyclones the model develops during the course of a forecast, but this capability is not used operationally.

5.1.1 Purpose of the vortex tracker

A numerical model produces an abundance of digital output, with up to hundreds of variables on dozens of vertical levels, including variables for mass, momentum, density, moisture, and various surface- and free-atmosphere fluxes. While a tropical cyclone's center is defined by its low-level circulation features, a comparison of synoptic plots of various low-level parameters will often reveal a range of variability in a storm's center position. This variability can be particularly great for storms that are either just forming or are undergoing extratropical transition. Figure 5.1 illustrates this variability for a case of Tropical Storm Debby (2006) in an analysis from the NCEP GFS. At this time, Debby was a weak, 40-kt tropical storm, and the variability in the center location fixes indicates that the model had not yet developed a coherent vertical structure for the storm.

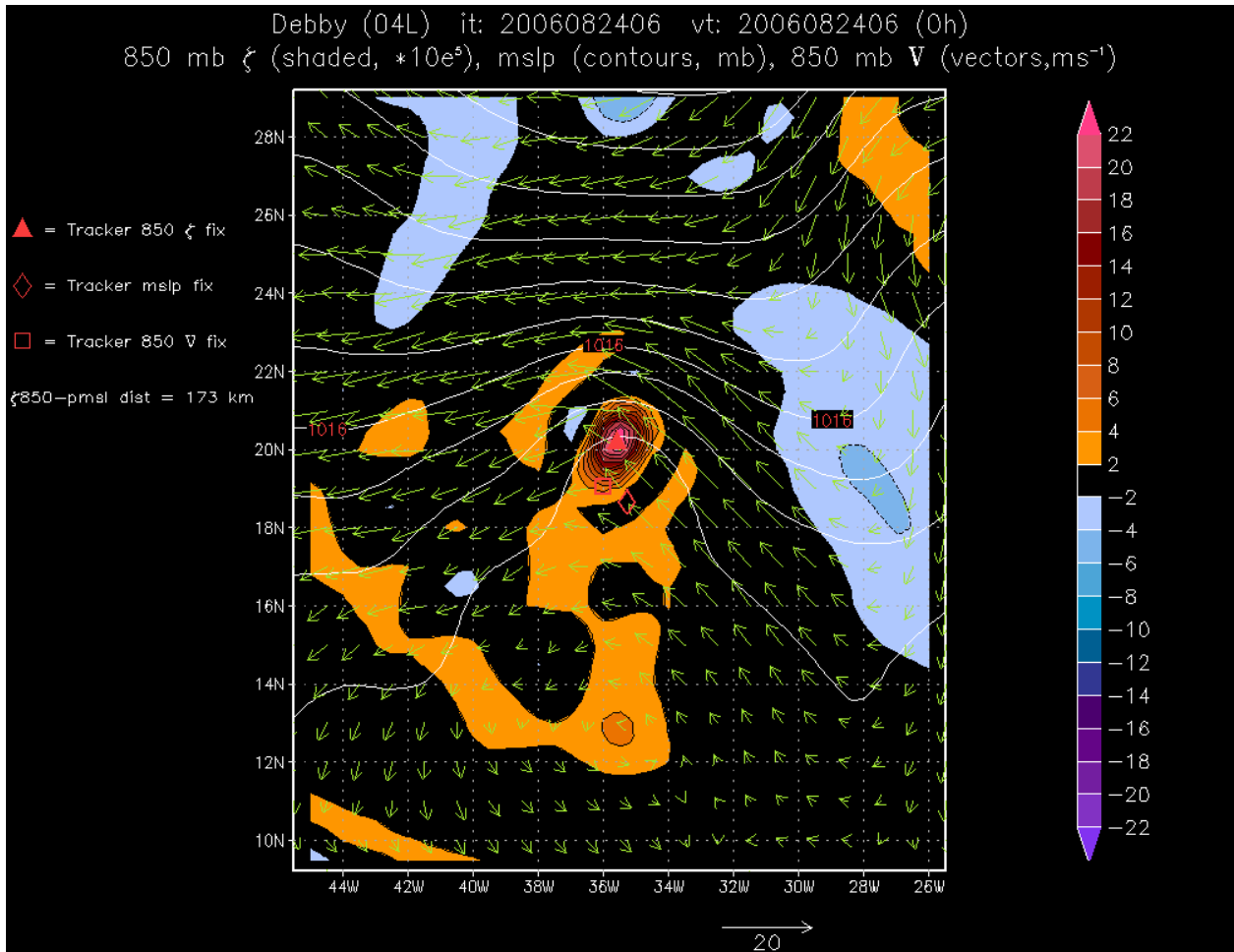


Figure 5.1: Mean sea-level pressure (contours, mb), 850-mb relative vorticity (shaded, $s^{-1} \times 10^5$) and 850-mb winds (vectors, ms^{-1}) from the NCEP GFS analysis for Tropical Storm Debby, valid at 06 UTC 24 August 2006. The triangle, diamond, and square symbols indicate the locations at which the GFDL vortex tracker identified the center position fix for each of the three parameters. The notation to the left of the synoptic plot indicates that the distance between the 850-mb vorticity center and the mslp center is 173 km.

A vortex tracker is needed to objectively analyze the data and provide a best estimate of the storm's central position and then track the storm throughout the duration of the forecast. Depending on the complexity of the tracker, additional metrics can be reported, including the minimum sea-level pressure, the maximum near-surface wind speed, the radii of gale-, storm- and hurricane-force winds in each storm quadrant, parameters that describe the thermodynamic structure or phase of the storm, and parameters that detail the spatial distribution of the near-surface winds. This document will focus primarily on the basic functioning of the tracker and its reporting of the track, intensity, and wind radii parameters.

5.1.2 Key issues in the design of a vortex tracker

When designing a tracking scheme, there are a couple of fundamental issues that must be considered. The first issue is deciding on the method used to locate a maximum or a minimum in some field of values. There are numerous methods that can be used for this purpose. The simplest method is to scan the field of values and pick out the maximum or minimum at one of the model output grid points. However, this method restricts the maximum or minimum value to being located at one of the fixed data points on the grid. For many grids, especially those with coarser resolutions, the actual maximum or minimum value may fall between grid points. The data can be interpolated to a finer resolution, but interpolation is a procedure that can be both expensive and complicated to generalize for usage with both regional and global grids over a range of resolutions. In addition, a problem can still remain after interpolation whereby the tracking scheme needs to choose between two or more candidate points with identical values that are located close to one another. The GFDL vortex tracker uses a scheme that employs a Barnes analysis of the data values at each candidate grid point to provide a field of values that have been weight-averaged based on distance from the candidate grid point. This technique, which will be described in detail below, helps to mitigate the issues described above.

The second issue involves finding the right balance between making the scheme sensitive enough so that it can detect and track weaker storms, and making it overly sensitive such that it continues tracking for too long and tracks weak remnants that no longer resemble a cyclone, or worse, it jumps to a stronger passing storm and begins tracking that storm instead. There are several checks that have been included in the GFDL vortex tracker, some with thresholds that can be adjusted either in the source code or via namelists as inputs to the executable. These will be described below.

The remainder of this document will describe in detail the design and functioning of the GFDL vortex tracker. Section 5.2 will focus on the design of the tracker and the input data that it needs. Section 5.3 presents a discussion of the various low-level parameters that are tracked and how they are combined to produce a mean position fix at a given lead time. Section 5.4 describes how the maximum wind and the various wind radii in each storm quadrant are obtained. Section 5.5 describes diagnostics that are performed by the tracker to analyze the thermodynamic phase of a model cyclone. Section 5.6 details usage of the tracker for the purpose of detecting and tracking new, model-generated storms, and Section 6.7 provides detail on the tracker output.

5.2 Design of the tracking system

5.2.1 Input data requirements

The GFDL vortex tracker can operate in two different modes. In the basic mode, it will perform tracking only for storms that have been numbered by a Regional Specialized Meteorological Center (RSMC), such as the National Hurricane Center (NHC). It can also operate in a mode in which it detects and tracks new storms a model generates during the course of a forecast.

5.2.1.1 Synoptic forecast data

The tracker requires input data to be in Gridded Binary (GRIB) version 1 format, on a cylindrical equidistant, latitude-longitude (lat/lon) grid. While the dx and dy grid increments each need to be uniform across the grid, dx does not need to be equal to dy. The data should be ordered so that j and i increment from north to south and east to west, respectively, such that point (1,1) is in the far northwestern part of the grid, and point (imax,jmax) is in the far southeastern part of the grid. Data files that instead have data values incrementing from south to north can be flipped prior to execution of the tracker using an external GRIB file manipulation tool.

The data files do not need to have regular spacing for the lead time intervals. This flexibility allows the user to obtain tracker output using output model data at more frequent time intervals around a particular time of interest. The tracker reads in a list of forecast lead times from a text file the user prepares. The tracker has the ability to process GRIB files that have the lead times identified in the Product Definition Section (PDS) of the GRIB header as either hours or minutes. The choice for using either minutes or hours is passed to the program via a namelist option. Regardless of which choice is made, those lead times must be listed in the user input text file as integers in units of minutes (the exact required format can be seen in the read statement in subroutine read_fhours), and then the tracker can manipulate the hours and minutes as needed.

5.2.1.2 Real-time observed storm data

The tracker works by searching for a vortex initially at a location specified by a 1-line text record produced by either NHC for storms in the Atlantic, eastern Pacific and central Pacific basins, or by the Joint Typhoon Warning Center (JTWC) for storms in other global basins. This record contains just the basic, vital information necessary to define the observed location and intensity parameters of the storm, and it is commonly referred to as the “TC vitals” record. An example TC vitals record is shown here for Katrina for the observed time of 00 UTC 29 August 2005:

```
NHC 12L KATRINA 20050829 0000 272N 0891W 335 046 0904 1006 0649 72 037  
0371 0334 0278 0334 D 0204 0185 0139 0185 72 410N 815W 0167 0167 0093 0167
```

The critical information needed from the TC vitals record for tracking is the Automated Tropical Cyclone Forecast (ATCF) ID number for the storm (12L), the observed time (20050829 0000), and the location of the storm, indicated here as “272N 0891W”, or 27.2° North, 89.1° West. For this example, the tracker would start looking for Katrina in the 00 UTC 29 August 2005 analysis for a given model at 27.2° North, 89.1° West, and if it finds a storm near there, it records its position, writes out a record in a specific text format that contains critical storm forecast location and intensity forecast data, and then makes a guess for the next position at the next forecast lead time to begin searching again.

5.2.2 The search algorithm

To locate a maximum or minimum value for a given variable, we employ a single-pass Barnes analysis (Barnes 1964, 1973) at grid points in an array centered initially around the NHC-observed position of the storm. We refer to this NHC-observed position as the initial guess position. For a given variable F , the Barnes analysis, B , at a given point, g , in this array is given as:

$$B(g) = \frac{\sum_{n=1}^N w_n F(n)}{\sum_{n=1}^N w_n} \quad (5.2.1.2.1)$$

where w is the weighting function defined by:

$$w = e^{-(d_n^2/r_e^2)} \quad (5.2.1.2.2)$$

and where d_n is the distance from a data point, n , to the grid point, g , and r_e is the e-folding radius. The e-folding radius is the distance at which the weighting drops off to a value of $1/e$, and this value can be adjusted. Currently, most regional and global model grids fall into a category with output file grid spacing between about 0.1° and 1.25° , and for those we use a value of $r_e = 75$ km. For any models with resolutions coarser than 1.25° , we use a value of $r_e = 150$ km. For model grids with a grid spacing finer than 0.1° , we use a value of $r_e = 60$ km. The overriding idea is that we want to find a balance whereby we include enough points in the averaging process to produce a weighted average from the Barnes function that is representative of the surrounding region, but not so many points that finer scale details are smoothed out to the point that it's difficult to differentiate the average value at one grid point from that of an adjacent point.

The Barnes analysis provides an array of Gaussian weighted-average data values surrounding the initial guess position. The center is defined as the point at which this function is maximized (e.g., Northern Hemisphere relative vorticity) or minimized (e.g., geopotential height, sea-level pressure, Southern Hemisphere relative vorticity), depending on the parameter being analyzed.

As described above, the center location for a given parameter will often lie between grid points, and this is especially true for coarser resolution grids. To produce a position fix with enough precision such that center fixes for variables with center locations between grid points can be properly represented, it may be necessary to perform several iterations of the Barnes analysis. In the initial iteration, a Barnes analysis grid is defined with grid spacing equal to that of the input data grid, and the weighted values from the Barnes analysis are assigned to the points on the analysis grid. The difference between the input data grid and the Barnes analysis grid is that the input data grid has specific (i,j) locations that are fixed, while for the analysis grid we can define an array of points, relative to the guess position in latitude-longitude space. After a position fix is returned from the first iteration of the Barnes analysis, we can perform an additional iteration of the Barnes analysis, this time centering the analysis grid on the position fix from the first iteration. In this second iteration, the search area for the center location is restricted, and the grid spacing of the Barnes analysis grid is halved in order to produce a finer resolution

position fix. We can iterate this process a number of times and run the Barnes analysis over increasingly finer resolution analysis grids in order to more precisely fix the center position. In the current version of the tracker, we specify a variable (“nhalf”) to indicate that five additional iterations of the Barnes analysis should be done for grids with spacing greater than 0.2° . For example, for a grid with original grid spacing of 1° , halving the analysis grid spacing five times would result in a final analysis grid spacing of approximately 3 km, which is already beyond the one-tenth of a degree precision contained in the observational Best Track dataset. For data grids with original spacing of less than 0.2° , such as the operational HWRF, only two additional Barnes iterations are performed, and for grids with spacing less than 0.05° , only one additional Barnes iteration is performed.

5.2.3 Tracking a vortex throughout a forecast

A tracking algorithm ultimately produces a set of points that contains information on the forecast location of the storm at discrete time intervals. The challenge is ensuring that the points that are connected from one lead time to the next do, in fact, represent points from the same storm and that there is no “contamination” introduced by accidentally having the tracker follow a different storm. This challenge becomes greater for model output with longer intervals between lead times. For example, it is far easier to know with certainty that a nearby storm is the same storm that we have been tracking up to this time if the last position fix only occurred 30 minutes ago in model time as opposed to it having occurred 12 hours ago. This section deals with how the model handles the tracking of a vortex from one lead time to the next and what types of quality control checks are applied.

5.2.3.1 Tracking from one lead time to the next

If the tracker finds a storm at a given lead time, it needs to know where to begin searching for the storm at the next lead time. There are two methods that the tracker employs for this purpose. In the first method, a Barnes analysis is performed for the location at which the tracker position fix was made for the current lead time. This analysis is performed for the winds at 500, 700, and 850 mb, using a relatively large e-folding radius of 500 km. The idea here is to create smoothed fields that represent the mean fields at each level. The mean values from these three levels are then averaged together to give a wind vector that can be used as a deep-layer mean steering wind. A hypothetical parcel is then advected according to the deep-layer mean wind for the length of the lead time interval in order to produce a dynamically generated guess position for the next lead time.

The second method uses a basic linear extrapolation of the current model storm motion. For all lead times after the initial time, this method can be employed by using the previous and current forecast position fixes. For the initial time, there is obviously no previous position from the current model forecast to use for an extrapolation; however, this extrapolation method is still used at the initial time by instead using the observed storm motion vector information that is read from the TC vitals record. However, this

method of using the storm motion vector is not as reliable because the observed storm motion vector may differ from the model storm motion vector.

The estimates from these two methods are averaged together to produce a position guess around which the tracker will begin searching for the storm at the next lead time. Both of these methods use estimates that are static in time, and therefore, error is introduced in the position guesses. Those errors obviously grow larger with increasingly longer lead-time intervals. However, it is important to note that these are only position guesses, and the tracker will allow a position fix to be made up to a certain distance from that position guess. Experience in operations has shown the combination of these two methods to be a reliable means of providing position guesses for successive lead times, even for model output with lead-time intervals of 12 hours. Cases that should be watched for trouble with the use of this method include those in which the storm begins to rapidly accelerate or decelerate, and those in which the storm is rapidly recurving into the westerlies.

5.2.3.2 Quality control checks

Once the tracker has produced a position fix at a given lead time, a number of checks are performed to help ensure that the system the tracker found is not only a storm, but also is the same storm that has been tracked to this point in the forecast. As a first check, the sea-level pressures of the points surrounding the position fix are evaluated to determine whether a pressure gradient exceeding a particular threshold exists and is sloped in the correct direction. This is a fairly easy criterion for a storm to satisfy since the requirement is only that it be satisfied for any azimuthal direction, and not that it be satisfied by a mean gradient value. The threshold can be set by the user in the run script by specifying its value in the “mslpthresh” variable. In the current version of the tracker, the mslpthresh variable is set to a value of 0.0015 mb/km, which is equivalent to 0.5 mb per 333 km.

A second check involves the wind circulation at 850 mb. The tangential component of the wind (V_T) is computed for all points within 225 km of the position fix, and the mean V_T must be cyclonic and exceed a user-specified threshold. This threshold is also set in the run script by specifying the value of the v850thresh variable. This variable has units of m/s and is set in the current version of the tracker to 1.5 m/s.

For a third check, the distance between the position fixes for two parameters is evaluated to ensure it does not exceed a specified distance. As will be described below in Section 5.3, the tracker finds the center location of several different low-level parameters. If the distance between the mean sea-level pressure (mslp) and 850-mb relative vorticity position fixes becomes too large, it could indicate either that the storm is becoming too disorganized due to dissipation or that it is undergoing extratropical transition and the tracker may have perhaps incorrectly “locked on” to a different storm nearby with one of those two parameter fixes. In either case, if that distance is exceeded, the tracker will stop tracking for this particular storm. That distance threshold is specified by the variable “max_mslp_850” in subroutine tracker, and it is currently set at 323 km for most models, including HWRF.

One final check is made of the model storm’s translation speed. The current and previous position fixes are used to calculate the average speed that the model storm must have

traveled in order to reach the current position, and if that speed exceeds a certain threshold, then the tracker assumes that it has incorrectly locked on to a different storm nearby and tracking is stopped for this storm. That speed is specified by the “maxspeed_tc” variable in module error_parms and is currently set to a value of 60 kt. It should be noted here that during the evaluation of model forecasts from the Hurricane Forecast Improvement Project (HFIP) High Resolution Hurricane (HRH) test in 2008, this storm translation speed check was responsible for erroneously stopping a number of forecasts. The problem arose for cases in which a very weak model storm center reformed after only 30 minutes of model time at a location more than 100 km away. While such behavior is reasonable for a very weak but developing storm to exhibit, this large shifting of storm position over a very short time period resulted in a computed translation speed that exceeded the threshold. If necessary, this problem can be circumvented by setting the maxspeed_tc threshold to an unrealistically high value.

It is important to point out that while these last two quality-control checks will occasionally terminate tracking for storms that are undergoing extratropical transition (ET), the intended purpose is not to stop tracking when ET is taking place. To the contrary, we want to continue tracking in order to provide track and intensity guidance for as long as possible in the forecast, and furthermore the model forecast of the onset of ET may not correspond at all to what happens with the observed storm. These last two checks are instead meant to stop tracking if the tracker detects that it may have erroneously begun to track a different, nearby storm.

The current version of the tracker has code in it that will report on the thermodynamic phase of the system, that is, whether the system is tropical, extratropical, etc. This code requires input data that has been interpolated to certain levels and/or averaged, as will be described in Section 5.5.

5.3 Parameters used for tracking

The GFDL vortex tracker produces position fixes for several low-level parameters. The position fixes are then averaged together to produce the mean position fix that is reported for that lead time. This section describes the various parameters and how the tracker combines them in order to produce the mean position fix.

5.3.1 Description of the primary and secondary tracking variables

There are six primary parameters and three secondary parameters that are used for tracking. All of these parameters are from the lower levels of the troposphere. The primary parameters include relative vorticity at 10 m and at 850 and 700 mb; mslp; and geopotential height at 850 and 700 mb. Most models, including HWRF, will output absolute vorticity, and for those models the tracker will subtract out the Coriolis component at each grid point. If vorticity is not included in the input GRIB data file, the tracker will compute it using the u- and v-components of the wind that have been read in. The Barnes analysis is performed for each of these six parameters. If the Barnes analysis returns a location for the maximum or minimum that is within a specified distance threshold, then that parameter’s location fix is saved for use later in computing the

average position fix. If it is not within that distance threshold, the position fix for that parameter is discarded for that lead time. If one or more of these parameters is missing from the input GRIB data file, the tracker simply continues tracking using the limited subset of available parameters.

The distance thresholds are defined initially by the “err_gfs_init” and “err_reg_init” parameters in module error_parms. Values for this initial error parameter vary according to the resolution of the data grid, with finer resolution grids being assigned a threshold of 275 km and coarser resolution global grids being assigned a less restrictive 300-km threshold. For lead times after the initial time, this distance threshold is defined as a function of the standard deviation in the positions of the parameter location fixes including up to the three previous lead times. For example, for very intense, steady-state storms that have strong vertical coherence in their structure, the various parameter fixes are likely to be located closely together. In these cases, the distance threshold defined by the standard deviation of the parameter fixes will be small, as will be the tolerance for outliers in the parameter fixes. For weak systems, or for storms that are undergoing ET, there is less coherence to the vertical structure and often wider variance in location of the parameter fixes. In these cases, the larger distance thresholds defined by the larger standard deviation allow more flexibility in accepting parameter fixes that are not located close to the guess position for a given lead time.

After the Barnes analysis is performed for the six primary tracking parameters, tracking is performed for three secondary wind-based parameters to refine the storm’s location fix. For these secondary parameters, a search is performed for the minimum in wind speed at the center of the storm at 10 m and at 850 and 700 mb. These are not included as primary parameters since, in an unrestricted search in the vicinity of a storm, it would be possible for the tracking scheme to focus in on a quiescent region outside of the storm instead of on the calm at the center of the storm. To help ensure that the search is focused as close to the storm center as possible, a modified guess position for the wind minimum search is created by averaging together the original guess position for this time and the locations of the primary parameter fixes for this lead time that are within 225 km of the original guess position. The Barnes analysis is then called to produce location fixes for the wind minimum at the three different vertical levels. It is important to note that if the tracker cannot make a position fix for any of the six primary parameters, then there will be no attempt to make a position fix using the three secondary wind-based parameters, and tracking will terminate for that particular storm.

5.3.2 Computation of the mean position fix

Once the Barnes analysis has been completed for the primary and secondary parameters, a mean location fix is computed for the storm. A parameter is only included in the mean computation if its location is found within the distance threshold, as described in Section 6.3a. The mean computation is performed in two steps. In the first step, a mean position is computed using all available parameters found within the distance threshold. In the second step, the distance of each parameter fix from that mean position is computed, as is the standard deviation of the parameter fixes. The mean position fix is then recalculated by using a Gaussian weighting controlled by the standard deviation of the position fixes.

The goal here is to minimize the impact of an outlier parameter fix by weighting the mean towards the larger cluster of parameter position fixes.

5.4 Intensity and wind radii parameters

The vortex tracker must also report on forecast data related to intensity and wind structure. For the mslp, the value that was reported during the search for the storm center was a smoothed value that came out of the Barnes analysis. A separate call is made to subroutine `fix_latlon_to_ij` in order to return the minimum gridpoint value of mslp near the storm center. The tracker then analyzes the near-surface wind data (10 m for HWRF and most other models) in order to report on the value of the maximum wind speed. For high resolution grids (spacing $< 0.25^\circ$), the search for the maximum wind is restricted to points within 200 km of the center. For coarser resolution grids with spacing up to 1.25° , the search can extend out to 300 km from the center. The value of the radius of maximum winds is obtained at the same time.

As large storms such as Katrina and Isabel have demonstrated, it is important to have guidance on the structure of the wind field in addition to having the forecast maximum wind value. The tracker provides for basic reporting of the forecast near-surface wind structure by obtaining the radii of 34-, 50- and 64-kt winds in each quadrant of the storm. The values that are reported indicate the maximum distance at which winds of these magnitudes were found anywhere in the quadrant and are not necessarily aligned along any particular azimuth within a quadrant. The values are then output in the standard ATCF text format, which will be described in Section 5.7 below.

The large wind field of Hurricane Sandy (2012) exposed an issue with the algorithm that diagnoses the wind radii in the model output. The maximum radius at which to search for the radii of 34-kt winds (R34) had been set at 650 km. The observed R34 values in Sandy easily exceeded 650 km, as did the forecast R34 values from many of the operational models. Simply increasing the maximum search radius by several hundred km is not advisable, since that could lead to the reporting of erroneous radii values for smaller storms. Instead, an iterative technique has been employed in which the maximum search radius is initially set to a small value (500 km), and if the diagnosed R34 value is returned as either 500 km or very close to it, then the search is done again, but after increasing the maximum search radius by 50 km. This may continue iteratively up to a maximum search radius of 1050 km. Results indicated much more reasonable results from a sample of storms with widely varying R34 values, including large storms such as Hurricane Sandy.

5.5 Thermodynamic phase parameters

The fundamental tracking algorithm of the tracker is designed such that it will analyze data to find the central location of a cyclone and report on its intensity. However, additional diagnostics can be performed after the tracker has located the cyclone center at a given lead time to determine whether a model cyclone is tropical or not. This section describes two different methods used in the tracker for diagnosing the thermodynamic phase of a cyclone.

The first method used by the tracker to diagnose the thermodynamic phase of cyclones is the cyclone phase space methodology developed by Hart (2003). The tracker ingests the average temperature from 300 to 500 mb and the geopotential height every 50 mb from 300 to 900 mb. There are three critical parameters that are diagnosed: (1) the storm motion-relative, left-to-right asymmetry in the lower-troposphere (900-600 mb); (2) warm- / cold-core structure in the lower troposphere (900-600 mb) as diagnosed by assessing the vertical variation of the near-storm isobaric height gradient; and (3) warm- / cold-core structure in the upper troposphere (600-300 mb) as diagnosed by assessing the vertical variation of the near-storm isobaric height gradient.

The second method used for diagnosing thermodynamic phase employs a more basic algorithm, loosely based on Vitart (1997), to determine the existence of a temperature anomaly in the 300-500-mb layer near the cyclone center. The tracker ingests a field containing mean temperatures in the 300-500 mb layer and it runs the tracking algorithm to locate the maximum temperature in that mean layer. It then calls a routine to analyze the 300-500 mean temperature field to determine whether a closed contour exists in the temperature field surrounding the maximum temperature. The value of the contour interval that is checked is set by the user as an input parameter in the script, and we have found empirically that setting the contour interval to 1°K provides an acceptable threshold.

Analyses for both the cyclone phase space and for the simple check of the warm-core return values which are output in a modified ATCF format, described below in Section 5.7. It is important to note that the calculations and determinations made by these thermodynamic diagnostics are provided as auxiliary information and will not affect how a cyclone is tracked or how long the cyclone is tracked. In particular, the tracker will not cease tracking a cyclone if the values returned from these thermodynamic phase diagnostics return values which indicate the storm has either begun or completed transition to an extratropical or subtropical cyclone. It is up to the user to interpret the tracking and phase diagnostic results that are reported in the ATCF output.

5.6 Detecting genesis and tracking new storms

As the forecasting community becomes increasingly interested in forecasts of cyclones at longer lead times, there is also increased interest in predicting cyclone genesis. In recent years, global models have shown the ability to develop cyclones without the aid of synthetic bogusing techniques. The tracker algorithm has been updated to detect genesis in numerical models and track any such new disturbances that the models develop.

Creating an algorithm for detecting new storms generated by a model presents a somewhat more complex problem than for tracking already-existing storms. For a storm that is already being tracked by an RSMC, an observed location is provided by that RSMC and the tracker begins searching near that location for what is known to be a coherent circulation in nature and is assumed to be a coherent circulation in the model. In the case of detecting genesis, no assumptions are made about the coherence of any circulation, and extra steps must be taken to ensure that any systems that are detected by the tracker in the model output are not only cyclones, but tropical cyclones. It is

important to note, however, that these additional checks to determine if the system is of a tropical nature are only done if the `trkrinfo%type` is set to “`tcgen`” in the input namelist file. If `trkrinfo%type` is instead set to “`midlat`”, then the tracker only uses `mslp` for locating the storm center, and no checks are performed to differentiate tropical from non-tropical cyclones.

The tracker begins by searching at the forecast initial time for any RSMC-numbered systems that may have been listed on the input TC vitals record (if provided). This is done so that these systems are properly identified by the tracker and are not then available to be detected and identified as new cyclones by the tracker. For each RSMC-numbered cyclone found, a routine named `check_closed_contour` is called. The primary purpose of this routine is to determine whether at least one closed contour in the `mslp` field exists surrounding the cyclone. An additional important function of this routine is to continue searching outwards from the center of the low in order to find all closed contours surrounding the low. All grid points contained within these closed contours are then masked out so that when the tracker searches for additional lows at the same lead time, any points that have been masked out will not be detected again as a new low.

After finding any RSMC-numbered systems and masking out grid points surrounding those systems, the tracker performs a two-step searching procedure over the remainder of the model domain. First, a search is performed to identify any candidate cyclones, and then a detailed tracking scan is performed to more accurately determine the location and intensity of the candidate cyclones found in the first search and to perform additional diagnostics.

In the first search to identify candidate cyclones, a looping procedure is conducted in which the grid points are scanned to find the lowest `mslp` on the grid. For the grid point with the lowest `mslp` found, a check is made to determine whether there is at least one closed `mslp` contour surrounding the system. If so, then this grid point is saved into an array as a candidate low to be analyzed in the second step. The looping procedure then continues searching for grid points with the next lowest `mslp`, and this procedure continues until the lowest pressure that is found is greater than one half standard deviation above the mean `mslp` on the grid.

In the second step, the candidate cyclones found in the first step are analyzed more critically using the full tracking algorithm outlined above in Section 5.2 to more accurately determine the location and intensity of the cyclone. The quality control checks outlined above in Section 5.2(c(ii)) are employed to ensure that the system being tracked has the fundamental characteristics of a cyclone and are used as input to determine whether or not to continue tracking for a given system.

Some of the more critical checks for newly detected storms include the check for a closed `mslp` contour as well as the check to determine if the azimuthally averaged 850-mb winds are cyclonic and exceed a user-specified threshold. However, due to the fact that incipient, developing cyclones have structures that are often weak and vacillating in intensity, there is some leniency used in the application of these checks from one lead time to the next for the purpose of genesis tracking. In particular, for the closed `mslp` contour check, the requirement is only that the checks return a positive result for at least

50% of the lead times over the past 24-h period to continue tracking. For the 850-mb circulation check, the threshold is a positive result returned for at least 75% of the lead times. The threshold is more rigorous for the 850-mb circulation check than for the mslp check since 850 mb is above the boundary layer and the storm circulation there is generally more inertially stable and less prone to high-frequency fluctuations in intensity than the surface layer.

Additional diagnostics can be performed at this time to determine the thermodynamic phase of the system, as described above in Section 5.6. Results from the thermodynamic phase diagnostics are included in the output, as described below in Section 5.7, but are not used in any algorithms for determining whether or not to continue tracking a system.

5.7 Tracker output

The motivation behind making this tracker operational in 1998 was to provide track and intensity guidance from forecasts for a number of models in as short a time as possible. One of the requirements was that the output data be in the same text ATCF format as that used by NHC. The two primary output files from the tracker include one file in ATCF format and another in a format just slightly modified from the ATCF format. The advantage of using the ATCF format is that user forecasts can easily be compared with those from some of the operational modeling centers.

5.7.1 Description of the ATCF format

The ATCF format contains information on the ocean basin, the storm number, the model ID, the initial date, the forecast hour, and various track, intensity and wind radii guidance. There can be up to three ATCF records that are output for each lead time. A sample segment with some ATCF records from a GFDL hurricane model forecast for Hurricane Emilia (2012) is shown here:

```
EP, 05, 2012071000, 03, GFDL, 000, 131N, 1118W, 98, 951, XX, 34, NEQ, 0080,
0072, 0057, 0078, 0, 0, 17, 0, 0, , 0, , 0, 0, , , , , 0, 0, 0, 0,
THERMO PARAMS, -9999, -9999, -9999, Y, 10, DT, -999
```

```
EP, 05, 2012071000, 03, GFDL, 000, 131N, 1118W, 98, 951, XX, 50, NEQ, 0056,
0047, 0036, 0053, 0, 0, 17, 0, 0, , 0, , 0, 0, , , , , 0, 0, 0, 0,
THERMO PARAMS, -9999, -9999, -9999, Y, 10, DT, -999
```

```
EP, 05, 2012071000, 03, GFDL, 000, 131N, 1118W, 98, 951, XX, 64, NEQ, 0040,
0028, 0017, 0037, 0, 0, 17, 0, 0, , 0, , 0, 0, , , , , 0, 0, 0, 0,
THERMO PARAMS, -9999, -9999, -9999, Y, 10, DT, -999
```

```
EP, 05, 2012071000, 03, GFDL, 006, 134N, 1129W, 80, 963, XX, 34, NEQ, 0100,
0084, 0057, 0088, 0, 0, 34, 0, 0, , 0, , 0, 0, , , , , 0, 0, 0, 0,
THERMO PARAMS, 45, 1405, 1742, Y, 10, DT, -999
```

EP, 05, 2012071000, 03, GFDL, 006, 134N, 1129W, 80, 963, XX, 50, NEQ, 0061,
0053, 0027, 0058, 0, 0, 34, 0, 0, , 0, , 0, 0, , , , , 0, 0, 0, 0,
THERMO PARAMS, 45, 1405, 1742, Y, 10, DT, -999

EP, 05, 2012071000, 03, GFDL, 006, 134N, 1129W, 80, 963, XX, 64, NEQ, 0045,
0034, 0008, 0038, 0, 0, 34, 0, 0, , 0, , 0, 0, , , , , 0, 0, 0, 0,
THERMO PARAMS, 45, 1405, 1742, Y, 10, DT, -999

EP, 05, 2012071000, 03, GFDL, 012, 137N, 1137W, 78, 964, XX, 34, NEQ, 0084,
0071, 0068, 0078, 0, 0, 22, 0, 0, , 0, , 0, 0, , , , , 0, 0, 0, 0,
THERMO PARAMS, 26, 1609, 1879, Y, 10, DT, -999

EP, 05, 2012071000, 03, GFDL, 012, 137N, 1137W, 78, 964, XX, 50, NEQ, 0054,
0048, 0041, 0050, 0, 0, 22, 0, 0, , 0, , 0, 0, , , , , 0, 0, 0, 0,
THERMO PARAMS, 26, 1609, 1879, Y, 10, DT, -999

EP, 05, 2012071000, 03, GFDL, 012, 137N, 1137W, 78, 964, XX, 64, NEQ, 0039,
0033, 0023, 0036, 0, 0, 22, 0, 0, , 0, , 0, 0, , , , , 0, 0, 0, 0,
THERMO PARAMS, 26, 1609, 1879, Y, 10, DT, -999

The first two columns represent the ATCF ID, here indicating that Emilia was the 5th named storm in the eastern Pacific basin in 2012. The next column indicates the initial time for this forecast. The “03” is constant and simply indicates that this record contains model forecast data. After the column with the model ID is a column indicating the lead time for each forecast record. Note that in the current version of the tracker, the frequency at which ATCF data are written out is defined by the atcffreq variable defined in the namelist. That variable should be specified as an integer * 100. The next two columns indicate the latitude and longitude, respectively, in degrees multiplied by 10. The next two columns, respectively, are the maximum wind speed, in kt, and the minimum sea-level pressure, in mb. The “XX” is a placeholder for character strings that indicate whether the storm is a depression, tropical storm, hurricane, subtropical storm, etc. Currently, that storm-type character string is only used for the observed storm data in the NHC Best Track data set.

The next six columns are for reporting wind radii forecast data. The first entry in those six columns is an identifier that indicates whether this record contains radii for the 34-, 50-, or 64-kt wind thresholds. The “NEQ” indicates that the four radii values that follow will begin in the northeast quadrant. Each subsequent value is from the next quadrant clockwise. The radii are listed in units of nautical miles (n mi). If the tracker has detected winds of at least 50 kt in the 10 m wind data, then an additional record will be output for this lead time. This record is identical to the first record, with the exception that the wind radii threshold identifier is “50” instead of “34”, and the radii values are included for the 50-kt threshold. Similarly, if the tracker has detected winds of at least 64 kt at this lead time, then an additional record is output containing those 64-kt wind radii. For any of these thresholds for which at least one quadrant has wind value exceedance, if one or

more of the remaining quadrants does not have exceedance, then for each of those quadrants a value of zero is output.

After the four quadrant values for wind radii, there are two placeholders that are always zero, and then a column that indicates the radius of maximum winds, in n mi. This value is reported using the location of the maximum wind speed that the tracker returned.

After the radius of maximum winds, there is a series of commas and zeroes, followed by a user-defined section of the ATCF record, which is used here to output the values for the thermodynamic diagnostics. The first three values listed after the "THERMO PARAMS" character string are the three cyclone-phase space parameters, and all values shown have been multiplied by a factor of 10. The values are listed in the following order: (1) Parameter B (left-right thickness asymmetry); (2) Thermal wind (warm/cold core) value for lower troposphere (900-600 mb); (3) Thermal wind value for upper troposphere (600-300 mb). Note that for the first lead time listed for a given model storm, the cyclone phase space parameters will always have undefined values of -9999. The reason for this is that the calculation of Parameter B is highly sensitive to the direction of motion, and for the first lead time listed for a storm, it is not possible to know which direction the model storm is heading.

After the cyclone phase space parameters is a character that indicates whether or not the simple check for a warm core in the 300-500 mb layer was successful. The possible values listed here are "Y", "N", and a "U" for "undetermined" if, for any reason, the warm-core check was unable to be performed. The next parameter indicates the value of the contour interval that was used in performing the check for the warm core in the 300-500 mb layer (that value is listed with a magnitude of *10). The last two parameters are currently unsupported and will always be listed as "DT, -999".

5.7.2 Output file with a modified ATCF format for sub-hourly lead times

As described in Section 5.2, the tracker can process lead times that are not regular intervals. In addition, it can process sub-hourly lead times (e.g., tracking using data every 20 minutes). However, the standard ATCF format described in the previous section cannot represent non-integral, sub-hourly lead times. To handle this problem, a separate file with a format just slightly modified from the standard ATCF format is also output. The only difference is that the lead time in the modified format contains five digits instead of three and is represented as the lead time * 100. For example, a lead time of 34 hours, 15 minutes would be 34.25 hours and would be represented in the modified ATCF format as 03425.

To summarize, the modified ATCF format can be output at every lead time, including sub-hourly, non-integral lead times. The standard ATCF format was only designed to handle integral, hourly lead times. Therefore, if a user is processing code that has data at sub-hourly temporal resolutions, a standard ATCF formatted record will not be output for those sub-hourly times.

5.7.3 Output file with a modified ATCF format for use with genesis tracking features

A modified ATCF format is required for the output from genesis tracking runs. In these runs, there will often be a mixture of RSMC-numbered storms as well as new storms that the model develops on its own. For the model-generated storms, a new storm-naming convention is devised to account for the fact that these storms have no previous, set identity as assigned by an RSMC, and the identifiers for the storms must be unique.

Included below is an example of output from a genesis tracking run for the NCEP GFS model. Shown is the output for one model-generated storm as well as for one RSMC-numbered storm, 99L. The first column is reserved for what will either be the ATCF basin ID (AL, EP, WP, etc.) for an RSMC-numbered storm or an identifier to indicate the type of tracking run that is being performed (“TG” = tropical cyclogenesis). The second column will either be the ATCF ID for an RSMC-numbered storm (e.g., 99L) or a tracker-defined cyclone ID for this particular tracking run. This cyclone ID is specific to this particular tracking run only, and it should not be used for any purposes of counting storms throughout a season, since that number may be repeated in the next run of the tracker, but for a different storm.

The third column contains the unique identifier for the storm. Using 2012080100_F150_138N_0805W_FOF from the first record below as an example, the first element indicates the initial date/time group for this particular tracker run, the “F150” indicates the forecast hour at which this particular storm was first detected in the model, and the next two elements (“138N_0805W”) indicate the latitude and longitude at which the storm was first detected. The “FOF” indicates that this storm was “Found On the Fly” by the tracker in a genesis tracking run, as opposed to being tracked from the initial time as an RSMC-numbered storm.

After the unique identifier in the third column, the format is the same as the standard ATCF described above in Section 5.7(a), through and including the wind radii values. After the wind radii values, the next two parameters listed are for the pressure and radius (n mi) of the last closed isobar (1009 and 196 in the first record below), and that is followed by the radius of maximum winds (n mi).

The next four values listed are for the thermodynamic diagnostics. The first three values listed are the three cyclone-phase space parameters, and all values shown have been multiplied by a factor of 10. The values are listed in the following order: (1) Parameter B (left-right thickness asymmetry); (2) Thermal wind (warm/cold core) value for lower troposphere (900-600 mb); and (3) Thermal wind value for upper troposphere (600-300 mb). Refer to Hart (2003) for interpretation of the three cyclone phase space parameters.

After the cyclone phase space parameters is a character that indicates whether or not the simple check for a warm core in the 300-500 mb layer was successful. The possible values listed here are “Y”, “N”, and a “U” for “undetermined” if, for any reason, the warm-core check was unable to be performed.

After the warm-core flag, the next two values (259 and 31 in record 1) indicate the direction and translation speed of storm motion, with the speed listed in m/s * 10. The final four values (112, 144, 69, 89) are, respectively, the values for the mean relative vorticity returned from the tracker at 850 mb, the gridpoint maximum vorticity near the cyclone center at 850 mb, the mean relative vorticity returned from the tracker at 700 mb, and the gridpoint maximum vorticity near the cyclone center at 700 mb. All vorticity values have been scaled by 1E6.

TG, 0048, 2012080100_F150_138N_0805W_FOF, 2012080100, 03, GFSO, 150, 138N, 805W, 18, 1008, XX, 34, NEQ, 0000, 0000, 0000, 0000, 1009, 196, 80, -999, -9999, -9999, N, 259, 31, 112, 144, 69, 89

TG, 0048, 2012080100_F150_138N_0805W_FOF, 2012080100, 03, GFSO, 156, 134N, 813W, 17, 1008, XX, 34, NEQ, 0000, 0000, 0000, 0000, 1010, 251, 98, 19, 106, -89, N, 252, 36, 126, 168, 67, 93

TG, 0048, 2012080100_F150_138N_0805W_FOF, 2012080100, 03, GFSO, 162, 134N, 816W, 17, 1008, XX, 34, NEQ, 0000, 0000, 0000, 0000, -999, -999, 55, -11, 162, 77, N, 266, 17, 110, 150, 70, 91

TG, 0048, 2012080100_F150_138N_0805W_FOF, 2012080100, 03, GFSO, 168, 133N, 818W, 16, 1007, XX, 34, NEQ, 0000, 0000, 0000, 0000, 1008, 92, 74, -27, 95, -26, N, 253, 16, 96, 118, 87, 113

TG, 0048, 2012080100_F150_138N_0805W_FOF, 2012080100, 03, GFSO, 174, 133N, 822W, 17, 1008, XX, 34, NEQ, 0000, 0000, 0000, 0000, 1010, 378, 56, -6, 100, -102, Y, 275, 24, 99, 139, 83, 105

TG, 0048, 2012080100_F150_138N_0805W_FOF, 2012080100, 03, GFSO, 180, 136N, 826W, 20, 1008, XX, 34, NEQ, 0000, 0000, 0000, 0000, 1009, 118, 57, -19, 123, -131, Y, 293, 29, 111, 150, 87, 113

TG, 0048, 2012080100_F150_138N_0805W_FOF, 2012080100, 03, GFSO, 192, 140N, 835W, 14, 1008, XX, 34, NEQ, 0000, 0000, 0000, 0000, 1009, 74, 62, -25, 137, -141, N, 294, 24, 108, 139, 96, 126

TG, 0048, 2012080100_F150_138N_0805W_FOF, 2012080100, 03, GFSO, 204, 143N, 846W, 17, 1009, XX, 34, NEQ, 0000, 0000, 0000, 0000, -999, -999, 159, -3, -41, -106, Y, 292, 30, 64, 73, 62, 68

TG, 0048, 2012080100_F150_138N_0805W_FOF, 2012080100, 03, GFSO, 216, 153N, 859W, 14, 1009, XX, 34, NEQ, 0000, 0000, 0000, 0000, 1012, 89, 155, 30, -19, -118, Y, 293, 31, 51, 56, 50, 55

AL, 99L, 2012080100_F000_097N_0430W_99L, 2012080100, 03, GFSO, 000, 105N, 430W, 28, 1012, XX, 34, NEQ, 0000, 0000, 0000, 0000, 1013, 68, 92, -999, -9999, -9999, N, 279, 83, 221, 267, 207, 258

AL, 99L, 2012080100_F000_097N_0430W_99L, 2012080100, 03, GFSO, 006, 110N, 443W, 33, 1011, XX, 34, NEQ, 0000, 0000, 0000, 0000, 1013, 178, 81, 41, 73, 112, Y, 286, 73, 265, 402, 230, 352

AL, 99L, 2012080100_F000_097N_0430W_99L, 2012080100, 03, GFSO, 012, 113N, 459W, 33, 1012, XX, 34, NEQ, 0000, 0000, 0000, 0000, 1014,

122, 68, 41, 278, 200, N, 282, 78, 302, 403, 257,
358
AL, 99L, 2012080100_F000_097N_0430W_99L, 2012080100, 03, GFSO, 018,
116N, 474W, 34, 1010, XX, 34, NEQ, 0000, 0000, 0000, 0000, 1012,
104, 61, 49, 379, 174, N, 280, 72, 283, 390, 225,
291
AL, 99L, 2012080100_F000_097N_0430W_99L, 2012080100, 03, GFSO, 024,
115N, 488W, 31, 1011, XX, 34, NEQ, 0000, 0000, 0000, 0000, 1013,
107, 72, 47, 427, 21, N, 271, 70, 255, 330, 189,
239
AL, 99L, 2012080100_F000_097N_0430W_99L, 2012080100, 03, GFSO, 030,
117N, 501W, 29, 1009, XX, 34, NEQ, 0000, 0000, 0000, 0000, 1011,
334, 79, 7, 494, 67, N, 278, 67, 240, 323, 175,
233
AL, 99L, 2012080100_F000_097N_0430W_99L, 2012080100, 03, GFSO, 036,
121N, 511W, 36, 1011, XX, 34, NEQ, 0083, 0000, 0000, 0000, 1013,
315, 62, 2, 471, 12, Y, 284, 62, 290, 505, 231,
400
AL, 99L, 2012080100_F000_097N_0430W_99L, 2012080100, 03, GFSO, 042,
123N, 526W, 39, 1009, XX, 34, NEQ, 0085, 0000, 0000, 0073, 1011,
114, 70, -10, 599, 217, Y, 277, 71, 359, 640, 302,
536
AL, 99L, 2012080100_F000_097N_0430W_99L, 2012080100, 03, GFSO, 048,
124N, 542W, 43, 1010, XX, 34, NEQ, 0094, 0000, 0000, 0072, 1012,
102, 70, -17, 620, 154, Y, 269, 78, 376, 627, 323,
543
AL, 99L, 2012080100_F000_097N_0430W_99L, 2012080100, 03, GFSO, 054,
123N, 560W, 39, 1008, XX, 34, NEQ, 0080, 0000, 0000, 0081, 1011,
216, 53, -31, 778, 249, Y, 270, 82, 336, 523, 280,
472
AL, 99L, 2012080100_F000_097N_0430W_99L, 2012080100, 03, GFSO, 060,
121N, 579W, 39, 1010, XX, 34, NEQ, 0075, 0000, 0000, 0067, 1013,
249, 56, -37, 810, 150, Y, 270, 84, 298, 457, 253,
398
AL, 99L, 2012080100_F000_097N_0430W_99L, 2012080100, 03, GFSO, 066,
121N, 596W, 34, 1009, XX, 34, NEQ, 0065, 0000, 0000, 0000, 1010,
71, 65, -41, 729, 63, N, 273, 77, 264, 415, 208, 320
AL, 99L, 2012080100_F000_097N_0430W_99L, 2012080100, 03, GFSO, 072,
122N, 611W, 34, 1010, XX, 34, NEQ, 0061, 0000, 0000, 0000, 1012,
146, 60, -34, 882, 35, N, 274, 71, 242, 376, 186,
273
AL, 99L, 2012080100_F000_097N_0430W_99L, 2012080100, 03, GFSO, 078,
125N, 626W, 31, 1009, XX, 34, NEQ, 0000, 0000, 0000, 0000, 1011,
228, 49, -48, 893, 12, N, 282, 74, 240, 342, 178,
262
AL, 99L, 2012080100_F000_097N_0430W_99L, 2012080100, 03, GFSO, 084,
127N, 644W, 30, 1011, XX, 34, NEQ, 0000, 0000, 0000, 0000, 1013,
125, 67, -23, 864, 3, N, 282, 80, 214, 289, 164,
213
AL, 99L, 2012080100_F000_097N_0430W_99L, 2012080100, 03, GFSO, 090,
131N, 659W, 29, 1009, XX, 34, NEQ, 0000, 0000, 0000, 0000, 1010,
66, 86, -32, 607, 86, N, 288, 73, 199, 251, 152, 204
AL, 99L, 2012080100_F000_097N_0430W_99L, 2012080100, 03, GFSO, 096,
134N, 674W, 29, 1010, XX, 34, NEQ, 0000, 0000, 0000, 0000, -999, -

999, 108, -48, 688, 59, N, 282, 71, 194, 249, 140,
178
AL, 99L, 2012080100_F000_097N_0430W_99L, 2012080100, 03, GFSO, 102,
137N, 692W, 31, 1009, XX, 34, NEQ, 0000, 0000, 0000, 0000, 1010,
73, 88, -51, 423, 123, N, 282, 79, 182, 250, 142, 191
AL, 99L, 2012080100_F000_097N_0430W_99L, 2012080100, 03, GFSO, 108,
140N, 711W, 29, 1011, XX, 34, NEQ, 0000, 0000, 0000, 0000, 1012,
83, 85, -45, 462, 49, N, 283, 84, 159, 217, 112, 154
AL, 99L, 2012080100_F000_097N_0430W_99L, 2012080100, 03, GFSO, 114,
145N, 729W, 28, 1010, XX, 34, NEQ, 0000, 0000, 0000, 0000, 1012,
83, 149, -74, 327, 174, N, 287, 80, 143, 204, 87, 125

6.0 The idealized HWRF framework

A mass-consistent idealized tropical cyclone initialization is available within the HWRF framework. The idealized simulation is configured for the operational HWRF triple-domain configuration with grid spacing 27, 9, and 3 km. The sea-surface temperature is constant in time and space (currently 302 K) as ocean coupling is not yet supported for the idealized configuration in HWRF. Initial conditions are specified using an idealized vortex superposed on a base state quiescent sounding.

To initialize the idealized vortex, the nonlinear balance equation in the pressure-based sigma coordinate system described in Wang (1995), and reported briefly in Bao et al. (2012) and Gopalakrishnan et al. (2011 and 2013), is solved within the rotated latitude–longitude E-grid framework. Sundqvist (1975) first used the balance equation to determine the wind (in terms of stream function) and the mass field (geopotential height). Kurihara and Bender (1980) adopted the inverse balance procedure to obtain mass field from wind field and then solved for surface pressure at the lower boundary of the sigma coordinates and geopotential elsewhere. A variant of this procedure, discussed in Wang (1995), is adopted in the HWRF system.

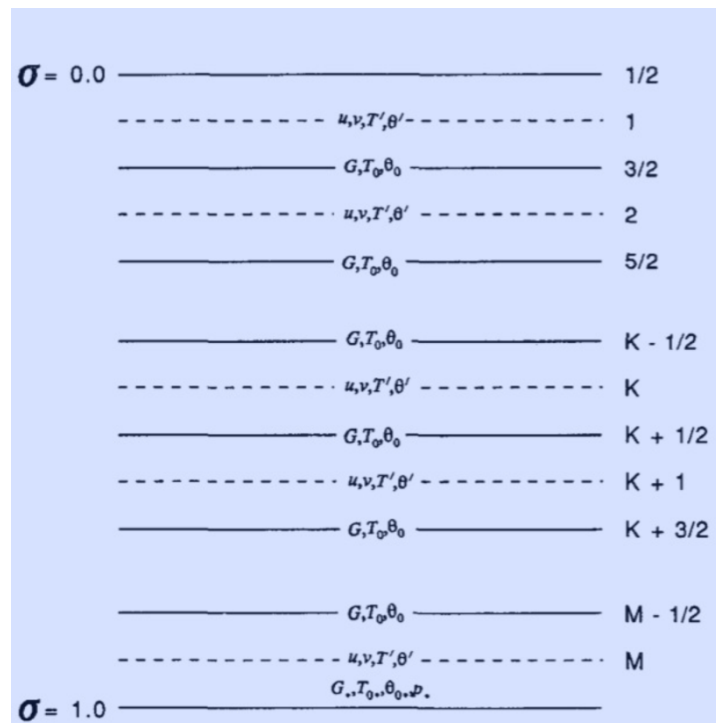


Figure 6.1. Vertical structure of the pressure-sigma coordinate used to create the idealized vortex.

Figure 6.1 provides an overview of the vertical structure of the sigma coordinate system used in the idealized initialization. The atmosphere is divided into M layers. The initial base state temperature (T_0), along with the forcing term G that approximates the

momentum fields, is provided at the interfaces. The zonal (u) and meridional (v) wind components, along with the temperature perturbation (T') from the initial base state, are computed at half levels between the interfaces. The forcing term and the pressure at the lower boundary ($\sigma=1$) are represented by G_d and p_* , respectively. The base state temperature and moisture fields, required in the hydrostatic equation to compute the geopotential from temperature and pressure, are prescribed in file *sound.d*. Wang (1995) provides an extensive overview of the initialization procedure. We describe here only the relevant equations as used in the code *module_initialize_tropical_cyclone.F*

The initial wind field, in cylindrical polar coordinates, is prescribed at each sigma level by:

$$V(r, \sigma) = V_m \left(\frac{r}{r_m} \right) \sin(\pi \sigma / 2) \exp\{1 - (r/r_m)^b\} / b \quad 6.1$$

where V_m is the maximum wind at radius r_m . Both these variables are supplied in file *input.d*. Parameter b is set to 1. The momentum field is a function of the u and v wind components and is given by:

$$G(u, v) = 2J(u, v) + f\zeta - u\beta \quad 6.2$$

where J is the Jacobian, f is the Coriolis parameter, ζ is the vorticity and beta is the meridional gradient of the Coriolis parameter.

$$\nabla^2 \ln(p_*) = G_d / RT_{0d} \quad 6.3$$

The pressure at $\sigma=1$ is obtained by solving the Poisson equation where subscript d denotes the variable evaluated at $\sigma=1$ and R is the gas constant. The temperature perturbations at the sigma levels are determined from solving the Poisson equation:

$$\nabla^2 T'_k = \nabla \cdot [(\partial T' / \partial \ln \sigma) \nabla \ln p_*]_k + [(\partial T_0 / \partial \ln \sigma) \nabla^2 \ln p_*]_k - [\partial G / R \partial \ln \sigma]_k \quad 6.4$$

Finally using the hydrostatic approximation, the geopotential heights are obtained from the total temperature and moisture fields.

Even though the generation of the idealized initial conditions are based on the base state sounding provided in file *sound.d* and on the vortex properties specified in file *input.d*, it is still necessary to provide the model with initial and boundary conditions from the GFS. The GFS-based initial and boundary conditions, processed through WPS, are overwritten with the idealized initialization in the `ideal_nmm_tropical_cyclone` code as explained in the HWRP Users Guide. The lateral boundary conditions used in the HWRP idealized simulation are the same as used in real data cases. This inevitably leads to some reflection when gravity waves emanating from the vortex reach the outer domain lateral boundaries.

In the experiments described by Bao et al. (2012) and Gopalakrishnan et al (2011, 2013), the simulations were performed on an f-plane centered at 12.5° . The idealized vortex initial intensity was 20 m s^{-1} with a radius of maximum winds of about 90 km, embedded in a uniform easterly flow of 4 m s^{-1} or in a quiescent ambient. The base-state temperature and humidity profile was based on Jordan's Caribbean sounding (Gray et al. 1975). In their experiments, the sea-surface temperature was set to 302 K, and no land was present in the domain.

The variables that can readily be customized for the HWRP idealized capability are the base-state sounding thermodynamic structure, the choice of f- or β -plane, the latitude of the storm, the radius of maximum wind, and the maximum wind speed. Sea-surface temperature can be changed in the source code. Additional settings may be changed by altering the source code, but these changes are not currently part of the code supported at the Developmental Testbed Center. Examples of possible changes are introduction of base-state non-zero winds, land surface, or coupling to an ocean model. Finally, all the operational physics, as well as the supported experimental physics options in HWRP, can be used in the idealized framework.

7.0 References

- Arakawa, A. and W. H. Schubert, 1974: Interaction of a Cumulus Cloud Ensemble with the Large-Scale Environment, Part I. *J. Atmos. Sci.*, **31**, 674-701.
- Bao, J.-W., S. G. Gopalakrishnan, S. A. Michelson, F. D. Marks, and M. T. Montgomery, 2012: Impact of physics representations in the HWRF on simulated hurricane structure and pressure–wind relationships. *Mon. Wea. Rev.*, **140**, 3278-3299.
- Barnes, S. L., 1964: A technique for maximizing details in numerical weather map analysis. *J. Appl. Meteor.*, **3**, 396-409.
- Barnes, S. L., 1973: Mesoscale objective analysis using weighted time-series observations. NOAA Tech. Memo. ERL NSSL-62, National Severe Storms Laboratory, Norman, OK 73069, 60 pp. [NTIS COM-73-10781].
- Bender, M. A. and I. Ginis, 2000: Real case simulation of hurricane-ocean interaction using a high-resolution coupled model: Effects on hurricane intensity. *Mon. Wea. Rev.*, **128**, 917-946.
- Bernardet, L. Tallapragada, V., Bao, S., Trahan, S., Kwon, Y., Liu, Q., Tong, M., Biswas, M., Brown, T., Stark, D., Carson, L., Yablonsky, R., Uhlhorn, E., Gopalakrishnan, S., Zhang, X., Marchok, T., Kuo, B., and Gall, R.: 2014, Community Support and Transition of Research to Operations for the Hurricane Weather Research and Forecast (HWRF) Model, accepted for publication in *Bull. Amer. Meteor. Soc*
- Bender, M. A., I. Ginis, R. Tuleya, B. Thomas and T. Marchok, 2007: The operational GFDL Coupled Hurricane-Ocean Prediction System and a summary of its performance. *Mon. Wea. Rev.*, **135**, 3965-3989.
- Bister, M. and K. A. Emanuel, 1998: Dissipative heating and hurricane intensity. *Meteor. Atmos. Phys.*, **65**, 233-240.
- Black, P. G., E. A. D'Asaro, W. M. Drennan, J. R. French, T. B. Sanford, E. J. Terrill, P. P. Niiler, E. J. Walsh and J. Zhang, 2007: Air-Sea Exchange in Hurricanes: Synthesis of Observations from the Coupled Boundary Layer Air-Sea Transfer Experiment. *Bull. Amer. Meteor. Soc.*, **88**, 357-374.
- Blumberg, A. F. and G. L. Mellor, 1987: A description of a three-dimensional coastal ocean circulation model. *Three-Dimensional Coastal Ocean Models*. N. Heaps, Ed., Vol. 4, Amer. Geophys. Union, 1-16.
- Boyer, T. P. and S. Levitus, 1997: *Objective Analysis of Temperature and Salinity for the World Ocean on a 1/4 Grid*. NOAA Atlas NESDIS 11, 62 pp.
- Braun, Scott A. and W.-K. Tao, 2000: Sensitivity of high-resolution simulations of hurricane Bob (1991) to planetary boundary layer parameterizations. *Mon. Wea. Rev.*, **128**, 3941–3961.

- Buehner, M., 2005: Ensemble-derived stationary and flow-dependent background-error covariances: Evaluation in a quasi-operational NWP setting. *Quart. J. Roy. Meteor. Soc.*, **131**, 1013–1043.
- Carnes, M. R., 2009: Description and evaluation of GDEM-V 3.0. Naval Research Laboratory, Stennis Space Center, MS 39529, 21 pp. [NRL/MR/7330--09-9165].
- Deardorff, J. W., 1978: Efficient prediction of groundsurface temperature and moisture, with inclusion of a layer of vegetation. *J. Geophys. Res.*, **83**, 1889-1903.
- Derber, J.C., and W.-S Wu, 1998: The use of TOVS cloud-cleared radiances in the NCEP SSI analysis system. *Mon. Wea. Rev.*, **126**, 2287-2299.
- Donelan, M. A., B. K. Haus, N. Reul, W. J. Plant, M. Stiassnie, H. C. Graber, O. B. Brown and E. S. Saltzman, 2004: On the limiting aerodynamic roughness of the ocean in very strong winds, *Geophys. Res. Lett.*, **31**, L18306.
- Emanuel, K. A., 2003: A similarity hypothesis for air-sea exchange at extreme wind speeds, *J. Atmos. Sci.*, **60**, 1420-1428.
- Falkovich, A., I. Ginis and S. Lord, 2005: Ocean data assimilation and initialization procedure for the Coupled GFDL/URI Hurricane Prediction System. *J. Atmos. Oceanic Technol.*, **22**, 1918-1932.
- Fels, S. B. and M. D. Schwarzkopf, 1975: The Simplified Exchange Approximation: A New Method for Radiative Transfer Calculations, *J. Atmos. Sci.*, **32**, 1475–1488.
- Fels, S., 1985: Radiative-dynamical interactions in the middle atmosphere, *Advances in Geophysics*, **28A**, 277-300.
- Ferrier, B. S., 2005: An efficient mixed-phase cloud and precipitation scheme for use in operational NWP models., *Eos., Trans. AGU*, **86(18)**, Jt. Assem. Suppl., A42A-02.
- Gamache, J. F., F. D. Marks Jr., and F. Roux, 1995: Comparison of three airborne Doppler sampling techniques with airborne in situ wind observations in Hurricane Gustav (1990). *J. Atmos. Oceanic Technol.*, **12**, 171–181.
- Gaspari, G., and S. E. Cohn, 1999: Construction of correlation functions in two and three dimensions. *Quart. J. Roy. Meteor. Soc.*, **125**, 723–757.
- Ginis, I, A. P. Khain and E. Morozovsky, 2004: Effects of large eddies on the structure of the marine boundary layer under strong wind conditions, *J. Atmos. Sci.*, **61**, 3049–3063.
- Gopalakrishnan, S. G., F. Marks, X. Zhang, J.-W. Bao, K.-S. Yeh, and R. Atlas, 2011: The experimental HWRF System: a study on the influence of horizontal resolution on the structure and intensity changes in tropical cyclones using an idealized framework. *Mon. Wea. Rev.*, **139**, 1762–1784.

- Gopalakrishnan, S. G., F. Marks Jr., J. A. Zhang, X. Zhang, J.-W. Bao, and V. Tallapragada, 2013: Study of the impacts of vertical diffusion on the structure and intensity of the tropical cyclones using the high-resolution HWRF system. *J. of the Atmos. Sci.*, **70**, 524-541.
- Gopalakrishnan, S. G., D. P. Bacon, N. N. Ahmad, Z. Boybeyi, T. J. Dunn, M. S. Hall, Y. Jin, P. C. S. Lee, R. V. Madala, R. A. Sarma, M. D. Turner and T. Wait, 2002: An Operational Multi-Scale atmospheric model with grid adaptivity for hurricane forecasting, *Mon. Wea. Rev.*, **130**, 1830-1847.
- Gray, W., E. Ruprecht, and R. Phelps, 1975: Relative humidity in tropical weather systems. *Mon. Wea. Rev.*, **103**, 685–690.
- Grell, G.A., 1993: Prognostic evaluation of assumptions used by cumulus parameterizations. *Mon. Wea. Rev.*, **121**, 764-787.
- Han, J. and H.-L. Pan, 2006: Sensitivity of hurricane intensity forecasts to convective momentum transport parameterization. *Mon. Wea. Rev.*, **134**, 664-674.
- Han, J. and H.-L. Pan, 2011: Revision of Convection and Vertical Diffusion Schemes in the NCEP Global Forecast System. *Wea. Forecasting*, **26**, 520-533.
- Harris, B. A. and Kelly, G. (2001), A satellite radiance-bias correction scheme for data assimilation. *Q.J.R. Meteorol. Soc.*, 127: 1453–1468.
doi: 10.1002/qj.49712757418
- Hart, R.E., 2003: A cyclone phase space derived from thermal wind and thermal asymmetry. *Mon. Wea. Rev.*, **131**, 585-616.
- Haus, B., D. Jeong, M. A. Donelan, J. A. Zhang, and I. Savelyev, 2010: The relative rates of air-sea heat transfer and frictional drag in very high winds. *Geophys. Res. Lett.* , **37**, doi:10.1029/2009GL042206.
- Hong, S.-Y. and H.-L. Pan, 1996: Nonlocal boundary layer vertical diffusion in a medium-range forecast model. *Mon. Wea. Rev.*, **124**, 2322-2339.
- Hong, S.-Y. and H.-L. Pan, 1998: Convective trigger function for a mass flux cumulus parameterization scheme. *Mon. Wea. Rev.*, **126**, 2621-2639.
- Janjic, Z. I., 1990a: The step-mountain coordinate: physical package. *Mon. Wea. Rev.*, **118**, 1429-1443.
- Janjic, Z. I., 1990b: The step-mountain coordinate model: further developments of the convection, viscous sublayer and turbulence closure schemes.. *Mon. Wea. Rev.* **122**, 927-945.
- Janjic, Z. I., 1994: The step-mountain Eta coordinate model – further developments of the convection, viscous sublayer and turbulence closure schemes. *Mon. Wea. Rev.*, **122(5)**, 927-945.

- Janjic, Z. I., 1996a: The Mellor-Yamada level 2.5 scheme in the NCEP Eta model. *Preprints*, 11th Conf. on Numerical Weather Prediction, Norfolk, VA, 19-23 August 1996; Amer. Meteor. Soc. Boston, MA, 333-334.
- Janjic, Z. I., 1996b: The surface layer in the NCEP Eta model. *Preprints*, 11th Conf. on Numerical Weather Prediction, Norfolk, VA, 19-23 August 1996; Amer. Meteor. Soc. Boston, MA, 354-355.
- Janjic, Z. I., 2000: Comments on "Development and Evaluation of a Convection Scheme for Use in Climate Models", *J. Atmos. Sci.*, **57**, p. 3686.
- Janjic, Z. I., 2002: Nonsingular Implementation of the Mellor–Yamada Level 2.5 Scheme in the NCEP Meso model, *NCEP Office Note*, No. 437, 61 pp.
- Janjic, Z. I., R. Gall and M. E. Pyle, 2010: Scientific Documentation for the NMM Solver. NCAR Technical Note NO. NCAR/TN–477+STR, 1-125, 53 pp. (Available from NCAR, P.O. Box 3000, Boulder, CO 80307)
- Jordi, A., and D.-P. Wang, 2012: sbPOM: A parallel implementation of Princeton Ocean Model. *Environ. Modelling & Software*, **38**, 59-61.
- Kain, J. S., and J. M. Fritsch, 1993: Convective parameterization for mesoscale models: The Kain-Fritsch scheme, The representation of cumulus convection in numerical models, K. A. Emanuel and D.J. Raymond, Eds., Amer. Meteor. Soc., 246 pp.
- Kleist, D. T., D. F. Parrish, J. C. Derber, R. Treadon, R.M. Errico and R. Yang, 2009: Introduction of the GSI into the NCEP Global Data Assimilation System. *Mon. Wea. Rev.*, **24**, 1691-1705.
- Kurihara Y. and R. E. Tuleya, 1974: Structure of a tropical cyclone developed in a three-dimensional numerical simulation model. *J. Atmos. Sci.*, **31**, 893–919.
- Kurihara, Y., and M. A. Bender, 1980: Use of a movable nested-mesh model for tracking a small vortex. *Mon. Wea. Rev.*, **108**, 1792–1809.
- Kwon Y. C., and S. Lord, B. Lapenta, V. Tallapragada, Q. Liu and Z. Zhang, 2010: Sensitivity of Air-Sea Exchange Coefficients (Cd and Ch) on Hurricane Intensity. [29th Conference on Hurricanes and Tropical Meteorology](#), **13C.1**
- Lacis, A. A. and J. E. Hansen, 1974: A parameterization for the absorption of solar radiation in the earth's atmosphere. *J. Atmos. Sci.*, **31**, 118–133.
- Lorenc, A. C., 2003: The potential of the ensemble Kalman filter for NWP—A comparison with 4D-VAR. *Quart. J. Roy. Meteor. Soc.*, **129**, 3183–3203.
- Lin, Y.-L., 2007. *Mesoscale Dynamics*. Cambridge University Press.
- Liu, Q., S. Lord, N. Surgi, Y. Zhu, R. Wobus, Z. Toth and T. Marchok, 2006b: Hurricane relocation in global ensemble forecast system. *Preprints*, 27th Conf. on Hurricanes and Tropical Meteorology, Monterey, CA, Amer. Meteor. Soc., P5.13.

- Liu, Q., T. Marchok, H.-L. Pan, M. Bender and S. Lord, 2000: Improvements in Hurricane Initialization and Forecasting at NCEP with Global and Regional (GFDL) models. *NCEP Office Note* 472.
- Liu, Q., N. Surgi, S. Lord, W.-S. Wu, S. Parrish, S. Gopalakrishnan, J. Waldrop and J. Gamache, 2006a: Hurricane Initialization in HWRF Model. *Preprints*, 27th Conference on Hurricanes and Tropical Meteorology, Monterey, CA.
- Makin, V. K., 2005: A note on the drag of the sea surface at hurricane winds, *Boundary-Layer Meteorol.*, **115**, 169-176.
- Marchok, T. P., 2002: How the NCEP tropical cyclone tracker works. *Preprints*, 25th Conf. on Hurricanes and Tropical Meteorology, Amer. Meteor. Soc., San Diego, CA, 21-22.
- McNally, A. P. (2000), Estimates of short-range forecast-temperature error correlations and the implications for radiance-data assimilation. *Q.J.R. Meteorol. Soc.*, 126: 361–373. doi: 10.1002/qj.49712656218
- Mellor, G. L., 1991: An equation of state for numerical models of oceans and estuaries. *J. Atmos. Oceanic Technol.*, **8**, 609-611.
- Mellor, G. L., 2004: *Users guide for a three-dimensional, primitive equation, numerical ocean model (June 2004 version)*. Prog. in Atmos. and Ocean. Sci, Princeton University, 56 pp.
- Mellor, G. L. and T. Yamada, 1982: Development of a turbulence closure model for geophysical fluid problems. *Rev. Geophys. Space Phys.*, **20**, 851-875.
- Michalakes, J., J. Dudhia, D. Gill, T. Henderson, J. Klemp, W. Skamarock and W. Wang, 2004: The Weather Research and Forecast Model: Software Architecture and Performance. *Eleventh ECMWF Workshop on the Use of High Performance Computing in Meteorology*, Reading, U.K., Ed. George Mozdzynski.
- Moon I.-J., T. Hara, I. Ginis, S. E. Belcher and H. Tolman, 2004a: Effect of surface waves on air–sea momentum exchange. Part I: Effect of mature and growing seas, *J. Atmos. Sci.*, **61**, 2321–2333.
- Moon I.-J., I. Ginis and T. Hara, 2004b: Effect of surface waves on air–sea momentum exchange. II: Behavior of drag coefficient under tropical cyclones, *J. Atmos. Sci.*, **61**, 2334–2348.
- Moon, I., I. Ginis, T. Hara and B. Thomas 2007: Physics-based parameterization of air-sea momentum flux at high wind speeds and its impact on hurricane intensity predictions. *Mon. Wea. Rev.*, **135**, 2869-2878.
- Pan, H.-L. and J. Wu, 1995: Implementing a Mass Flux Convection Parameterization Package for the NMC Medium-Range Forecast Model. NMC Office Note, No. 409, 40 pp. [Available from NCEP, 5200 Auth Road, Washington, DC 20233]

- Pan, H.-L., 2003: The GFS Atmospheric Model. NCEP Office Note, No. 442, 14 pp. [Available from NCEP, 5200 Auth Road, Washington, DC 20233].
- Parrish, D. F. and J. C. Derber, 1992: The National Meteorological Center's spectral statistical-interpolation system. *Mon. Wea. Rev.*, **120**, 1747–1763.
- Phillips, N. A., 1957: A coordinate system having some special advantages for numerical forecasting. *J. Meteor.*, **14**, 184-185.
- Powell, M. D., P. J. Vickery and T. A. Reinhold, 2003: Reduced drag coefficient for high wind speeds in tropical cyclones, *Nature*, **422**, 279-283.
- Price, J., 1981: Upper ocean response to a hurricane. *J. Phys. Oceanogr.*, **11**, 153-175.
- Reynolds, R. W. and T. M. Smith, 1994: Improved global sea surface temperature analyses using optimum interpolation. *J. Climate*, **7**, 929-948.
- Roberts, R.E., J. E. A. Selby and L. M. Biberman, 1976: Infrared continuum absorption by atmospheric water-vapor in 8–12 um range. *Applied Optics*, 1-91.
- Rodgers, C. D., 1968: Some extensions and applications of the new random model for molecular band transmission. *Quart. J. Roy. Meteor. Soc.*, **94**, 99–102.
- Ryan, B. F., Wyser, K. and P. Yang, 1996: On the global variation of precipitating layer clouds. *Bull. Amer. Meteor. Soc.*, **77**, 53-70.
- Sasamori T., J. London and D. V. Hoyt, 1972: Radiation budget of the Southern Hemisphere. *Meteor. Monogr*, **35**, 9–23.
- Schwarzkopf, M D. and S. Fels, 1985: Improvements to the algorithm for computing CO2 transmissivities and cooling rates. *J. Geophys. Res.*, 90(C10), 10,541-10,550.
- Schwarzkopf, M. D. and S. Fels, 1991: The simplified exchange method revisited: An accurate, rapid method for computation of infrared cooling rates and fluxes. *J. Geophys. Res.*, **96(D5)**, 9075-9096.
- Sirutis, J. J. and K. Miyakoda, 1990: Subgrid scale physics in 1-month forecasts. Part I: Experiment with four parameterization packages. *Mon. Wea. Rev.*, **118(5)**, 1043-1064.
- Skamarock, W. C., J. B. Klemp, J. Dudhia, D. O. Gill, D. M. Barker, M. G. Duda, X –Y. Huang, W. Wang and J. G. Powers, 2008: A Description of the Advanced Research WRF Version 3, NCAR Technical Note NO. NCAR/TN–475+STR, 1-125
- Smagorinsky, J., 1963: General circulation experiments with primitive equations. Part I: The basic experiments. *Mon. Wea. Rev.*, **91**, 99-164.
- Sundqvist, H., 1975: Initialization for models using sigma as the vertical coordinate. *J. Appl. Meteor.*, **14**, 153–158.

- Tallapragada, V., C. Q. Kieu, Y.C. Kwon, S.G. Trahan, Q. Liu, Z. Zhang, and I.-H. Kwon, 2014: Evaluation of Storm Structure from the Operational HWRF Model during 2012 Implementation. *Mon. Wea. Rev.* (in press). doi: <http://dx.doi.org/10.1175/MWR-D-13-00010.1>.
- Teague, W. J, M. J. Carron and P. J. Hogan, 1990: A comparison between the Generalized Digital Environmental Model and Levitus climatologies. *J. Geophys. Res.*, **95**, 7167-7183.
- Tiedtke, M., 1989: A comprehensive mass flux scheme for cumulus parameterization in large-scale models. *Mon. Wea. Rev.*, **117**, 1779–1800.
- Troen, I. and L. Mahrt, 1986: A simple model of the atmospheric boundary layer: Sensitivity to surface evaporation. *Bound. Layer Meteor.*, **37**, 129-148.
- Tuleya, R. E., 1994: Tropical storm development and decay. Sensitivity to surface boundary conditions. *Mon. Wea. Rev.*, **122**, 291-304.
- Vickers, D. and L. Mahrt, 2004. Evaluating formulations of the stable boundary layer height. *J. of Appl. Meteor.*, **43**, 1736-1749.
- Vitart, F., J. L. Anderson, and W. F. Stern, 1997: Simulation of the interannual variability of tropical storm frequency in an ensemble of GCM integrations. *J. Climate*, **10**, 745-760.
- Wang, X., C. Snyder, and T. M. Hamill, 2007a: On the theoretical equivalence of differently proposed ensemble/3D-Var hybrid analysis schemes. *Mon. Wea. Rev.*, **135**, 222–227.
- Wang, X., T. M. Hamill, J. S. Whitaker, and C. H. Bishop, 2007b: A comparison of hybrid ensemble transform Kalman filter-OI and ensemble square-root filter analysis schemes. *Mon. Wea. Rev.*, **135**, 1055–1076.
- Wang, X., 2010: Incorporating ensemble covariance in the Gridpoint Statistical Interpolation (GSI) variational minimization: A mathematical framework. *Mon. Wea. Rev.*, **138**, 2990–2995.
- Wang, Y., 1995: An inverse balance equation in sigma coordinates for model initialization. *Mon. Wea. Rev.*, **123**, 482–488.
- Yablonsky, R. M. and I. Ginis, 2008: Improving the ocean initialization of coupled hurricane-ocean models using feature-based data assimilation. *Mon. Wea. Rev.*, **136**, 2592-2607.
- Yablonsky, R. M. and I. Ginis, 2009: Limitation of one-dimensional ocean models for coupled hurricane-ocean model forecasts. *Mon. Wea. Rev.*, **137**, 4410–4419.
- Yablonsky, R. M., I. Ginis, E. W. Uhlhorn and A. Falkovich, 2006: Using AXBTs to improve the performance of coupled hurricane–ocean models. *Preprints, 27th Conf. on Hurricanes and Tropical Meteorology*, Monterey, CA, Amer. Meteor.

Soc., 6C.4. [Available online at
<http://ams.confex.com/ams/pdfpapers/108634.pdf>.]

- Yablonsky, R. M. and I. Ginis, 2013: Impact of a warm ocean eddy's circulation on hurricane-induced sea surface cooling with implications for hurricane intensity. *Mon. Wea. Rev.*, **141**, 997-1021.
- Yablonsky, R. M., I. Ginis, B. Thomas, V. Tallapragada, D. Sheinin, and L. Bernardet, 2014a: Performance of the ocean component of NOAA's operational Hurricane Weather Research and Forecasting (HWRF) Model through 2013. *J. Atmos. Oceanic Technol.*, in review.
- Yablonsky, R. M., I. Ginis, and B. Thomas, 2014b: MPIPOM-TC: A new ocean modeling system with flexible initialization for improved coupled tropical cyclone-ocean model forecasts. *Environ. Modell. Softw.*, in review.
- Zhang, C, Y. Wang, and K. Hamilton, 2011: Improved Representation of Boundary Layer Clouds over the Southeast Pacific in ARW-WRF Using a Modified Tiedtke Cumulus Parameterization Scheme. *Mon. Wea. Rev.*, **139**, 3489–3513.
- Zhang, J. A., S. Gopalakrishnan, F. Marks, R. F. Rogers, and V. Tallapragada, 2012: A developmental framework for improving hurricane model physical parameterizations using aircraft observations. *Trop. Cycl. Res. And Rev.*, **1**, 1-11.
- Zhang, J. A., P. G. Black, J. R. French, and W. M. Drennan, 2008: First direct measurements of enthalpy flux in the hurricane boundary layer: The CBLAST results. *Geophys. Res. Lett.*, 35(11):L14813, doi:10.1029/2008GL034374.
- Zeng, X., M. Zhao and R. E. Dickinson, 1998: Intercomparison of bulk aerodynamic algorithms for the computation of sea surface fluxes using TOGA COARE and TAO data, *J. Climate*, **11**, 2628-2644.